Mesoporous and Microporous Titania Membranes

Graduation committee:

Chairman:	Prof. dr. ir. J.F.J. Engbersen	University of Twente
Promotor:	Prof. dr. ing. D.H.A. Blank	University of Twente
Assistant promotor:	Dr. ir. J.E. ten Elshof	University of Twente
Committee members:	Dr. ir. K. Kaizer	University of Twente
	Prof. dr. ing. M. Wessling	University of Twente
	Dr. ir. Z.A.E.P. Vroon	TNO-TPD
	Prof. dr. F. Kapteijn	Delft University of Technology
	Dr. R. Bredesen	SINTEF
	Prof. dr. S. Putić	University of Belgrade

The research described in this thesis was carried out in the Inorganic materials science group at the University of Twente. Financial support is provided by the Commission of the European Communities in the framework of the Growth Programme, "INMEMPERV - High performance microporous inorganic membranes for pervaporation and vapour permeation technology", contract no. G1RD-CT-1999-00076.

Mesoporous and microporous titania membranes
J. Sekulić-Kuzmanović
ISBN 90-365-2107-6

Printed by Febodruk BV, Enschede, The Netherlands.

MESOPOROUS AND MICROPOROUS TITANIA MEMBRANES

DISSERTATION

to obtain
the doctor's degree at the University Twente,
on the authority of the rector magnificus,
prof. dr. F.A. van Vught,
on account of the decision of the graduation committee,
to be publicly defended
on Friday 29th October 2004 at 16.45

by

Jelena Sekulić-Kuzmanović

born on 26th January 1972

in Niš, Serbia

The dissertation is approved by the promotor
Prof. dr. ing. D.H.A. Blank and the assistant promotor Dr. ir. J.E. ten Elshof

Table of contents

1

Introduction

A semi-permeable active or passive barrier, which permits passage of one or more species or components of a gaseous or liquid mixture or solution is called a membrane [1]. Development of synthetic membranes evolved as a scientific discipline in the middle twentieth century, although numerous examples of naturally occurring membranes were known long before. Due to the increasing energy costs in the past few decades, membrane separation processes are becoming more and more attractive in comparison with the conventional separation processes (such as distillation, adsorption, absorption, extraction, crystallisation etc), fitting within the global view of technology for a sustainable economy.

The separating ability of a membrane is determined both by its structure, expressed in terms of porosity and pore size, and by the material it is made of. IUPAC classifies membrane according to the pore size into macroporous (pore size >50 nm), mesoporous (pore size 2-50 nm), and microporous (pore size <2 nm) membranes [2]. On the other hand, depending on the driving force and the physical size of the separated species, membrane processes are classified into microfiltration, ultrafiltration, nanofiltration, reverse osmosis, dialysis, electrodialysis, pervaporation and gas separation [3]. The choice of the membrane material is dictated by the application conditions, separation mechanisms on which membrane operates, and by economic considerations. Both organic (polymeric) and inorganic (ceramic or carbon) membranes are widely used. Advantages of inorganic membranes compared to the polymeric ones are their high thermal, mechanical and chemical stabilities. On the other hand, they are brittle (hence a supporting system is needed) and have high installation and modification costs. Contrary to the undoubtful

potential of inorganic membranes for application in separations, only a very few actual industrial processes based on this technology can be found [1,3,4-7]. Some examples are drinking and wastewater treatment, separation in organic media, purification of used oil, etc. [5-7].

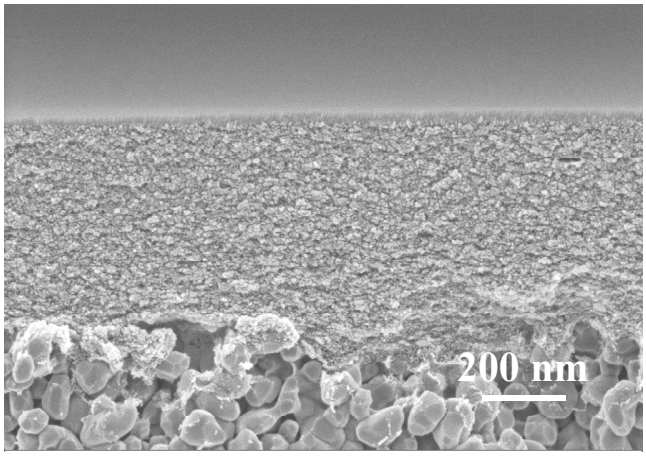

Figure 1.1: Scanning electron microscopy (SEM) micrograph of a composite ceramic membrane system.

Ceramic membranes are usually composite systems consisting of several layers of one or more different oxidic materials. Generally, they have a macroporous support, a mesoporous intermediate layer, and a microporous top layer. The first two layers provide mechanical support for the third one, where the actual separation occurs. Commonly suggested oxidic materials for ceramic membranes are Al_2O_3, TiO_2, ZrO_2, SiO_2, and their combinations. Figure 1.1. shows an example of a membrane system, consisting of an α-alumina macroporous support, a titania mesoporous intermediate layer, and a microporous silica top layer. The separation characteristics of the top layer are determined by its microstructure (mainly its pore size distribution), which is formed during the synthesis procedure. Hence, to prepare a membrane with the required properties, it is important to understand the relationship between the synthesis conditions and the resulting structure. Several approaches are known for the preparation of ceramic porous membranes: the sol-gel method [8], the pyrolysis of a polymeric precursor [9], chemical vapour infiltration [10], leaching [11], etc. Among these processes, the sol-gel technology has shown to be the most suitable for making thin porous films with desired properties [8], mainly due to the relative simplicity, low production costs and possibility of good control over the whole process, allowing synthesis of “tailor-made” materials.

For successful implementation of inorganic membranes in separation technologies in a large-scale industrial environment, several requirements still have to be met: specific combinations of high separation factors and high permeability, reliability, long-term stability, commercial availability, low production and maintenance costs, etc. From the materials point of view, long-term thermal and chemical stabilities are important issues that are, surprisingly, addressed scarcely in literature [12-22]. Although the stability of inorganic membranes is the most often emphasised advantage over their organic counterparts, exposure to extreme conditions can still alter their microstructure during application or cleaning.

A membrane is thermally stable at a certain temperature when its properties (phase structure, mechanical strength, and most importantly, pore structure) remain unchanged or change negligibly at that temperature in a period of time comparable to the practical application lifetime. The thermal stability is often determined by the temperature of crystallographic phase transformations. Beyond this temperature, structural changes may occur, often accompanied by the generation of cracks due to significant volume changes. Apart from phase transformation, the tendency to decrease the surface area at high temperature in order to decrease the total surface energy of the system is of great importance in porous materials. Considering the sintering properties, alumina and silica membranes are thermally the most stable [12,17], whereas anatase titania and zirconia are known for their limited thermal stability caused by the relatively low phase transformation temperature [15,19].

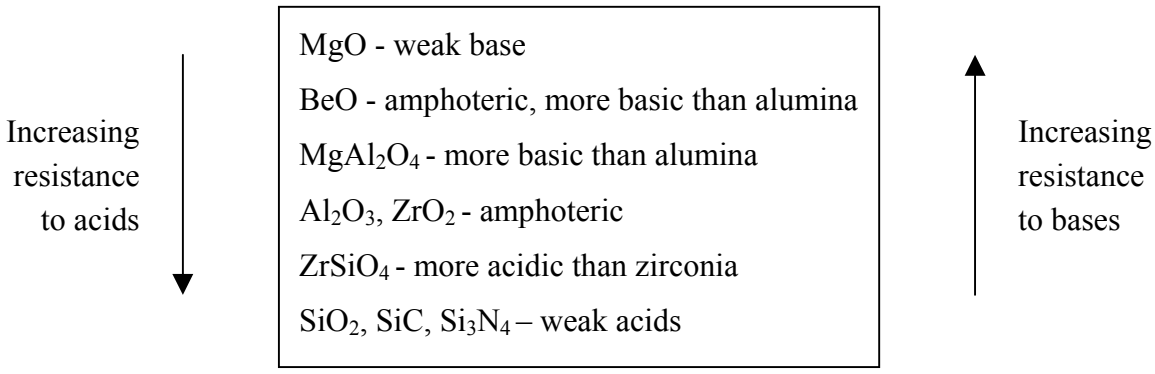

Figure 1.2: Relative resistance of various ceramic materials to acids and bases [1].

The chemical stability of a membrane is often defined as the resistance against aggressive liquids and vapours. The issue of chemical resistance is relevant not only during

application, but also during membrane cleaning operations, which often involve strong acids and bases, and sometimes also peroxides.

A relative comparison of the resistance to acids and bases of various metal oxides and ceramics is shown in Figure 1.2. As a general rule, the more acidic a metal oxide or ceramic is, the greater its resistance towards acids. However such materials are also more prone to attack by bases, and vice versa. For example, considering the weakly acidic nature of silica, a limited resistance to various chemicals can be expected, especially in basic environment. In addition, an extremely poor hydrothermal stability, caused by the high affinity of the silica surface to water, limits its application potential [16]. Furthermore, the chemical resistance may vary with the allotropic state (phase). For example, α-alumina is very stable towards strong acids and bases, but the γ-alumina phase is known for its poor chemical stability [1]. On the other hand, the excellent chemical resistance of titania and zirconia membranes have received considerable interest in recent years [22,23].

1.1 Motivation and objectives

The aim of the work presented in this thesis is to develop mesoporous and microporous ceramic membranes that would contribute to the removal of some of the existing limitations that are detaining broader application of ceramic membrane technology in the chemical industry. These limitations are mainly related to membrane reliability and chemical stability in combination with the required separation properties.

At present, the composite membrane system α-alumina – γ-alumina – silica shows promising results for pervaporation and gas separation applications [24-26]. Moreover, the γ-alumina membrane is widely used as ultrafiltration membrane [24], while silica is the only available truly microporous material (pore size <0.6 nm) that can be employed in applications which require molecular sieving properties [25-27]. However, silica is known to decompose in strong alkaline environments (pH≥9), and γ-alumina is unstable at pH≤4 and pH≥9 [21,22]. Having in mind the limited chemical stability of both of these two materials and the inapplicability of microporous silica in nanofiltration due to its too low pore size, the development of membranes made of new oxide materials is a logical next step.

Because of its superior chemical stability, titania is the most promising membrane material to replace both γ-alumina and silica [22,28-29]. A crystalline mesoporous titania

membrane could be a suitable supporting material, but could also serve as micro- or ultrafiltration membrane [28], while microporous titania with a pore size slightly larger than silica could successfully cover the nanofiltration range, and be applied in gas separation and pervaporation [29]. However, due to the highly sensitive synthesis procedure for both mesoporous and microporous titania membranes, literature reports limited success in their manufacturing and application. Therefore, the presented research concentrates on the development and study of titania membranes. The objectives can be summarized as follows:

1. The study and understanding of the sol-gel chemistry of transition metal alkoxides and the relationship between synthesis conditions and properties of the obtained oxidic membrane materials.
2. The development of reproducible procedures for mesoporous and microporous titania membrane synthesis.
3. Evaluation of membrane systems containing Al_2O_3, SiO_2 and TiO_2 for potential membrane applications in gas separation, nanofiltration and pervaporation technology.

1.2 Outline

Chapter 2 covers the theoretical background of ceramic membrane formation and characterisation.

In chapter 3, the synthesis procedure and characteristics of a mesoporous titania, and a zirconia doped titania membrane are described. A doping mechanism for incorporation of zirconia into the titania structure is proposed, and its influence on microstructure, thermal and chemical stability and liquid permeability was investigated.

Chapter 4 deals with the synthesis and properties of amorphous microporous TiO_2 membranes. The sol-gel chemistry of titanium alkoxides and some synthesis-properties relationship were explored by studying the influence of several processing variables on particle size and sol stability. The thermal phase evolution, microstructural characteristics, thermal and chemical stability, as well as the gas and liquid permeation properties of thin titania films were investigated.

In Chapter 5 the pervaporation characteristics of amorphous microporous titania membranes in dewatering of binary liquids are described. The influence of process

parameters (temperature and feed component concentrations) on the pervaporation properties was studied on the example of ethylene glycol/water mixture.

Finally, in chapter 6 the pervaporation characteristics of three types of asymmetric stacked membrane systems (based on the materials described in chapters 3 and 4) are discussed with respect to separation mechanism, chemical stability and possible applications.

References

1. H.P. Hsieh, "Inorganic membranes for separation and reaction*",* Elsevier, Amsterdam, 1996.
2. W.J. Koros, Y.H. Ma, T. Shimidzu, "Terminology for membranes and membrane process", IUPAC; Comission on membrane nomenclature, 1995.
3. A.J. Burggraaf, L.Cot, "Fundamentals of inorganic membranes science and technology", Elsevier, Amsterdam, 1996.
4. R.R. Bhave, "Inorganic membranes: synthesis, characteristics, and applications", Van Nostrand Reinhold, New York, 1992.
5. K. Londsdale, "The growth of membrane technology", J. Membr. Sci. 10 (1982) 81-181.
6. R.D. Noble, "An overview of membrane separations", Sep. Sci. Tech. 22 (1987) 731-743.
7. L. Shi-Hee, C. Koo-Chun, S. Min-Chul, D. Jong-In, L. Hee-Soo, A. Keun Ho, "Preparation of ceramic membrane and application to the crossflow microfiltration of soluble waste oil", Mater. letters, 52, 4-5 (2002) 266-271.
8. C.J. Brinker, "Sol-gel science: the physics and chemistry of sol-gel processing", Harcourt Brace Jovanovich, Boston, 1990.
9. H. Mori, S. Mase, N. Yoshimura, T. Hotta, K. Ayama, J. Tsubaki, "Fabrication of supported Si_3N_4 membranes using the pyrolysis of liquid polysilane precursor", J. Membr. Sci. 147, 1 (1998) 23-33.
10. A. Nijmeijer, B.J. Bladergroen, H. Verweij, "Low-temperature CVI modification of γ-alumina membranes", Micropor. Mesopor. Mater. 25, 1-3 (1998) 179-184.
11. H. Wang, G.R. Gavalas, "Mesoporous glass films supported on α-Al_2O_3", J. Membr. Sci. 176, 1 (2000) 75-85.
12. Y.S. Lin, C.H. Chang, R. Gopalan, "Improvement of thermal stability of porous nanostructured ceramic membranes", Ind. Eng. Chem. Res. 33 (1994) 869-870.
13. I. Voigt, P. Puhlfurss, J. Topfer, "Preparation and characterisation of microporous TiO_2 membranes", Key. Eng. Mater. 132-136 (1997) 1735-1737.
14. A. Larbot, J. Fabre, C. Guizard, L. Cot, "New Inorganic ultrafiltration membranes: titania and zirconia membranes", J. Am. Ceram. Soc. 72, 2 (1989) 257-261.
15. K.-N.P. Kumar, J. Tranto, J. Kumar, J.E. Engell, "Pore structure and phase transformation in pure and M-doped (M=La, Ce, Nd, Gd, Cu, Fe) alumina membranes and catalyst supports", J. Mater. Sci. Letters: Pore structure and stability, 15, (1996) 3-9.
16. H. Imai, H. Morimoto, A. Tominaga, H. Hirashima, "Structural changes in sol-derived SiO_2 and TiO_2 films by exposure to water vapour", J. Sol-Gel Sci. Tech. 10 (1997) 45-54.
17. R.S.A. Lange, K. Kaizer, A.J. Burggraaf, "Ageing and stability of microporous sol-gel modified ceramic membranes", Ing. Eng. Chem. Res. 34 (1995) 3838-3847.
18. G.R. Gallaher, P.K.T. Liu, "Characterisation of ceramic membranes; I: Thermal and hydrothermal stabilities of commercial 40 A membranes", J. Membr. Sci. 92 (1994) 29-44.

19. C.–H. Chang. R. Gopalan, Y.S. Lin, "A comparative study on thermal and hydrothermal stability of alumina, titania and zirconia membranes", J. Membr. Sci. 91 (1994) 27-45.
20. R.S.A. de Lange, J.H.A. Hekkink, K. Keizer, A.J. Burggraaf, "Formation and characterization of supported microporous ceramic membranes prepared by sol-gel modification techniques", J. Membr. Sci. 99,1 (1995) 57-75.
21. J. Sekulic, M.W.J. Luiten, J.E. ten Elshof, N.E. Benes, K. Keizer, "Microporous silica and doped silica membrane for alcohol dehydration by pervaporation", Desalination, 148 (2002) 1-3.
22. T. Van Gestel, C. Vandecasteele, A. Buekenhoudt, C. Dotremont, J. Luyten, B. Van der Bruggen, G. Maes, "Corrosion properties of alumina and titania NF membranes", J. Membr. Sci. 214,1 (2003) 21-29.
23. J.M. Hofman-Zuter, "Chemical and thermal stability of (modified) mesoporous ceramic membranes", PhD thesis, Twente University, 1995.
24. A. Larbot, S. Alami-Younssi, M. Persin, J. Sarrazin, L. Cot "Preparation of a γ-alumina nanofiltration membrane", J. Membr. Sci. 97 (1994) 167-173.
25. R.M. de Vos, H. Verweij, "High-Selectivity, High-Flux Silica Membranes for Gas Separation", Science, 279 (1998) 1710-1711.
26. H.M. van Veen, Y.C. van Delft, C.W.R. Engelen, P.P.A.C. Pex, "Dewatering of organics by pervaporation with silica membranes", Separat. Purif. Techn. 22-23 (2001) 361-366.
27. L. Cot, A. Ayral, J. Durand, C. Guizard, N. Hovnanian, A. Julbe, A. Larbo, "Inorganic membranes and solid state sciences", Solid State Sciences, 2, 3 (2000) 313-334.
28. T. Tsuru, D. Hironaka, T. Yoshioka, M. Asaeda, "Titania membranes for liquid phase separation: effect of surface charge on flux", Separ. Purif. Tech. 25, 1-3 (2001) 307-314.
29. P. Puhlfürß, A. Voigt, R. Weber, M. Morbé, "Microporous TiO_2 membranes with a cut off <500 Da", J. Membr. Sci. 174, 1 (2000) 123-133.

2

Theoretical background of sol-gel membrane formation and characterisation techniques

Abstract

Membrane synthesis by the sol-gel process includes sol manufacturing, layer application, drying and thermal treatment. In this chapter, the discussion that concerns sol manufacturing is mainly concentrated on the sol-gel chemistry of transition metal precursors and the control of hydrolysis and condensation reactions through control of synthesis process parameter. Furthermore, the basis of the layer application by dip-coating, calcination procedures and the standard synthesis procedures for state-of-the-art α-alumina, γ-alumina and silica membranes are described. Prepared membranes can be evaluated and compared through the characterisation procedure. An appropriate study of the structure of porous materials should include an analysis of pore size distribution, pore morphology, total porosity, the thickness of the different layers or porous clusters, etc. Morphological structure of a membrane is usually studied by the microscopic methods that provide images of the surface or cross-sections of the membrane. Porosity and pore size can be studied by sorption measurements (if material is in the powder form), or by the liquid–liquid and air–liquid displacement techniques (if material is in the thin layer form). Theoretical backgrounds of some of the mentioned techniques are described in more detail in this chapter and will not be further addressed.

2.1 Membrane synthesis by sol-gel technique

Sol-gel is a general name for a process that converts a colloidal or polymeric "solution" (sol), to a gelatinous substance (gel) [1]. Sol-gel processing has gained scientific interest and technological importance during the last decades mainly due to the relative simplicity of the procedure and the almost unlimited number of possibilities for the formation of materials with improved or new properties. Applied in a membrane production process, it includes sol manufacturing, layer application, drying and thermal treatment. Although each step may be critical for the success of the membrane synthesis, it is widely believed that the final membrane properties are to a large extent determined by the structure and chemistry of the sol. The sol-gel chemistry of silica is one of the most widely studied topics in this area [1]. However, the sol-gel chemistry of transition metal alkoxides is more complex than that of silicon alkoxides, because transition metal precursors are highly reactive (they have a low electronegativity and can exhibit various coordination numbers). Since one of the key objectives of this thesis is the development of a microporous titania membrane, the discussion below will be mainly concentrated on the sol-gel chemistry of the polymeric route with transition metal precursors. Furthermore, the theoretical background of membrane layer formation will be briefly addressed, and the standard synthesis procedures for state-of-the-art α-alumina, γ-alumina and silica membranes will be described.

2.1.1 Sol-gel chemistry of transition metal alkoxides

The chemistry involved in the sol-gel process is based on so-called inorganic polymerisation [1-4]. It involves the hydrolysis and condensation reactions of metal alkoxide precursors dissolved in water or an organic solvent, leading to the formation of a metal-oxo-based macromolecular network. Precursors are usually metallo-organic compounds such as alkoxides – $M(OR)_n$ (M=Si, Ti, Zr, Al; OR=$OC_nH_{2\,n+1}$).

The overall hydrolysis-condensation reactions can be written as

Hydrolysis:	$M\text{-}OR + H_2O \rightarrow M\text{-}OH + R\text{-}OH$	
Condensation:	$M\text{-}OH + M\text{-}OX \rightarrow M\text{-}O\text{-}M + X\text{-}OH$	Oxolation
	$M\text{-}OH + M\text{-}XOH \rightarrow M\text{-}OH\text{-}M + X\text{-}OH$	Olation
	(X=H, or X=R)	

The hydrolysis reaction replaces alkoxide groups with hydroxyl groups. Subsequent condensation occurs through formation of OH bridges via olation, and formation of oxygen bridges via oxolation.

Two kinds of sol-gel routes are generally described in literature, differing in the structure of the obtained sol species. The so-called colloidal or "particulate" route is based on the formation of colloids in aqueous media, where the particles are prevented from agglomeration by mutual repulsion of similar charges at the particle surface. The transition from sol into gel in these systems is a result of electrolytic effects, which also determines the particle distance at the gelling point, thus influencing the capability of the gel to remain monolithic during drying. Colloidal (particulate) sols are generally used for the production of crystalline, mesoporous materials. The second type of sol-gel route leads to polymeric sols from which amorphous and microporous materials may be formed. In the polymeric route, metal-organic precursors are reacted in alcoholic media, where the polymeric particles remain separated because of their small size. Gelling in polymerised systems from metal-organic precursors occurs as a result of polymerisation.

In general, different products (colloidal/polymeric sol species, gels or precipitates) can be obtained depending on the relative hydrolysis and condensation rates, as suggested in Table 2.1. This table illustrates commonly accepted rules of thumb used as a starting point in sol-gel chemistry and materials development [2].

Table 2.1: Expected product of the sol-gel process depending on the hydrolysis and condensation rates.

Hydrolysis rate	Condensation	Result
slow	slow	colloids/sols
fast	slow	polymeric sols/gels
fast	fast	colloidal gel or precipitate
slow	fast	controlled precipitation

In conclusion, the success of the sol-gel route to get a stable sol with required properties depends on the ability to control the hydrolysis-condensation process. The control of hydrolysis and condensation rates is performed through control of several process parameters, which will be discussed in the following sections.

2.1.1.1 Influence of process parameters

Precursor; In order to gain control over the hydrolysis-condensation process, the precursor reactivity during the process has to be decreased. It is a well-known fact that the hydrolysis rate of a metal alkoxide decreases with increasing size of the alkyl group (e.g. ethoxide > propoxide > butoxide). This is a consequence of the positive partial charge of the metal atom, which decreases with alkyl chain length. On the other hand, steric hindrance effects also have to be taken in to account, as it has been shown that the hydrolysis rate decreases in the order tertiary > secondary > normal. The third property of the metal alkoxide that has to be taken into account is its molecular structure. The full coordination of many metals often can not be satisfied in metal alkoxides $M(OR)_n$. This is due to the fact that the oxidation state Z of the metal is lower than its usual coordination number N. For example, the oxidation state of titanium is Z=4 while its usual coordination number is N=6. In such cases coordination expansion of the metal alkoxide may occur via oligomerisation or charge transfer complex formation. In a weak complexing medium, coordination expansion involves alkoxy-bridging. Metal alkoxides are oligomers rather than monomers. As shown by Manzini *et al.*, $Ti(Oi\text{-}Pr)_4$ is a tetracoordinated monomer (no Ti-Ti correlation is found) while $Ti(OBu)_4$ and $Ti(OEt)_4$ form a pentacoordinated oligomer with Ti-Ti distances of 3.09 Å. [5]. As a general rule, because of steric hindrance, titanium alkoxides with primary alkoxy groups form trimers with Ti surrounded by five ligands, while those with secondary or tertiary alkoxy groups remain monomeric with Ti in fourfold coordination. [6]. This is confirmed by the calculated free energy of hydrolysis: ΔG_o=110 kJ/mol for ethoxide side groups, and ΔG_o=90 kJ/mol for iso-propoxide and tert-butoxide [6]. The larger ΔG_o value calculated for $Ti(OEt)_4$ is attributed to the energy required to break the trimeric species.

However, alkoxy bridging is not the only way for coordination expansion. As an alternative process, the addition of another donor ligand from the solution can also occur. The most often used additives are acetic acid and acetylacetone [7,8]. This complexation reaction seems to be highly favored when the electrophilic power and the coordinative unsaturation (expressed by the difference N-Z) of the metal atom are large. Strongly complexing species remain bound to the metal.

Theoretically, the most logical choice of a precursor that would provide slow hydrolysis and condensation rates would be an alkoxide with a long normal alkyl chain that forms trimeric species in an alcoholic solution. However, the actual choice will also depend on some other process characteristics. For example, long chain alkoxides are less soluble in

alcohol and will therefore be more difficult to remove later. In addition, a number of authors showed that beside precursor type, the oligomerisation and/or inhibition ratio are dominant factors in the control of the hydrolysis and condensation reaction [6,9-11].

Hydrolysis ratio; The hydrolysis ratio is defined as the ratio of molar concentration of water and metal alkoxide (titanium in this case):

$$r_w = \frac{[H_2O]}{[Ti]} \tag{2.1}$$

Two major domains are defined for the case of titania alkoxide hydrolysis, based on the stoechiometrically needed number of molecules of water per molecule of titania for complete hydrolysis (that equals to 4):

- $r_w \leq 4$

  At hydrolysis ratio lower that s stoechiometrically needed, the so-called polymeric sol-gel process may occur (when other conditions are also favourable), so that a network of partially hydrolysed and polycondensed oligomers diluted in the solvent is formed.

- $r_w > 4$

  In this case olation (not oxolation) is the predominant pathway for condensation, which leads to the formation of cross-linked polymers, particulate sols (gels), or precipitates. The use of excess of water is a standard route for colloidal ("particulate") sol preparation.

Inhibitors; The normal course of hydrolysis-condensation reactions of titanium alkoxides in solution leads to precipitation of titanium-oxo polymers. The control of hydrolysis-condensation reactions is therefore usually performed through the use of catalysts or inhibitors, which may be inorganic acids or complexing ligands such as organic acids, beta-diketones or related derivates [7,9]. The addition of such inhibitors can prevent precipitation, force growth to gel state or stop it. The simplest and most commonly used inhibitors for condensation reactions are H^+ ions [10]. The inhibition ratio (r_a) is defined as the ratio of molar concentration of H^+ ions and metal alkoxide:

$$r_a = \frac{[H^+]}{[Ti]} \tag{2.2}$$

At the same time, inorganic acids favour the hydrolysis reaction by making protonated alkoxy ligands better leaving groups. However, depending on the proton concentration, nucleophilic species (Ti-OH) may be protonated, causing selective inhibition of some condensation reactions. Moreover, acidic condensations may help to break the titanium oxo or titanium hydroxo bridges, thereby enhancing reverse (dissolution) reactions.

Solvent influence; Metal alkoxides are often dissolved in organic solvents before hydrolysis is performed. The most often used solvents are parent alcohols, which have the same number of carbon atoms in the alkyl group as in the alkoxy group of the metal alkoxide (for example, ethanol is the most suitable solvent for a metal ethoxide). As a general rule, dilution should lead to higher alkoxide association, and the formation of oligomers rather than monomers. However, solvents are often not chemically inert toward metal alkoxides and the metal alkoxide reactivity can be easily modified by changing the solvent. Sanchez *et al*. report alcohol interchange as one of the methods of chemical modification of alkoxide precursors to change the gelation time and even the properties of the oxide [11]. Metal alkoxides react with a variety of alcohols to form the following type of equilibrium [11-13]:

$$M(OR)n + xR'OH \Leftrightarrow M(OR)n\text{-}x(OR')x + xROH$$

In general, the ability for interchange increases when the steric hindrance of the alkoxy group decreases. For example, it was proven by Sanchez *et al*. that alcohol interchange occurs when $Ti(OEt)_4$ is dissolved in ethanol, n-butanol or t-butanol [11]. However, a higher degree of interchange is achieved when ethanol or n-buthanol are used, and a lower in the case of t-butanol, probably because metal alkoxides form oligomers in primary alcohols, while they stay monomeric in other alcohols.

2.1.1.2 Particle growth mechanisms

Colloidal sol; The growth of colloidal particles from nuclei proceeds by diffusion of solute precursors onto the existing nuclei. In general, the formation of monodisperse particles is favoured when nuclei are small and their size distribution is narrow. Hence, the control of particle growth can be achieved already during hydrolysis and condensation reactions through the control of process parameters. An example of uncontrolled particle growth is the phenomenon known as "Ostwald ripening" [6]. Once primary particles are formed, the small ones dissolve, and the product species are incorporated into the large particles (Figure 2.1), which leads to disappearance of small particles while large particles become

bigger. Particle growth can also continue through an aggregation process, the prevention or control of which is often described as sol stability. Sol stabilization techniques are mainly based on increasing steric hindrance or electrical repulsion between sol particles, but also on the employment of protective agents such as inert solvents, bulky organic ligands or micelles [6].

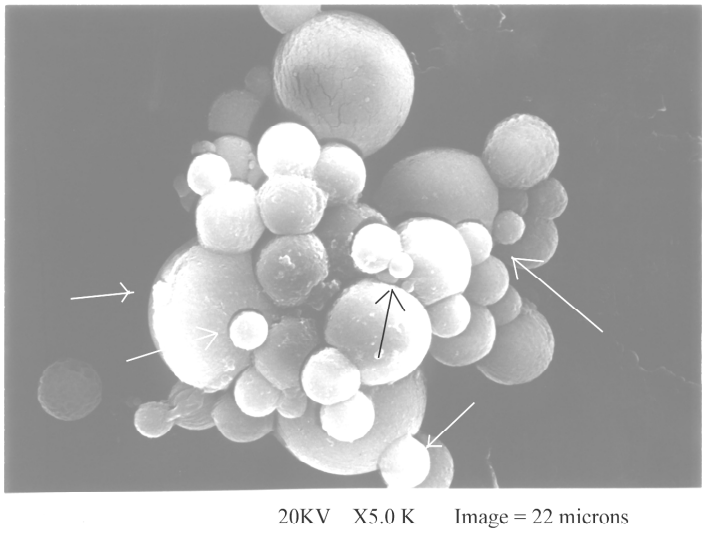

Figure 2.1: SEM micrograph showing Ostwald ripening; the arrowheads indicate the smaller particles precipitated on the larger ones.

Polymeric sol; Hydrolysis and condensation reactions carried out under certain carefully controlled conditions may lead to the formation of a three-dimensional network of branched polymers. These polymeric systems grown by random processes are fractal objects and can be represented by a mass fractal dimension (D_f) that relates the mass m to the radius r of the sol particle via

$$m \propto r^{D_f} . \tag{2.3}$$

D_f has an upper limiting value of 3, where the object is Euclidean. As D_f decreases, the object will look sparser, giving essentially a linear object when D_f=1. The fractal dimension of polymeric species in the sol can be measured by means of small angle X-ray scattering (SAXS), and hence the polymeric growth process can be monitored, as described in section 2.2.2.

The growth of polymeric species has been explained by a number of equilibrium and kinetic growth processes [14-18], but only a few of the most commonly accepted views will be briefly described.

According to the particle-cluster aggregation model, developed by Witten and Sander, individual particles, diffusing due to Brownian motion, stick onto a single growing aggregate one after another [15]. For many cases however, this model leads to more compact structures than observed experimentally.

Thus, an alternative model was developed by Meakin, the so-called the cluster-cluster aggregation model [16]. It describes an aggregation process, where all reacting species initially are present in the defined space (a "sea of monomers" is present). The aggregation process is governed by collisions between diffusing clusters. The resulting structure is much more open compared with the particle-cluster model. Another important difference is the shape of the structures. While particle-cluster aggregates exhibit a roughly spherical shape with a well-defined centre around which growth takes place, cluster-cluster aggregates are of an ellipsoidal shape, anisotropic with no recognizable centre (Figure 2.2).

Figure 2.2: Comparison of particle-cluster (a) and cluster-cluster (b) growth models, made by computer simulation [16].

An extension of the cluster-cluster aggregation model that considers a lower degree of interpenetration of the reacting species is developed by Jullien [17]. This so called tip-to-tip model emphasizes sticking on tips, which is physically justified when considering electrostatic forces in the case of polarisable clusters. When two particles approach each other, opposite charges appear on the nearest tips and the clusters stick on these tips. However, all the models mentioned before assume a constant reactivity of the aggregating species. In practical simulations, this is not always true. For example, the reactivity of an alkoxide monomer for hydrolysis under acid-catalysed conditions decreases with the number of hydrolysed groups. This is incorporated in the aggregation model of Kallala *et al.* [18], by introducing a relative reactivity of monomers during the polymerisation process. Contrary to the models described above, a continuous range of final products can be obtained.

2.1.2 Membrane layer formation

After the sol has been formed, further membrane manufacturing involves layer deposition, drying and a calcination step.

During the layer deposition process, capillary forces drive the dispersion medium through the support, forming a layer of concentrated sol on the surface. Film formation may proceed according to two mechanisms, namely slip casting and film coating, depending on sol properties and coating parameters [19,20]. During a slip casting process a layer forms by capillary suction of the fluid medium of the dipping solution by the support pores. The process is time dependent and the thickness of the formed layer will increase with duration of dipping. The film coating mechanism generally occurs when the dipping time is short and the viscosity of the suspension is high. This is because an adhering dispersion layer is retained as a result of the drag force exerted by the substrate during withdrawal from the dispersion. The thickness of the layer adhered increases with the withdrawal speed and dispersion viscosity, but is not dependent on the dipping time. When particulate sols are deposited, the dipping solution is usually a mixture of the sol and organic polymer additives, so-called binders [23]. Binders lower the surface tension and improve the visco-elastic properties and the stress relaxation behaviour of the gel layer during drying. Due to their organic nature and low decomposition temperature they are burnt out during the firing step. Polymeric sols are usually dissolved in alcohol, the obtained layer is thinner and in general it dries faster, while organic additives that would suppress stresses during drying are not necessary. Layer deposition is typically carried out by means of dip coating or spin coating [19-22]. In the dipping process a porous support is brought into contact with the dip-solution for a few seconds, resulting in film formation. The dip-coating parameters, such as suspension viscosity and dipping time, play a critical role in determining the thickness of the wet cake and consequently, the thickness of the final ceramic membrane [22,24,25].

One of the most critical steps in membrane formation is the drying process, because large stresses develop due to the capillary force of the pore fluid that cannot be relaxed by shrinkage because of the presence of the rigid support [26]. Also, the stress field in the top layer can become inhomogeneous around hard agglomerates. If the stress exceeds a certain limit, the top layer cracks and peels off from the support. However, drying stress may also play a positive role in the membrane formation process. It causes weak aggregates to break down into primary particles and may help in further rearrangement and ordering of the

primary particles. In the case of polymeric films, an additional problem can be caused by overlap of the drying and gelation processes, due to the fact that volatile compounds (solvent) evaporate faster than the others (water, acid, precursor), thus increasing the concentration of the reacting species. Therefore, films are usually processed from the aged sols in which polymeric species already have a final size and morphology, in order to avoid hydrolysis and condensation reactions under uncontrolled conditions.

The last step in membrane manufacture is calcination (annealing, sintering), which gives the microstructural, mechanical and chemical integrity to the system [26-28]. During calcination physically adsorbed water (or any other solvent), residual organics and nitrates will be removed. In the initial stage of sintering, , a "physical reaction" takes place on the contact points between primary particles, which results in the formation of necks between the particles. Continued heating leads to neck broadening and increasement of shrinkage and consequently, densification. The change of porous structure is particularly profound around the phase transition temperature. During the heating and cooling process, stress develops due to a thermal expansion mismatch between support and top layer, and/or shrinkage. If not carefully controlled, this may lead to microstructural changes, layer cracking or delamination. The main sintering mechanisms can be described as (1) solid state diffusion from areas with relative small curvature to areas with relative large curvature, typically in the neck area along the grain boundary in the neck, which is characteristic for "grainy", crystalline structured materials, and (2) viscous sintering of amorphous or glassy structures by viscous flow and particle deformation. In both cases, the driving force for sintering is a decrease of the surface energy of the system.

2.1.3 Synthesis procedures for α-alumina/γ-alumina/silica membrane system

Synthesis procedures for the state-of-the-art membrane system α-alumina/γ-alumina/silica, that is also used in this study, were previously developed and are well established. Therefore, the manufacturing process will be described in this chapter and will not be discussed further in this thesis.

Flat disc-shaped supports are prepared using a colloidal filtration method [29]. The colloidal suspension is prepared from pure α-alumina powder (AKP30, Sumimoto, Japan). To ensure electrostatic stabilisation of the suspension [30], the powder is dispersed in a solution of HNO_3 and ultrasonically treated for 15 minutes. The resulting stable solution is poured into a round mould with a polyester filter (pore size 0.8 μm, ME 27,

Schleicher & Schuell, Germany). Casts are formed using a vacuum pump. The obtained casts are dried overnight in ambient air, and sintered at 1100 ^{o}C for 1 h. After sintering, cutting and polishing are done to achieve the standard shape for the support (2 mm thickness and 39 mm diameter). Subsequently, the supports are polished (polishing machine Jean Wirtz, Germany) to achieve as "shiny" a surface as possible, without any visible defects. The resulting α-alumina supports have a porosity of around 30%, and a pore size of ~100 nm [31].

The γ-alumina intermediate layers are made by dip coating boehmite (γ-AlOOH) sols onto the α-alumina supports, under class 1000 clean room conditions. The boehmite sol is prepared by the colloidal sol-gel route. The theoretical background of this route is discussed in detail in section 2.1 of this chapter. Aluminium-tri-sec-butoxide is added to water heated to 90 ^{o}C, with a hydrolysis ratio (r_w=[H_2O]/[Al]) of 140. After addition the mixture is kept at 90 ^{o}C for 1 h to evaporate sec-butanol. Subsequently, the solution is cooled down to 60 ^{o}C, and peptised with 1M HNO_3 at pH 2.8. The resulting boehmite mixture is refluxed for 20 h at 90 ^{o}C, resulting in a homogeneous, stable 0.5 M boehmite sol. The dipping solution is made by mixing the sol with a PVA solution, which acts as a binder. After dipping the membrane is dried in a climate chamber at 40 ^{o}C and 60% relative humidity for 3 h. The γ-alumina membranes are formed by calcination at 600 – 650 ^{o}C for 3 h in air. The resulting membranes have an average thickness of ~1 μm and a pore size of 5-7 nm [32]. A porosity, measured on unsupported material, is ~55%.

Standard silica membranes were prepared by dip-coating a supported γ-alumina membrane in a diluted sol, followed by thermal treatment. The standard silica sol is prepared by acid-catalysed hydrolysis and condensation of tetra-ethyl-ortho-silicate (TEOS) in ethanol. The reaction mixture had a final molar [Si]:[EtOH]:[H_2O]:[H^+] ratio 1:3.8:6.4:0.085, in accordance with the "standard" recipe of silica sol preparation, described by de Lange [33]. A mixture of acid and water is carefully added to a mixture of TEOS and ethanol under vigorous stirring followed by 3 h heating at 60 °C. After dip-coating, membranes were calcined for 3 h at 400 ^{o}C.

Unsupported material is prepared by evaporation the sol (or dipping solution) in a 10 cm diameter petri-dish at room temperature. Calcination of the resulting dry powder is performed under the same conditions as for supported material.

2.2 Experimental techniques for membrane characterisation

Separation properties, and hence applicability of porous membranes are directly determined by characteristics of the porous structure: pore size, shape, connectivity, particle packing, surface area etc. Proper characterisation of porous structures is crucial for the scientific development and industrial application of inorganic membranes. Characterisation of supported membranes is generally more demanding than characterisation of most of the other porous materials because the separation layer is thin, with often anisotropic and microporous structure. Therefore, specialised characterisation techniques are required. Characterisation techniques for porous materials are generally mentioned as static or dynamic methods, according to the nature of obtained parameters: morphology related parameters, and permeation related parameters (concerning active pores only), respectively. Although the literature describes a large number of available characterisation techniques, they often have limitations that make characterisation process difficult and somewhat uncertain [34]. Problems are especially pronounced in description of microporous structures. Further, problems are related to the absence of standard characterisation methods, i.e. absence of experimental and data analysis protocols, as well as standards for experimental conditions. The IUPAC has addressed this problem recently in the project: "Standardisation of methods for the characterisation of inorganic membranes" [35].

In this section, basis of some characterisation techniques used in the present research are described. Their theoretical background and applicability for the determination of a certain characteristic of a porous structure are explained.

2.2.1 Imaging techniques in material characterisation

Stereology is a term that is usually used to describe the visual examination techniques of the surface and cross-section morphology of materials by means of optical or electron microscopes. These techniques mostly provide information about particle size and shape, surface roughness, layer continuity and thickness and they are considered as standard techniques in materials characterisation. The most often used are Scanning Electron Microscopy (SEM) [36], Transition Electron Microscopy (TEM) [36] and Atomic Force Microscopy (AFM) [37]. The main common drawback of scanning and transition electron microscopy (SEM and TEM) is that sample preparation is required, which can influence the real porous structure. On the other hand, the interpretation of results from the AFM

technique is subjective to some extent and can therefore be difficult, especially in the case of the microporous materials.

In this study, supported membranes were examined by high resolution scanning electron microscopy (LEO Gemini 1550 FEG - SEM, UK), transition electron microscopy (Philips M30 Twin/STEM, The Netherlands) [38] and an AFM Nanoscope IIIa set-up (Digital instruments, USA) [39].

2.2.2 Porosity and pore size measurements

Gas adsorption/desorption isotherms (physisorption); This technique is one of the most widely used in characterisation of porous materials for the determination of pore volume, specific surface area and pore size distribution of materials with spherical, cylindrical or slit-shaped pores. However, real solid/gas interfaces are complex and different mechanisms may contribute simultaneously to physisorption. Consequently, the interpretation of physisorption data may not be strictly straightforward [40].

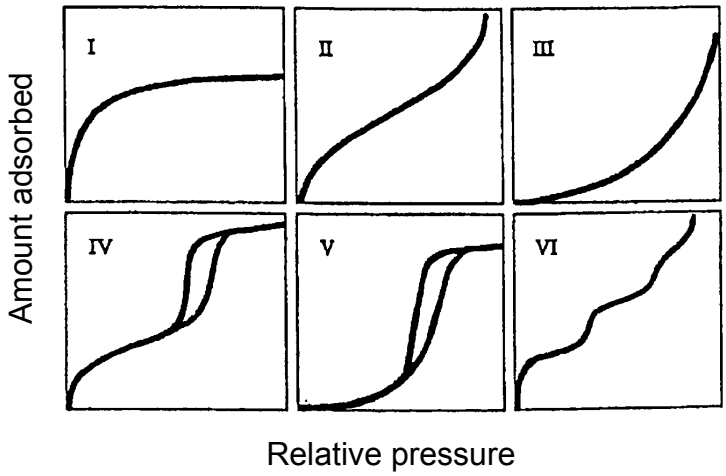

Figure 2.3: Six types of physisorption isotherms [40].

The adsorption and desorption isotherms of a non-reactive gas (typically N_2 at 77 K) on an outgassed sample are determined as a function of the relative pressure (i.e. the ratio between the applied pressure and the saturation pressure of the gas). The adsorption isotherm is determined by measuring the quantity of gas adsorbed at a series of relative pressures (i.e. the ratio of applied pressure and saturation pressure). The adsorption isotherm starts at low relative pressure. At a certain minimum pressure, the smallest pores will be filled with liquid nitrogen. As the pressure is increased further, larger pores are filled, and near the saturation pressure, all pores are filled. The total pore volume is

determined by the quantity of gas adsorbed near the saturation pressure. Desorption occurs when the pressure is decreased from the saturation pressure downward. The majority of physisorption isotherms can be grouped into the six types [40] that are shown in Figure 2.3. The type I isotherm is typical for microporous solids and chemisorption isotherms. Type II is observed on finely divided non-porous solids. Type III and type V are typical for vapour adsorption (e.g. water vapour on hydrophobic materials). Type IV and V feature a hysteresis loop; desorption on mesopores occurs at lower pressures than those at which adsorption in similar-sized pores would take place. Finally, the rare type VI step-like isotherm is seen on special types of carbons.

A number of calculation models can be applied to different regions of the adsorption isotherms to evaluate the specific surface area (e.g. BET method, Dubinin method, Langmuir adsorption isotherm, etc.), or the micro- and mesopore volume and pore size distributions (e.g. BJH method, Horvath and Kawazoe method, Saito- Foley method, etc.) [41-43]. The microporous volume is usually determined by the t-plot method of de Boer, the nonane preadsorption technique and the Dubinin-Radushkevich equation [41-43]. The most widely used method for pore size estimation is the Horvath and Kawazoe method for slit shaped pores [42] and cylindrical pores [43]. It calculates the average potential function inside the micropores, relating the average fluid-fluid and solid-fluid interaction energy of an adsorbed molecule to its free energy change upon adsorption. Mesopore size calculations are usually based on the Kelvin equation [40].

The sorption measurements described in this thesis were carried out at 77 K using N_2 as the condensable gas using an adsorption porosimeter (ASAP 2400 Micromeritics, USA).

Permporometry; This is a useful and commonly used method for the characterisation of the active pores of ultrafiltration membranes. With this technique, pores in the range of 3 to 100 nm can be determined. The method was first developed by Eyraud *et al.* [44] as gas-liquid permporometry and later improved into the gas-vapour permporometry method [45,46]. A schematic drawing of the measurement principle is given in Figure 2.4.

Permporometry is based on the controlled blocking of pores by capillary condensation and the simultaneous measurement of a gas diffusion flux through the remaining open pores. When a condensable vapour (e.g. cyclohexane) is introduced at low vapour pressure, first a molecular adsorption layer (the so-called “t-layer”) is formed on the inner surface of the pores. When the relative vapour pressure P/P_0 of the condensable gas is increased further from zero to unity, pores with increasingly large radius become blocked due to capillary

condensation. The simultaneous non-condensable gas (e.g. oxygen) flux through the remaining open pores provides a measure for the fraction of pores with pore size larger than the pores that are already blocked. Upon desorption the same processes occur in reverse order. The pore size distribution is usually determined upon desorption (lowering P/P_0).

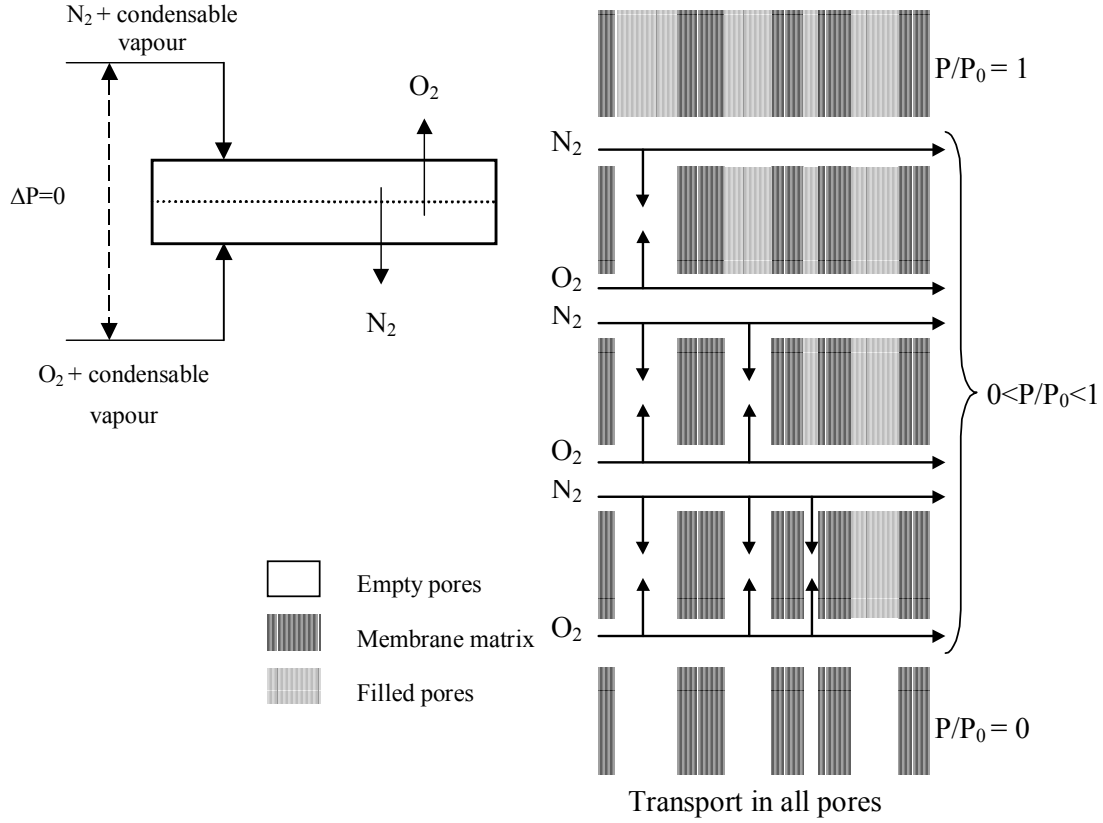

Figure 2.4: Schematical drawing of the permporometry principle.

The relationship between relative vapour pressure and the capillary condensation of pores with Kelvin radius r_K upon desorption is given by the following equation:

$$\ln(P/P_0) = -\frac{2\gamma_s V_m}{r_K RT}, \tag{2.4}$$

where γ_s and V_m are the surface tension and molar volume of the condensable vapour, respectively, R is the gas constant and T the temperature.

The relationship between the real pore width (d_p) and the Kelvin radius (r_K) is given as:

$$d_p = 2(r_K + t), \tag{2.5}$$

where t is the thickness of the "t-layer" formed on the inner surface of the pores, which is usually 0.3-0.5 nm.

The number of pores (n) can be obtained from the gas flow [47]:

$$J_i = \frac{2\pi n r^3 \Delta p_i}{3 A_m R T \tau l} \sqrt{\frac{8RT}{\pi M_W}} \tag{2.6}$$

where J is the gas flux through the membrane, Δp_i - gas partial pressure difference across the membrane, A_m – geometrical membrane area, τ - tortuosity, l - membrane thickness, and M_w - gas molecular weight.

2.2.3 Small angle X-ray scattering (SAXS)

SAXS is a well-established scattering technique that operates at small angles in the vicinity of the primary beam and extending to less than 2 degrees for standard wavelengths. The scattering features at these angles correspond to structures ranging from tens to thousands of angstroms. It has proven to be a useful tool to monitor the sol-gel process, especially because of the property of polymeric species in the sol to be fractal objects [33,48].

Polymeric systems grown by a random process are fractal-like objects and can be represented by a mass fractal dimension (D_f) that relates mass (M) and size (R) via $M \propto R^{D_f}$. D_f has a limiting value of three, where the object is Euclidian. As the fractal dimension decreases the structure will look sparser, giving essentially a linear configuration when D_f=1. In the case of polymeric sols, the fractal dimension of the species can be correlated with their ability to inter-penetrate and form a microporous structure.

The tendency of fractal system to interpenetrate, which is inversely related to the mean number of intersections $M_{1,2}$ of two mass fractal objects of size R and mass fractal dimension D_f is defined as:

$$M_{1,2} \propto R^{(D_{f1}+D_{f2}-3)} \tag{2.7}$$

If $D_{f1}=D_{f2}+D_f$, it can be seen from the equation that polymeric structures can interpenetrate very well when their fractal dimension is D_f<1.5 [48]. When the fractal dimension is higher than 1.5, i.e, highly branched polymers are present, the fractal objects become dense, and their ability to interpenetrate decreases.

Small angle scattering experiment yield a scattering intensity (I) as function of the modulus of the scattering vector Q (nm^{-1}), which is defined as:

$$Q = \frac{2\pi}{\lambda}\sin(2\Theta) \tag{2.8}$$

where λ is the wave length (nm) of radiation used and *2*Θ is the scattering angle.

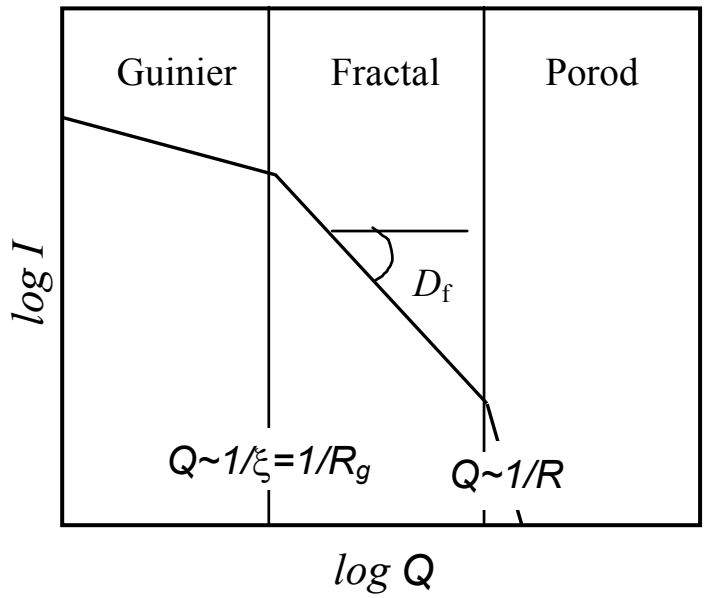

Figure 2.5: Typical small-angle scattering curve.

In a typical scattering curve (*log I – log Q*), as shown in Figure 2.5, three regions can be identified. The Guinier region, above the upper cut-off size, the Porod region below the lower cut-off size, and the intermediate fractal region. The cut-off *Q* values from fractal to Guinier region and from fractal to Porod region yield approximate values for *1/*ξ and *1/*R_o. The upper cut-off length ξ is correlated with the radius of gyration (*Rg*) of the sol particles, and *Ro* is correlated to the size of the primary building blocks. From the slope of the curve in the fractal region, where the intensity follows a power law, the dimension D_f can be calculated.

Interpreting SAXS data can be a very difficult task unless the sample fits one of the many idealised models that have been developed over the years [33,48]. Data analysis in the present study was carried out using the Texeira function, as shown by Eq. (2.9) [49]. It was chosen because it yields results that are not very sensitive to the angular interval over which the fitting is carried out.

$$I(Q) = 1 + \frac{D_f \Gamma(D_f - 1)}{(QR_o)^{D_f}\,(1 + 1/Q^2\xi^2)^{(D_f-1)/2}}\sin((D_f - 1)\tan^{-1}(Q\xi)) \tag{2.9}$$

I(Q) - scattering intensity as a function of scattering vector Q

Γ - gamma function (Γ(n+1)=n!)

ξ - cut-off distance of the order of the radius of inertia R_g

R_o - radius of the individual scatter.

Small angle x-ray scattering experiments were performed with an X-ray difractometer with Cu Kα radiation (PW 3011/20, Philips, The Netherlands), by PanAlytical, Almelo, The Netherlands.

2.2.4 X-ray reflectivity

X-ray reflectivity is a non-destructive technique used for estimation of layer thickness, density and surface (or interface) roughness. It is based on the total external reflection of x-rays and measurement of scattering from a series of layers (not atomic planes) that have a contrast of density and scattering power [50,51]. An advantage of the method is that it is insensitive to the layer crystallinity and it may therefore be applied to amorphous, polycrystalline or monocrystalline layers. A schematic representation of the reflectivity technique is given in Figure 2.6, and a typical reflectivity curve that explains the basic information that is contained within the curve is shown in Figure 2.7.

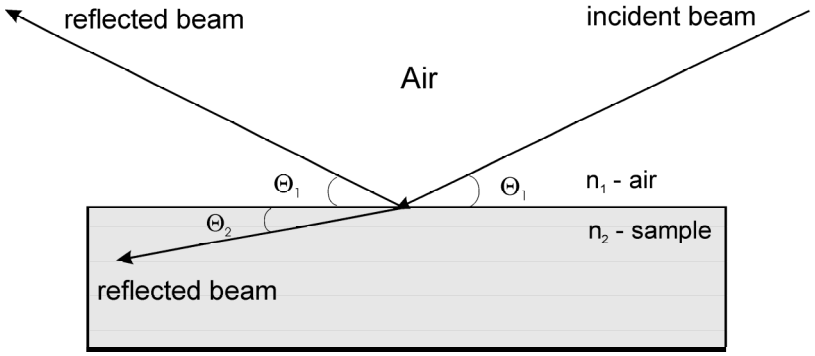

Figure 2.6: Schematic representation of reflectivity technique.

The density is estimated from the critical angle of incidence in the following way. For X-rays the refractive index *n* of any medium is defined as:

$$n=1-\delta-i\beta, \qquad (2.10)$$

where δ is a term that specifies the dispersion of the x-ray beam, and the imaginary part β indicates the absorption of x-rays.

$$\delta = \frac{\rho_e r_e \lambda^2}{2\Pi} \tag{2.11}$$

$$\beta = \frac{\mu\lambda}{4\Pi} \tag{2.12}$$

Here ρ_e is the electron density, λ the wavelength of the x-rays, μ the linear adsorption coefficient, and r_e the classical electron radius ($=e^2/mc^2$).

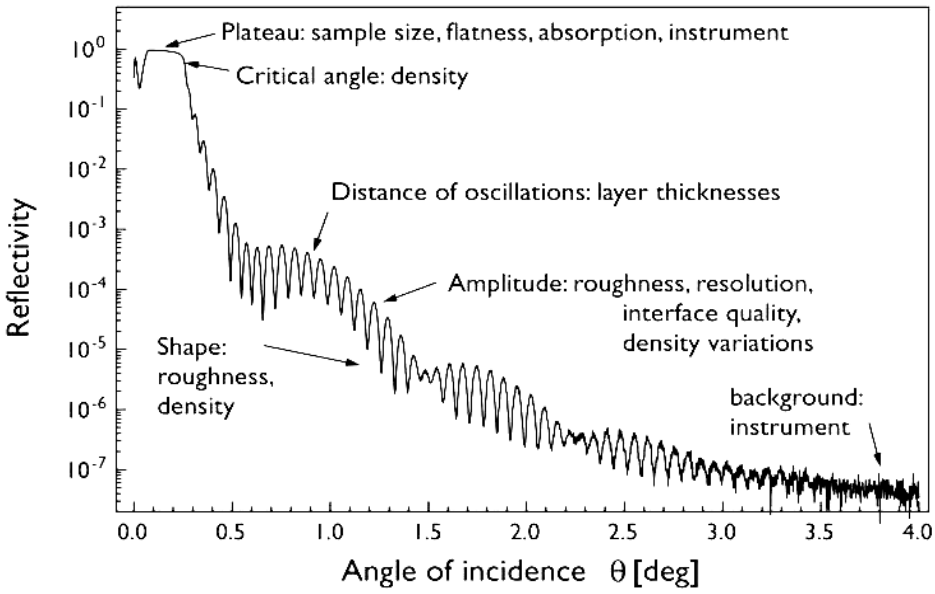

Figure 2.7: Typical reflectivity curve.

According to Snell's law:

$$n_1 cos\,\Theta_1 = n_2 cos\Theta_2 \tag{2.13}$$

n_1-index of refraction of air (~1)

n_2-index of refraction in solid (<1)

An X-ray beam that strikes a solid surface at a small angle (0-2°) is completely reflected. Above the critical angle of total reflectance θ_c the beam penetrates the sample, whereby the angle of refraction θ_2 is smaller than the angle of incidence θ_1 (the refractive index of X-rays in solids is smaller than in air). Bellow a certain critical angle total reflection occurs (Θ_2=0), so that:

$$cos\Theta_c = n_2 = 1 - \delta_2 \tag{2.14}$$

and

$$\Theta_c = \sqrt{2\delta_2}\,. \tag{2.15}$$

In practice, the mean mass density ρ_m that is of interest is related to δ_2 by the equation:

$$\rho_m = \frac{\delta_2 A}{N_A Z}, \tag{2.16}$$

where Z is the atomic number, A is the mass number, and N_A is the Avogadro constant.

Applying the same theory to thin layers (angle of refraction θ_2 corresponds to the refraction from the interface of the layer and support), the following equation can be derived:

$$\Theta_1 = \frac{\lambda^2}{4t^2} n^2 + 2\delta_2 \qquad (y=ax+b), \tag{2.17}$$

where λ is wave length and t layer thickness. The layer thickness can be calculated from the parameters of $\theta_1 - n$.

The reflectivity can be calculated using the Fresnell equations [51]. In the simple case of one substrate + one layer, it can be written as:

$$R = \left| \frac{R_1 + R_2 e^{\frac{4\pi i \Theta_2 t_2}{\lambda}}}{1 + R_1 R_2 e^{\frac{4\pi i \Theta_2 t_2}{\lambda}}} \right| \tag{2.18}$$

where R_1 and R_2 are the Fresnell reflectivity coefficients of the free surface and the substrate interface, respectively.

Finally, the surface roughness (σ) is derived from the amplitude of oscillations or:

$$R = \frac{\Theta_1 - \Theta_2}{\Theta_1 + \Theta_2} e^{\frac{-4\pi^2 \Theta_1 \Theta_2 \sigma^2}{\lambda^2}}. \tag{2.19}$$

Reflectivity measurements were performed [52] on a high-resolution 4-circle diffractometer (Philips, The Netherlands). Data processing was carried out using Philips software X'Pert Reflectivity.

2.2.5 Positron annihilation analysis

Detailed information about the porous structure of a material can obtained from positron annihilation studies. This technique is based on a positron “interaction” with a porous structure [53]. The positron is the antiparticle of the electron, it has the same mass and

spin, but opposite charge and magnetic momentum. A schematic representation of the positron-electron annihilation process is given in Figure 2.8. In matter positrons annihilate with electrons via the emission of 2γ-quanta [54]. In the centre of mass the total momentum of an electron-positron pair is zero and therefore, due to momentum and energy conservation laws, the resulting photons are emitted in opposite directions, each of them with energy of 511 keV. In the laboratory frame, however, the electron-positron pair has a non-zero momentum, mainly because the electron is thermalised before annihilation takes place. Therefore, there is a shift (ΔE) in the energy of the two photons and they are emitted with small deviations (Θ and φ) from collinearity, as represented in Figure 2.8.

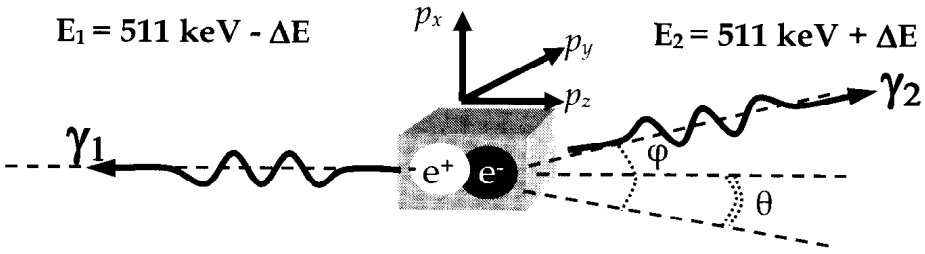

Figure 2.8: Schematic representation of the positron-electron annihilation process.

Apart from the annihilation process, the positron can capture an electron and form a bound state called positronium (Ps) in some low-density materials. Positronium can be considered as a very light tracer "atom" with the physical size of a hydrogen atom wandering around in the porous structure. Their behaviour in a porous material can be described as hot particles with 1 eV initial kinetic energy, which lose their energy by frequent collisions with the atoms of the pore walls. For low-*k* coatings five annihilation states can be distinguished: *para*-positronium (*p*-Ps), *o*-Ps annihilation via the pore wall, *o*-Ps self-annihilation, positron annihilation inside the walls separating the pores, and the fraction of Ps that escapes from the film. The ground state of positronium consists of a singlet state called *para*-positronium (p-Ps), with the spins of electron and positron oriented antiparallelly, and a triplet state called *ortho*- positronium (o-Ps) with parallel spins.

Several analysis techniques are used to obtain information about material structure: Doppler broadening of annihilation radiation (DBAR), tow-dimensional angular correlation of annihilation radiation (2D-ACAR) and positron annihilation lifetime [54]. Measurements of Doppler broadening effects are generally characterised by the S (shape) parameter, which is defined as the ratio between the central part of the annihilation spectra and the total spectra. This parameter reflects the positron annihilation with valence

electrons (low momentum). In general, a high value of S indicates positron annihilation in open volume defects. A second useful parameter for the analysis of Doppler broadening is the W (wing) parameter, which reflects the positron annihilation with high momentum electrons (core electrons). This parameter is related to the chemical environment where annihilation takes place. In the study of interfaces, both parameters can be combined in S-W maps, with a third variable (i.e. implementation energy, temperature, strain etc) as running parameter.

An important experimental parameter (*f*-Ps), obtained from so-called positronium fraction measurements, represents the fraction of implanted positrons that is related to *ortho*-positronium self-annihilation via 3-γ events. This parameter is generally related to pores with sizes >1 nm, combined with percolation inside the samples. The *f*-Ps technique determines the type of porosity (open or closed in terms of positronium escape) in thin film materials and it is defined such that for highly porous material with large pores *f*-Ps=100%. All experiments were performed with the positron beams at the Delft Positron Center [54]. The analysis of data was done with the aid of the VEPFIT program [55]. This program provides an algorithm that simulates the implementation and solves the diffusion equation, taking into account the trapping and annihilation of positrons in the material.

References

1. C.J. Brinker, G.W. Scherer, "Sol-gel science: The physics and chemistry of sol-gel processing", Academic press, INC, 1990.
2. J J. Livage, M. Henry, C. Sanchez, "Sol-gel chemistry of transition metal oxides", Prog. Solid State Chem. 18 (1988) 259-341.
3. J. Blanchard, S. Barboux-Doeuff, J. Maquet, C. Sanchez, "Investigation on hydrolysis-condensation reaction of titanium (IV) butoxide", New J. Chem. 19 (1995) 929-936.
4. D.C. Bradley, R.C. Mehrota, D.P. Gaur, "Metal Alkoxides", Academic Press, London, 1978.
5. I. Manzini, G. Antonioli, D. Bersani, P.P. Lottici, G. Gnappi, A. Montenero, "X-ray absorption spectroscopy study of crystallization processes in sol-gel-derived TiO_2", J. Non-Cryst. Solids, 192–193 (1995) 519-523.
6. J. Livage, M. Henry, J.P. Jolivet, C. Sanchez, "Chemical synthesis of fine powders", MRS Bull. (1990) 18-25.
7. S. Barboux-Doeuff, C. Sanchez, "Synthesis and characterisation of titanium oxide-based gels synthesised from acetate modified titanium butoxide precursors", Mat. Res. Bull. 29 (1993) 1-14.
8. A. Bleuzen, S. Barboux-Doeuff, P. Flaud, C. Sanchez, "Rheological study of titanium oxide-based gels", Mat. Res. Bull. 29 (1994) 1223-1232.
9. S. Benfer, U. Popp, H. Richter, C. Siewert, G. Tomandl, "Development and characterization of ceramic nanofiltration membranes", Sep. Purif. Tech. 22-23 (2001) 231-238.
10. M. Kallala, C. Sanchez, B. Cabane, "SAXS study of gelation and precipitation in titanium-based systems", J. Non-Cryst. Solids, 147-148 (1992) 189-196.
11. C. Sanchez, J. Livage, M. Henry, F. Babonneau, "Chemical modification of alkoxide precursors", J. Non-Cryst. Solids, 100 (1988) 65-71.
12. M. Nabavi, S. Doeuff, C. Sanchez, J. Livage, "Chemical modification of metal alkoxides by solvents: A way to control sol-gel chemistry", J. Non-Cryst. Solids, 121 (1990) 31-34.
13. M.T. Harris, C.H. Byers, "Effect of solvent on the homogeneous precipitation of titania by titanium ethoxide hydrolysis", J. Non-Crystal. Solids, 103,1 (1988) 49-64.
14. K.D. Keefer, D.W. Schaefer, "Growth of Fractally Rough Colloids", Phy. Rev. Letter, 56 (1986), 2376-2379.
15. T.A. Witten, L.M. Sander, "Diffusion limited aggregation, a kinetic critical phenomenon", Phy. Rev. Lett. 47, 19 (1981) 1400-1403.
16. P. Meakin, "Formation of Fractal Clusters and Networks by Irreversible Diffusion-Limited Aggregation", Phys. Rev. Letters, 51 (1983) 1119-1122.
17. R. Jullien, "A new model of cluster aggregation", J. Phys. (A), 19 (1986), 2129-2136.
18. M. Kallala, R. Jullien, B. Cabane, "Crossover from gelation to precipitation", J. Phys. (II) France, 2, (1992) 7-25.
19. Y. Gu, G. Meng, "A model for ceramic membrane formation by dip-coating", J. Europ. Ceram. Soc. 19 (1999) 1961–1966.

20. F.M. Tiller, C.D. Tsai, “Theory of filtration of ceramics: I. Slip casting”, J. Am. Ceram. Soc. 69 (1986), 882–887.
21. J.D. Le Roux, D.R. Paul, “Preparation of composite membranes by a spin coating process”, J. Membr. Sci. 74, 3 (1992) 233-252.
22. C.J. Brinker, A.J. Hurd, P.R. Schunk, G.C. Frye, C.S. Ashley, “Review of sol-gel thin film formation”, J. Non-Cryst. Solids, 147-148, (1992) 424-436.
23. C.K. Lambert, R.D. Gonzalez, “Effect of binder addition on the properties of unsupported -Al_2O_3 membranes”, Mater. Letters, 38, 2 (1999) 145-149.
24. M. Guglielmi, S. Zenezini, “The thickness of sol-gel silica coatings obtained by dipping”, J. Non-Cryst. Solids, 121, 1-3 (1990) 303-309.
25. Q. Chang, R. Peng, X. Liu, D. Peng, G. Meng, “A modified rate expression of wet membrane formation from ceramic particles suspension on porous substrate”, J. Membr. Sci. 233, 1-2 (2004) 51-55.
26. K.-N.P. Kumar, “Nanostructured ceramic membranes”, PhD Thesis, University of Twente, 1993, pp 96-99.
27. R.M. German, “Sintering theory and practice”, New York, Wiley, 1996.
28. G.W. Scherer, “Sintering of sol-gel films”, J.Sol-Gel. Sci. Tech. 8 (1997) 353-363.
29. I.A. Aksay, C.H. Schilling, “Molecular and colloidal engineering of ceramics”, Ceramics International, 17, 5 (1991) 267-274.
30. J.H. Green, G.D. Parfitt, “Stability of non-aqueous dispersions. Paper 7. Electrostatic stabilization of concentrated colloidal dispersions”, Colloids and Surfaces, 29, 4 (1988) 391-402.
31. F.F. Lange, “Powder processing science and technology for increased reliability”, J. Am. Ceram. Soc. 72,1 (1989) 3-15.
32. J. van Vuren, B.C. Bonekamp, K. Keizer, R.J.R. Uhlhorn, H.J. Veringa, A.J. Burggraaf, “Formation of ceramic alumina membranes for gas separation”; pp. 2235-45 in: High Tech Ceramics. Edited by P. Vincenzini. Elsevier Science Publ. B.V., Amsterdam, Oxford, New York, Tokyo, 1987.
33. R.S.A. de Lange, “Microporous sol-gel derived ceramic membranes for gas separation”, PhD thesis, Unversity of Twente, 1993.
34. A.J. Burggraaf, L. Cot, “Fundamentals of inorganic membrane science and technology”, Elsevier, Amsterdam, 1996.
35. http://www.iupac.org/projects/2000/2000-002-2-100.html
36. S.L. Flegler, J.W. Heckman, “Scanning and transmission electron microscopy: an introduction”, Oxford University Press, Oxford, 1994.
37. C.F. Quate, “The AFM as a tool for surface imaging”, Surface Science, 299 (1994) 980-995.
38. http://www.mesaplus.utwente.nl/
39. http://mtp.ct.utwente.nl/
40. K.S.W. Sing, D.H. Everett, R.A.W. Haul, L. Moscou, R.A. Poerotto, J. Rouquerol, T. Siemieniewska, “Reporting physisorption data for gas/solid system with special reference to the determination of surface area and porosity”, Pure Appl. Chem. 57 (1985) 603-19.

41. R.G. Avery, J.D.F. Ramsay, "The sorption of nitrogen in porous compacts of silica and zirconia powders", J. Colloid. Interface Sci. 42 (1973) 597-609.
42. G. Horvath, K. Kawazoe, "Method for the calculation off effective pore size distribution in molecular sieve carbon", J. Chem. Eng. Jpn. 16 (1983) 470-478.
43. A. Saito, H.C. Foley, "Curvature and parametric sensitivity in modelsin models for adsorption in microporous, AIChE J 37,3 (1991) 429-435.
44. C. Eyraud, M. Betemps, J.F. Quinson, F. Chatelut, M. Brun, B. Rasneur, "Détermination de la répartition des rayons de pores d'un ultrafiltre par "permporométrie gaz-liquide" comparaison entre porométrie d'écoulement et porométrie d'équilibre de condensat", Bull. Soc. Chim. France, 9-10 (1984) 237.
45. F.P. Cuperus, "Characterization of ultrafiltration membranes", Ph.D. Thesis, University of Twente (1990).
46. G.Z. Cao, J. Meijerin, H.W. Brinkman, A.J. Burggraaf, "Permporometry study on pore size distribution af active pores in porous ceramic membranes", J. Membr. Sci. 83 (1993) 221-235.
47. A.W. Adamson, "Physical chemistry of surfaces", Whiley, New York, 5th edition, 1990.
48. B.N. Nair, "Structure-property relations in silica sols, gels and molecular-sieving membranes" PhD Thesis, University of Tokyo, Japan, 1998.
49. J. Teixeira, "Small-angle scattering by fractal systems", J. Appl. Cryst. 21 (1988) 781-786.
50. V. Kogan, K. Bethke, R. de Vries, "Appling X-rays in material analysis", Nuclear Instruments and Methods in Physics Research (A), 509 (2003), 290-293.
51. S. Kundu, "Interface modification of Ag/Co system: X-ray reflectivity study", Nuclear Instruments and Methods in Physics Research, Section B: Beam Interactions with Materials and Atoms, 212 (2003) 489.
52. www.dannalab.com
53. I. Proszhak, Materials Structure, 8,2 (2001) 55-59.
54. A. van Veen, R. Escobar Galindo, H. Schut, S. W. H. Eijt, C. V. Falub, A. R. Balkenende, F. K. de Theije, "Positron beam analysis of structurally ordered porosity in mesoporous silica thin films", Mater. Sci. Eng. (B), 102, 1-3 (2003) 2-8.
55. A. van Veen, H. Schut, M. Clement, J. M. M. de Nijs, A. Kruseman, M. R. Ijpma, "VEPFIT applied to depth profiling problems", Applied Surface Science, 85 (1995) 216-224.

3

Mesoporous TiO_2 membranes and influence of ZrO_2 addition on microstructure and liquid permeability

Abstract

A procedure for the synthesis of crystalline, mesoporous TiO_2 membranes by the colloidal sol–gel technique is established. The influence of several processing variables on particle size and sol stability was investigated. It was found that ultrasonic after-treatment plays a crucial role in breaking weak agglomerates and obtaining stable sols with an average particle size of 15-18 nm. Crack-free layers with an average pore size of 7 nm can be obtained with a reproducibility of around 50%. The influence of binders and calcination conditions on cracking and membrane mechanical stability was studied. Phase transformation of the anatase to rutile crystallographic phase, as well as considerably large stresses that develop during calcination were identified as the main causes of layer instability. The influence of up to 30 mol% zirconia doping on microstructure, liquid permeability, thermal and chemical stability of mesoporous composite titania/zirconia membranes was investigated. It was demonstrated that zirconia retards the phase transformation of anatase until at least 700 ^{o}C. Moreover, the mechanical strength of the titania membranes is significantly improved by addition of zirconia. Consequently, crack-free layers calcined at 450-700 ^{o}C can be formed with reproducibility of nearly 100%. The pore size decreases gradually to 3.6 nm by addition of up to 20 mol% zirconia, while nitrogen sorption experiments shows that the porosity, BET surface area and pore connectivity increases. Chemical stability tests showed that undoped titania and composite titania/zirconia materials were stable in the pH range 1-13 at room temperature. The permeability of titania and titania/zirconia composite membranes is 8 times larger than that of γ-alumina and it is not affected by the level of zirconia doping or by the nature of the permeating liquid.

3.1 Introduction

Ceramic membranes are gaining more and more importance in separation technology, especially in combination with catalytic processes. Commonly mentioned positive characteristics are their high permeability and chemical and thermal resistance [1,2]. In recent years titania membranes have received significant attention mainly because of their superior chemical resistance, compared to other membrane materials including γ-alumina and silica. Beside membrane applications, thin porous or dense titania layers can be used as antireflectance coating for solar cells [3,4], photocatalyst for organic pollutant treatment of industrial air and water [5], in nanocell photovoltaic systems [6], etc. They also attract attention of researchers in biomaterials science: an anatase surface layer promotes the bioactivity of titanium and its alloys significantly, which is of practical importance for them to be used as orthopaedic and dental implants [7].

The current limitation to practical application of titania-based membranes appears to be the limited success that was met in producing crack-free layers by the sol-gel technique, due to the fact that a partial kinetic anatase-to-rutile phase transformation occurs in titania upon calcination of the layer at temperatures of ~350 °C or higher [8,9]. The phase transformation takes place by coalescence of small anatase particles into larger rutile grains, and is accompanied by considerable grain and pore growth. However, a minimum calcination temperature of 450 °C is required to obtain well-defined, mechanically stable layers. As was suggested by Kumar, there are two basic approaches to avoid phase transformation [8]: (a) direct synthesis of rutile-phase titania, or (b) retarding phase transformation (and accompanying grain growth) to a temperature above the normal calcination temperature. Although the first approach can be a fast and effective way towards crack-free layer formation, the minimum grain size of the rutile phase is ~50 nm, which leads to the formation of a mesoporous membrane with ~20 nm pore size [10]. On the other hand, the anatase grain size, and consequently, pore size can be much smaller, which is preferred for many applications.

With respect to the second strategy mentioned above, it was observed that the presence of alumina as an inert second phase in a titania membrane increases the phase transformation temperature from 350 ^{o}C for unsupported mesoporous anatase to 700 ^{o}C for the anatase phase of an unsupported titania-alumina composite membrane [8]. It has been suggested that the presence of alumina decreases the sub-coordination number of the anatase particles

in the nano-composite matrix [8,11]. The sub-coordination number is defined as the number of neighbouring particles belonging to the same phase and having actual contact with the particle under consideration. A lower sub-coordination number leads to a situation in which anatase particles have a lower number of contact points, which decreases the probability of their coalescence into a larger rutile particle.

However, numerous examples show that although some dopants retard the phase transformation of anatase, others promote it. It has therefore been suggested that dopant valence may also have an effect on the transformation behaviour of titania. Yang and Fereire [12] studied the mechanism of acceleration and inhibition of the anatase-to-rutile transformation. They reported that additives such as WO_3 and P_2O_5 retard the phase transformation process, whereas others, such as CuO and Fe_2O_3, accelerate the process. These effects were explained by the change of oxygen vacancy concentration in the anatase structure due to the presence of substitutional or interstitial dopant ions in the crystal lattice. Additives with a lower metal ion valence than that of Ti^{4+} may increase the oxygen vacancy concentration, thereby acting as promoters for phase transformation. On the other hand, cations with a higher valence may reduce the oxygen vacancy concentration and act as inhibitors. The same authors also showed that addition of ZrO_2 had an inhibiting effect on the anatase-to-rutile phase transformation, even though no oxygen vacancy concentration change was expected in this case. The inhibiting effect of ZrO_2 was explained in terms of an increase of strain energy resulting from the substitution of Ti^{4+} ions with Zr^{4+}, which is believed to lower the driving force for phase transformation [13].

Okada *et al.* [14] proposed that the incorporation of foreign cations with valence larger than 4 may retard the transition by forming interstitial Ti^{3+} cations that suppress atomic transport in the anatase structure, while dopants with valence equal to 4 may affect the phase transformation by anatase lattice deformation, the extent of which is influenced by the difference in ionic radius between the foreign cation and Ti^{4+}. Provided that the ionic radius of a foreign cation is smaller than that of Ti^{4+}, it may be incorporated in the anatase structure, otherwise it can only coexist as a separate second phase. For example, the radius of Zr^{4+} is ~20% larger than the radius of Ti^{4+}, hence it is not expected to replace Ti^{4+}, while Si^{4+} with a radius that is considerably smaller than Ti^{4+} may become substitutionally incorporated in the anatase lattice. Using anatase lattice parameters and XPS data, Okada *et al.* [14] proposed a model for the state of Si in the anatase phase: Si^{4+} is thought to be incorporated in the TiO_2 xerogel and remains in the anatase structure after crystallisation,

but is gradually expelled at higher heating temperatures to form an amorphous surface SiO_2 layer that coats the anatase particle. Sanchez-Soto *et al.* proposed that amorphous zirconia might also coat the crystalline (anatase) particles [15]. Upon heating this composite the titania and zirconia phases may react and produce zirconium-titanate.

In conclusion, a large number of dopants has been identified that can inhibit the anatase-to-rutile phase transformation of titania [15-21]. However, to our knowledge a systematic quantitative comparison of efficiency between various dopants has not been performed. The most widely used and supposedly efficient dopants are alumina and silica. However, only a few authors mentioned one of the major disadvantages of these composite systems, which is the significant decrease of chemical stability in strongly alkaline or acidic media [19]. Van Gestel *et al*. [19] demonstrated that the alumina phase of a titania/alumina composite dissolved in harsh environments ($pH \leq 3$ or $pH \geq 11$), which led to a collapse of the pore structure. In this respect, zirconia has been found to be more suitable, as it has a beneficial influence on both thermal and chemical stability [19-21].

In this chapter a procedure for the synthesis of crystalline, mesoporous TiO_2 membranes by the colloidal sol–gel technique is established. The influence of binders and calcination conditions on cracking occurrence and membrane mechanical stability is also studied. Zirconia doping is utilised to stabilise the anatase phase of mesoporous titania membranes. The beneficial influence of doping on microstructure and membrane performance, as well as the applicability of zirconia-doped titania membranes in a wide interval of temperature and pH is indicated.

3.2 Experimental

3.2.1 Synthesis

Particulate titania sols were prepared from titanium alkoxides, as described in more detail by Kumar [8]. An alcoholic solution of titanium-isopropoxide or titanium tert-butoxide (obtained from Aldrich chemicals) was reacted with a solution of water ($[H_2O]/[Ti] \geq 20$). Isopropanol was used as solvent for Ti-isopropoxide, while tert-butanol or ethanol were used to dissolve Ti-tert-butoxide. High dilution ratios (<0.5 mol Ti/dm^3, and <1 mol H_2O/dm^3 alcohol) were desirable to keep the local concentration of water and pre-cursor low so that small particles can be obtained. After the hydrolysis reaction has been completed, the remaining white gelatinous slurry was filtered and washed with large

quantities of water to remove any alcohol still present. The washed filtrate was redispersed in water and electrostatically stabilised with a HNO_3 solution ($[H^+]/[Ti]=0.4$). The peptization process was carried out by refluxing at 80 ^oC for 16 h, after which a stable sol with weakly agglomerated particles was obtained. To break the agglomerates the sol was treated ultrasonically for 1 h.

Two-component sols were made using the so-called sol-solution method [21], in which an appropriate amount of zirconium-oxy-nitrate hydrate ($ZrO(NO_3)_2 \cdot xH_2O$, Fluka Chemika) solution was directly added to the titania sol.

Mesoporous titania and titania/zirconia layers were applied by dip-coating onto α-alumina supports (disc-shaped, diameter 39 mm, thickness 2 mm, mean pore radius 100 nm, porosity ~35% [22]). Combinations of hydroxy-propyl cellulose and polyvinyl-alcohol were used as binders. All membranes were dried for 3 h at 40 ^oC at a relative humidity of 60%, and subsequently calcined for 3 h at various temperatures. If necessary, the coating, drying and calcination steps were repeated to repair defects present in the first layer. Unsupported material was prepared by drying and subsequent calcination of mixed sols under the same conditions as used to make supported membranes.

3.2.2 Characterisation

The particle size distribution in the sol was measured by dynamic light scattering (ZetaSizer 3000HSa, Malvern, UK). The internal surface area, pore volume, and average pore size distribution of titania powders were obtained from nitrogen sorption isotherms using an adsorption porosimeter (Micromeretics, ASAP 2400). The Berret-Joyner-Halenda (BJH) method was used in the data processing. Assuming cylindrical pore geometry, the pore sizes were calculated from the Kelvin equation [23]. The crystal structures of the samples were identified by X-ray diffraction (XRD, Philips, SR5056, Panalytical, Almelo, the Netherlands). Supported membranes were examined by scanning electron microscopy (LEO Gemini 1550 FEG - SEM, UK) and atomic force microscopy (AFM, Nanoscope IIIa set-up, Digital instruments, US). X-ray Photoelectron Spectroscopy (XPS, PHI Quantera Scanning ESCA Microprobe, USA) with Ar^+ sputtering was carried out to identify the atomic concentrations of zirconia and titania by measuring the Zr 3*d* and Ti 3*d* spectra as a function of depth inside the layer.

The mean pore size (diameter) of the mesoporous membrane layers was measured using the permporometry technique [24]. These experiments were performed with a homemade

set-up using cyclohexane as condensable gas and oxygen as non-condensable gas. Permporometry is based on the controlled blocking of pores by capillary condensation and the simultaneous measurement of a gas diffusion flux through the remaining open pores. When a condensable gas (cyclohexane) is introduced at low vapour pressure, first a molecular adsorption layer (the so-called "t-layer") is formed on the inner surface of the pores. When the relative vapour pressure P/P_0 of the condensable gas is increased further from zero to unity, pores with increasingly large diameter become blocked due to capillary condensation. The simultaneous gas flux through the remaining open pores provides a measure for the fraction of pores with pore size larger than the pores that are already blocked. Upon desorption the same processes occur in reverse order. The relationship between relative vapour pressure and the capillary condensation of pores with Kelvin radius r_K upon desorption is given by Eq. (3.1):

$$\ln(P/P_0) = -\frac{2\gamma_s V_m}{r_K RT}, \tag{3.1}$$

where γ_s and V_m are the surface tension and molar volume of the condensable gas, respectively, R is the gas constant and T the temperature.

The relationship between the real pore diameter (d_p) and the Kelvin radius (r_K) is given by Eq. (3.2):

$$d_p = 2(r_K + t), \tag{3.2}$$

where t is the thickness of the "t-layer" formed on the inner surface of the pores, which is usually 0.1-0.5 nm. A more detailed description of the permporometry principle and set-up can be found in the articles of Cuperus *et al.* [24] and Cao *et al.* [25].

The chemical stability of the material was determined at room temperature by static solubility tests [19] in water at pH values of 1-13 using calcined unsupported material. In all cases 1 g of powder was immersed in 50 ml of water solution. The pH of the solutions was adjusted with nitric acid or ammonium hydroxide and the total weight loss of the powder after 120 h immersion was calculated by measuring the concentration of dissolved titania in the solution using atomic absorption spectroscopy (AAS, Thermo-Optec BV SOLAAR system 939). The material was regarded as stable when the amount of dissolved titania in the solution was lower than or close to the AAS detection limit of 0.1 mg/l for titanium.

The water permeability of the membranes was measured in a pressurized dead-end filtration cell with fully desalinated, pre-filtered water and hexane as permeation liquids to compare the permeabilities of hydrophilic and hydrophobic solvents [25-26]. The applied pressure was in the range of 0-12 bar.

3.3 Results and discussion

3.3.1 Titania and zirconia-doped titania membrane synthesis

All process parameters were adjusted to obtain stable sols with minimal particle sizes. The alkoxide to water molar ratio was kept at 1:20. Particulate sols are expected to be formed when $[H_2O]/[Ti]$ ratios above the stoichiometrically required value for full hydrolysis of the alkoxides (4 in this case) are used [28]. The optimal $[H^+]/[Ti]$ peptization ratio was found to be 0.4, since this resulted in sols that were stable for several months. The use of titanium-iso propoxide and titanium-tert-butoxide as precursors did not result in a significant decrease of the average particle size in the sol (Figure 3.1), although Ti-tert-butoxide gave a much broader distribution. For both precursors, higher dilution ratios resulted in smaller particles and a sharper size distribution. Based on these results, titanium-isopropoxide dissolved in iso-propanol (<0.4 mol Ti/dm^3) was used as a precursor in all further experiments.

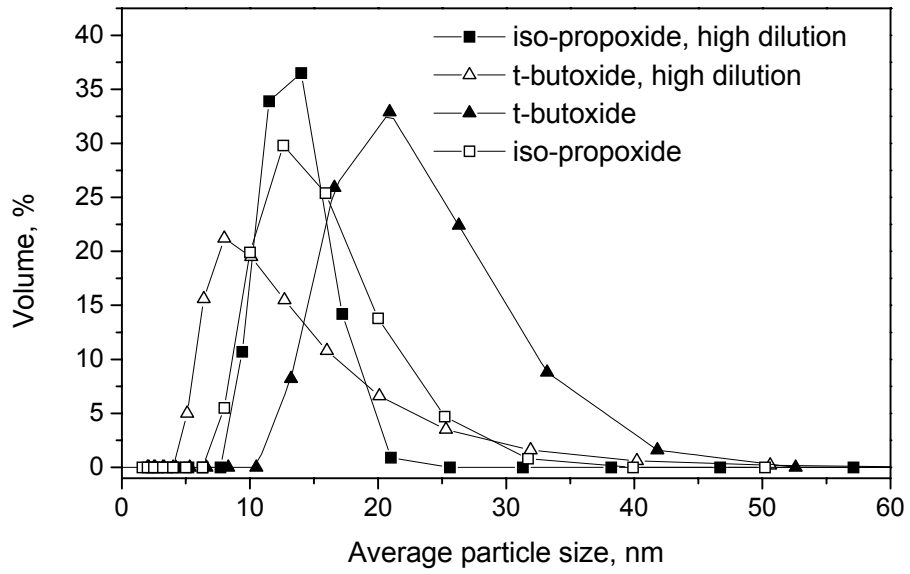

Figure 3.1: Particle size distribution in the sol, measured after ultrasonic treatment, depending on the precursor used and ratio of dilution.

Variation of process parameters (type of precursor, dilution ratio, water and acid concentrations) caused significant differences in agglomerate size after sol peptisation. Typically the agglomerate sizes were in the range of 60 nm to 1 μm. However, the primary particle sizes measured by dynamic light scattering after ultrasonic treatment were always in the range of 15–18 nm. It appears that this is a minimum particle size that can be obtained by this method. Similar results were previously reported by Lijzenga *et al.* [29].

A temperature of 450 ^{o}C is suggested as the most suitable for titania membrane calcination. At this temperature, no grain growth or visible "neck" formation between grains that would indicate the occurrence of a sintering process is observed, as can be seen on the AFM picture shown in Figure 3.2. An average grain size of 16 nm that can estimated from the AFM studies is equal to the particle size in the sol.

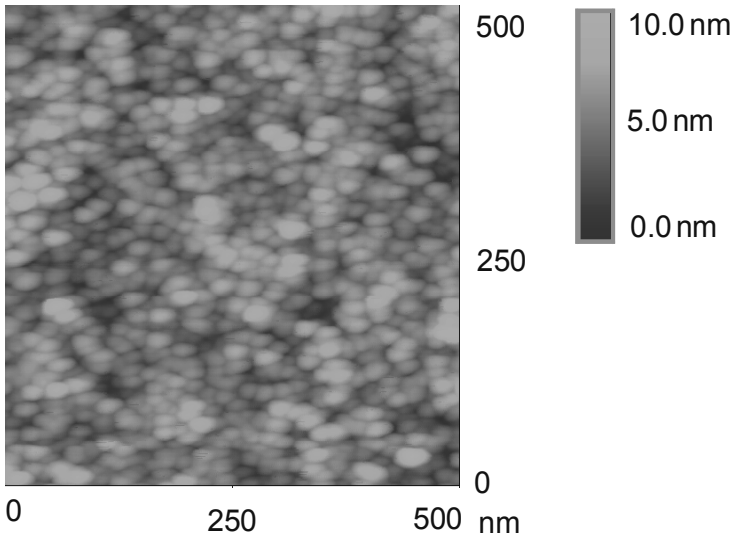

Figure 3.2: AFM picture of titania membrane calcined at 450 ^{o}C.

It was found that both PVA and HPC as binders are necessary to obtain a layer with desired thickness. Since a high PVA content causes flocculation of the titania sol, and a high HPC content decreases the viscosity of the sol to the extent that no layer can be formed, coating solutions in general contained very low amounts of binders, hence the development of large stress during drying and calcination can be expected. Therefore, drying is conducted in a high humidity atmosphere (R.H. 60%), and heating and cooling rates during the calcination process were kept as low as 10 ^{o}C/h. An extra dwell step at 200 ^{o}C during the cooling process was introduced to allow stresses to be released. However, severe cracking occurred in some cases either during calcination or even long

term storage. Consequently, the reproducibility of the formation of crack-free titania layers was approximately 50%.

The zirconia content was varied from 0-40 mol%, calculated on total metal concentration. Independent of the actual zirconia content, only a slight increase of the average particle size occurred upon addition of the zirconium-based solution (≤1 nm), but no negative effect on the sol stability was observed. It was found that the same binder content, drying and calcinations procedure as in the case of pure titania membrane can be utilized. Crack-free layers, with the thickness 0.2-0.5 μm were obtained.

3.3.2 Structural characterisation of titania and zirconia-doped titania material

Microstructural changes due to the presence of zirconia were investigated by comparison of adsorption/desorption isotherms of undoped and zirconia-doped titania powders, as shown in Figure 3.3. The physisorption isotherm of zirconia-doped titania is of type IV, similar as for pure titania, but the hysteresis loop changes from type H2 towards type H3 with increasing zirconia content [30]. An H2 hysteresis loop is characteristic for a mesoporous material consisting of spherical particles, with a relatively wide pore size distribution and a pore shape that is often described as "ink bottle"-type. A change of the hysteresis loop shape towards H3 type indicates that the mesopore size and shape changes, and an increased level of microporosity can be observed (see Figure 3.3 (b)).

Table 3.1: Properties of unsupported titania material doped with various zirconia contents, calcined at 450 ^{o}C.

ZrO_2 content, mol%	BET surface area, m^2/g	Porosity, %	Pore size, nm
0	73.0	28	4.5
5	120.0	38	4.1
10	142.0	38	3.9
20	165.1	40	3.6
30	151.0	47	5.4

At a content of 30 mol% zirconia, the hysteresis loop showed a typical H3 shape, characteristic for a material with a considerable number of slit-like pores. The main factors that can cause narrowing of the hysteresis loop are increased pore connectivity and/or decreased tortuosity [31]. According to percolation theory [31] the more highly connected

the pore network is, the easier it becomes for vapour-filled pores to form a spanning cluster, and consequently the hysteresis loop will become narrower. High tortuosity values are normally associated with wide hysteresis loops provided that there is no substantial interference of capillary condensation metastability effects [31].

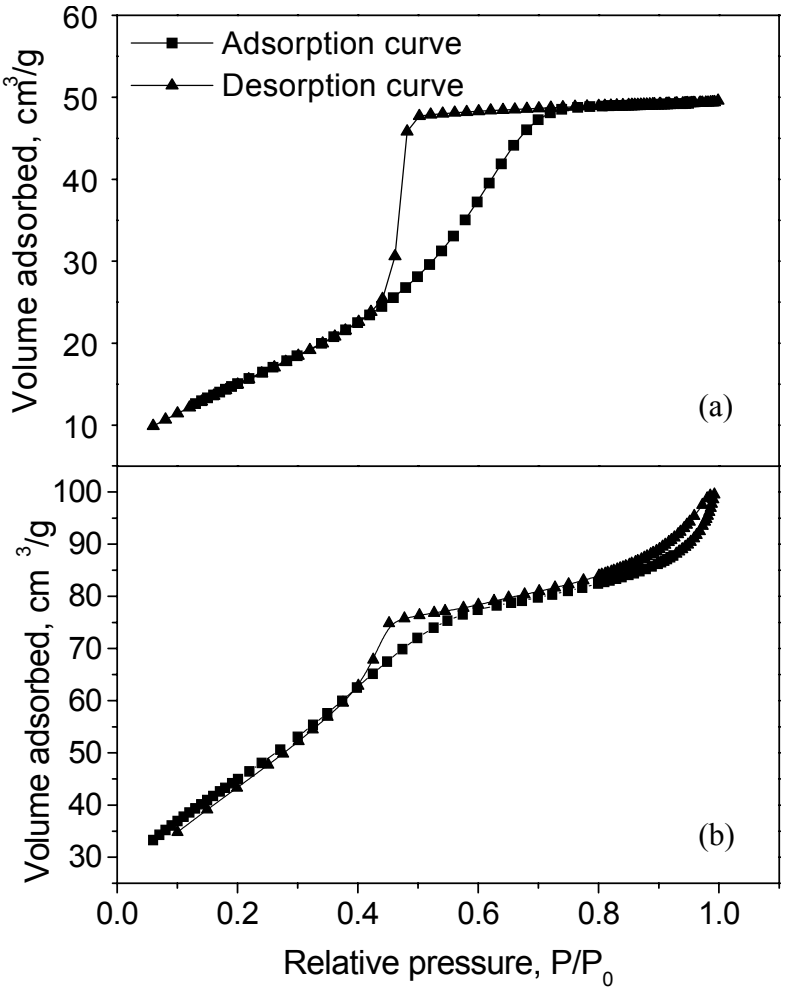

Figure 3.3: Sorption isotherms for (a) pure TiO_2, and (b) TiO_2 80 mol% / ZrO_2 20 mol%, both calcined at 450 °C.

Quantitative nitrogen sorption data are listed in Table 3.1, where the internal BET surface area, average pore size calculated from the BJH model and porosity calculated from cumulative pore volume data are presented for titania and titania/zirconia composites. Already at low dopant contents a significant increase of the surface area and total porosity was observed, while the pore size decreased. The trend continued with increasing dopant content until the zirconia concentration exceeded 20 mol%. These results are in accordance with the hysteresis loop change described above and may be explained by assuming that small ZrO_2 clusters form between the necks of neighbouring titania grains. These clusters lead to an effective reduction of the pore size until a certain critical zirconia concentration

is exceeded and large clusters of crystalline zirconia are formed. It was found that smooth and continuous thin layers on macroporous supports could be obtained when up to 30 mol% of zirconia was present in the titania layer. Layers with 30 mol% zirconia or more were very rough, with a considerable increase of the average pore size.

3.3.3 Mechanical, thermal and chemical stability of the membrane layers

In the absence of zirconia, mechanically poor layers were formed. This is illustrated in Figure 3.4 (a), where a cross section of an undoped mesoporous titania membrane with a microporous silica top layer is shown. Although the mesoporous layer was initially intact after calcination at 450 °C, cracking occurred upon deposition and drying of the silica sol. Most likely the cracks were induced by capillary forces resulting from solvent that had penetrated from the silica sol into the underlying mesoporous layer. The figure clearly demonstrates that the crack propagates along large rutile grains that are embedded in the small-grained anatase microstructure.

The mechanical strength at the same calcination temperature was found to be largely improved by the addition of zirconia. Moreover, reproducibility of procedure that results in crack-free layer was improved from ~50% for pure titania membrane, to nearly 100% for doped one. A uniform, crack-free titania/zirconia layer on an α-alumina support is shown in Figure 3.4 (b). The average thickness of a singly coated layer is ~1 μm.

The mean membrane pore size measured with permporometry and calculated from Eq. (3.2) was found to be in the range of 5.4-7.8 nm. Figure 3.5 shows the oxygen flux as a function of relative pressure of cyclohexane (Figure 3.5 (a)) and pore size distributions in the mesoporous layers (Figure 3.5 (b)) at various dopant levels. The pore size distributions were calculated from the range of relative pressures where the flux behaviour is ruled by capillary condensation (P/P_0=0.4-0.6). However, some oxygen permeation remained above this range, showing the presence of larger pores. From the decrease of oxygen flux in the region P/P_0=0.9-1.0, the presence of some pores of up to 60 nm could be estimated. It is clear from Figure 3.4 (a) that the range of relative pressures, where the flux behaviour is ruled by capillary condensation and Eq. (3.2) can be applied, shifts to the left upon going from pure titania to a membrane with 20 mol% zirconia. Accordingly, the addition of 7 mol% ZrO_2 decreased the average pore size from 7.8 nm in pure titania to 5.8 nm, and narrowed the pore size distribution. Higher dopant contents did not lead to a further

decrease of the pore size, but the number of pores and consequently, the internal surface area increased significantly.

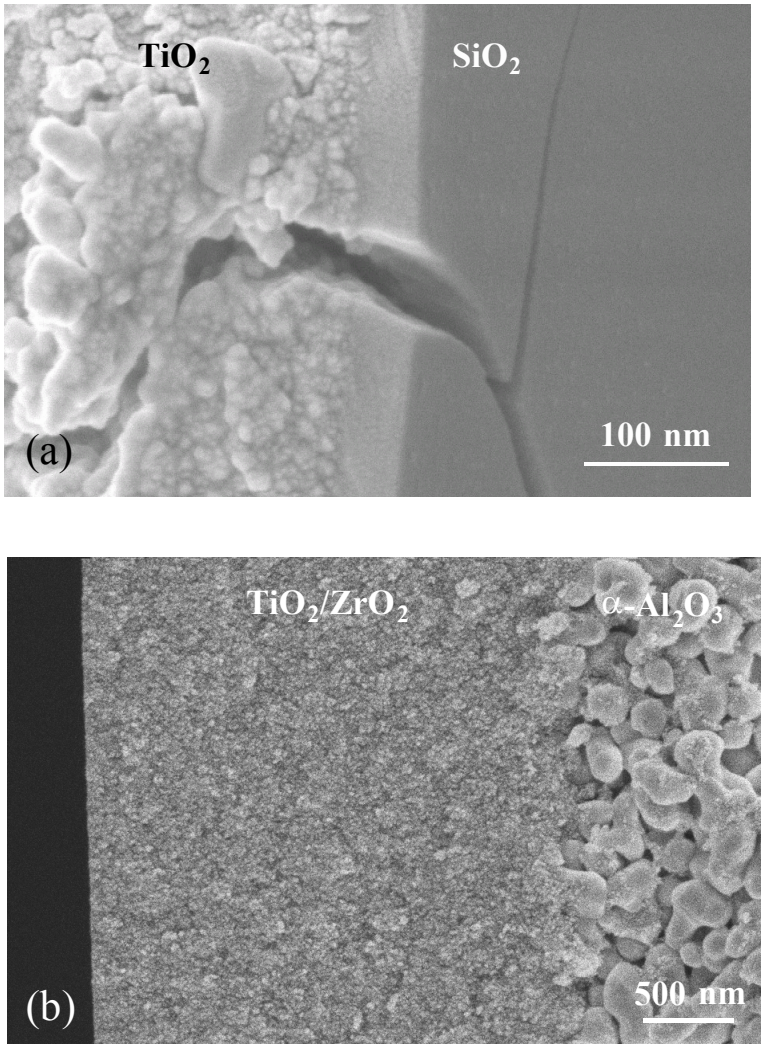

Figure 3.4: SEM pictures of (a) a cross section of a TiO_2 layer with microporous SiO_2 membrane on top, and (b) double-coated TiO_2 80 mol% /ZrO_2 20 mol% membrane.

The observed differences in pore size distribution between supported (measured by permporometry) and unsupported material (measured by nitrogen sorption) can be assigned to constraint effects caused by the rigid support. This has an effect on the crystallite size and pore growth during calcination, leading to a more open structure and larger pores in the titania film [8].

Chemical stability tests showed that both undoped titania and composite titania/zirconia materials did not dissolve at room temperature in aqueous solutions in the pH range 1-13. Namely, the weight loss of titania was below the detection limit, which is for atomic absorption 0.1 mg/l of titanium.

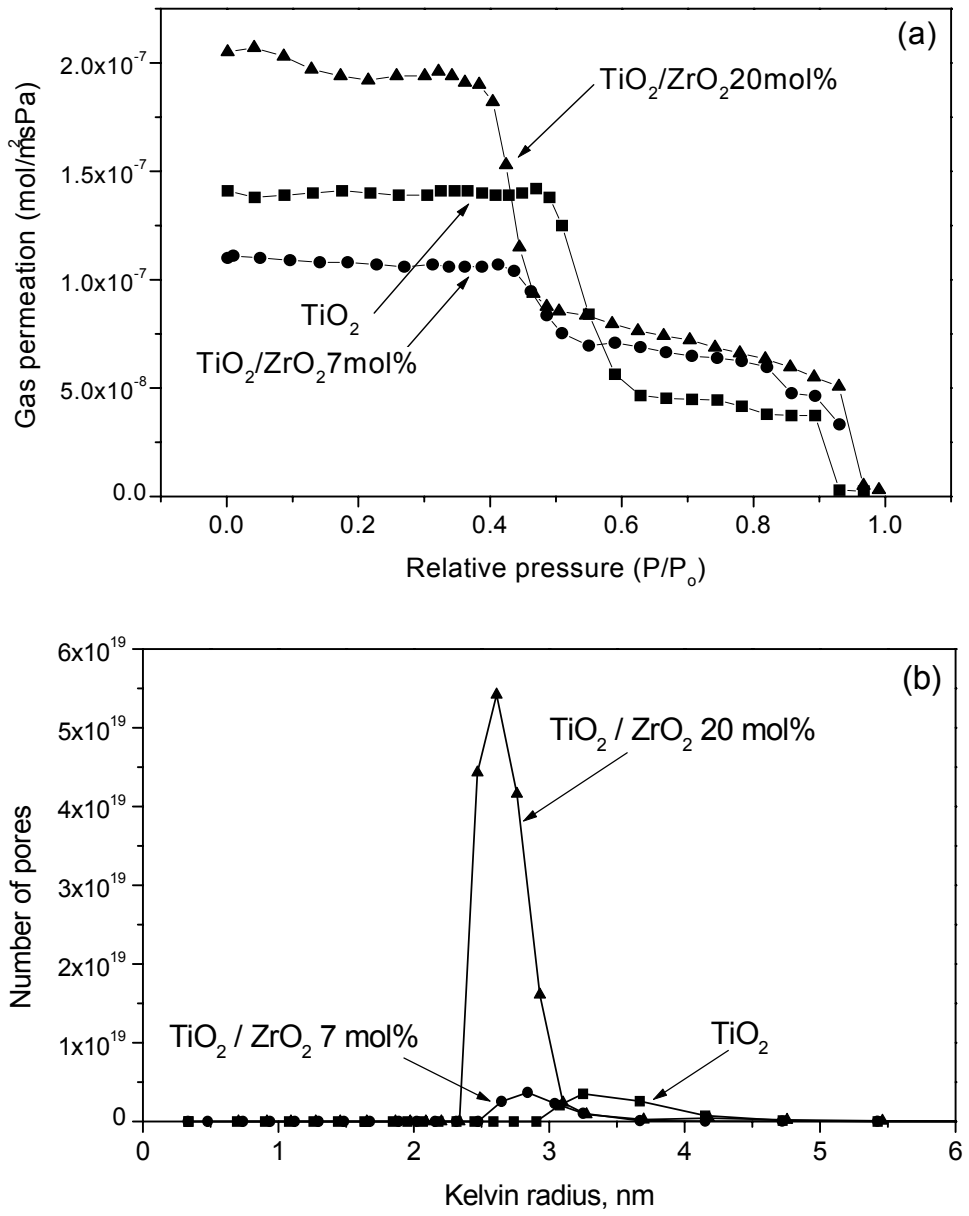

Figure 3.5: Oxygen permeation flux as a function of relative pressure (a) and pore size (defined by Eq. 3.2) distribution (b) for TiO_2, TiO_2 93 mol% / ZrO_2 7 mol% and TiO_2 80 mol% / ZrO_2 20 mol% membranes obtained by permporometry.

The phase transformation from anatase to rutile in pure TiO_2 membranes is a kinetic transition that occurs at any temperature. For sol-gel derived titania it starts to proceed at measurable rates at 350 °C. The rutile content after calcination at 450 °C for 3 h was estimated to be about 10 mol% from XRD data. It appears that this amount was not sufficient to cause immediate cracking of the layer. However, cracking was often observed upon application of a microporous top layer, as illustrated in Figure 2 (a), or even after long-term storage under ambient conditions. This indicates poor mechanical layer strength

and may be due to the low calcination temperature that may not be high enough to stabilize the layer mechanically. Another possible reason is the presence of large rutile grains that either cause stress in the layer, and/or decrease the number of connections (necks) between grains per unit volume of titania. It is for these reasons that thermal stabilization of the anatase phase is required.

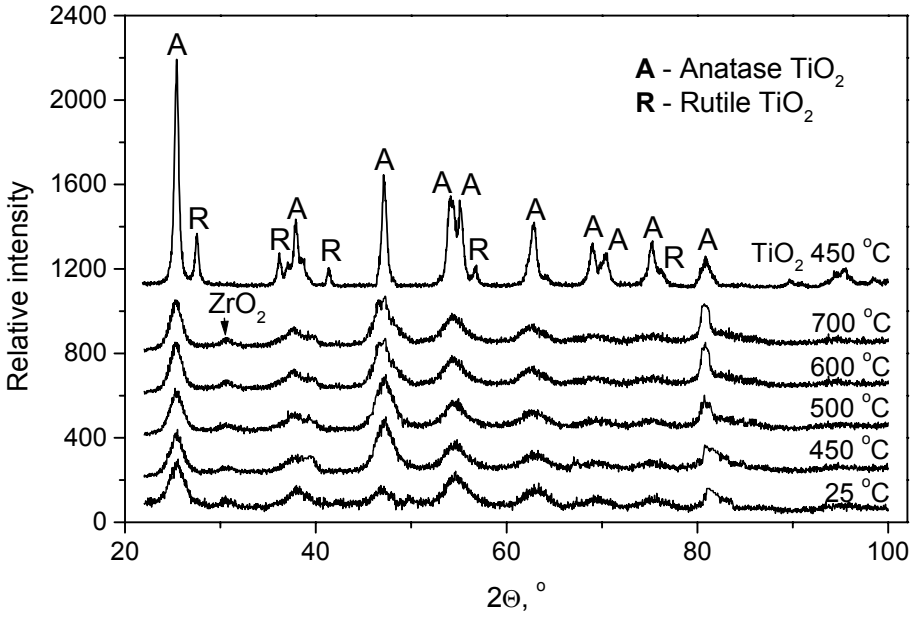

Figure 3.6: In situ high temperature XRD diagrams of TiO_2 90 mol% / ZrO_2 10 mol% and XRD spectrum of pure TiO_2 calcined at 450 °C.

Temperature programmed XRD diagrams of TiO_2 90 mol% / ZrO_2 10 mol% composite powder and undoped TiO_2 calcined at 450 °C (upper line) are shown in Figure 3.6. The X-ray difractograms indicate that the doped material is a mixture of pure anatase and a small fraction of poorly crystallized zirconia until at least 700 °C. The same crystalline structure is observed for zirconia contents of 5-40 mol%. In contrast, the undoped titania shows clear rutile peaks already at 450 °C, while no rutile was found up till 700 °C when zirconia was present in the sample.

Crystalline zirconia was not observed at concentrations below 7 mol%. This may be explained by the observation of Yang *et al.* that the maximum solubility of zirconia in titania at 900 °C is about 7.5 mol% [12]. However, our experiments were carried out at temperatures of 400-700 °C, hence the formation of a thermodynamically equilibrated solid solution is not ensured. Alternatively, the absence of zirconia peaks may indicate that zirconia is present in amorphous form, or that the amount of crystalline zirconia is below the detection limit of the XRD equipment. On the other hand, the presence of crystalline

zirconia at higher zirconia loading does indicate the existence of a separate second phase and the formation of a composite microstructure. This supports the theory of thermal stabilization by an inert second phase (impurity) that decreases the sub-coordination number of the anatase particles in the nanocomposite matrix [10].

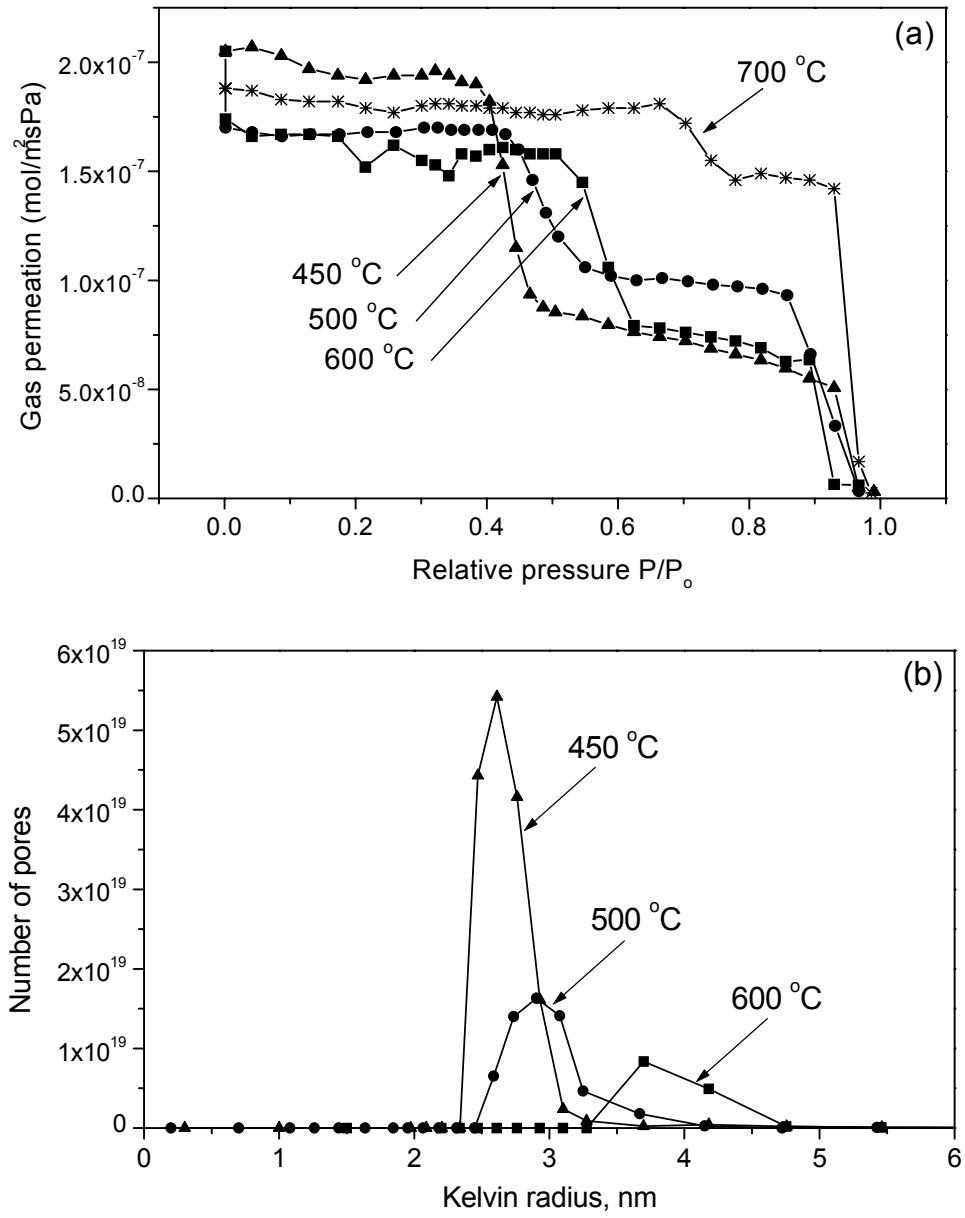

Figure 3.7: Oxygen permeation flux as a function of relative pressure (a) and pore size (defined by Eq. 3.2) distribution (b) for TiO_2 80 mol% / ZrO_2 20 mol% membrane calcined at 450 °C–700 °C.

The theory of thermal stabilisation by an impurity presence is additionally supported by angle-dependent XPS measurements that showed no shift in binding energy of the Zr 3*d* level over the examined depth (~6 nm) into the titania grains, and no increase of the local

zirconia concentration at the anatase grain surface. The presence of zirconia in only one chemical form, homogeneously distributed through the layer, excludes the existence of a coating on the surface of the anatase particles, as proposed for silica-doped and zirconia-doped titania [14,15].

Unlike undoped titania membranes, the ZrO_2-doped layers remained crack-free at calcination temperatures of 700 ^oC. The range of relative pressures where capillary condensation is observed shifted to larger values (Figure 3.7 (a)) with increasing calcination temperature. Figure 3.7 (b)) shows that the pore size distribution became wider and the pore size increased with calcination temperature as a consequence of (anatase) grain growth.

3.3.4 Liquid permeability

As shown in Figure 3.8, the volume water flux at steady state showed a linear dependency on the pressure applied across the membrane. This indicates that the pressure difference is the only driving force for permeation. For transport driven only by convection the volume flow rate (F) is proportional to the pressure difference (ΔP) according to Darcy's law:

$$F = \frac{B^o}{\eta} \Delta P \tag{3.3}$$

where η is the liquid viscosity and B^o the total permeability, which is defined as

$$B^o = \frac{\varepsilon r_p^2}{8\tau L} \tag{3.4}$$

where r_p is the (hydrodynamic) pore radius, L the membrane layer thickness, ε the porosity, and τ the tortuosity.

Water fluxes of 7 - 45 dm^3/m^2h were measured at 2 - 12 bar applied pressure. The high permeabilities of the titania membranes can be explained by the relatively large pores (5-8 nm) and the high porosities (30-40%), but also by the small layer thickness (~2 μm).

Figure 3.8 also shows the fluxes obtained with an α-alumina support and an α-alumina supported ~2 μm thick mesoporous γ-alumina nanofiltration membrane (pore size ~4.5 nm [26]). All titania membranes had a considerably higher permeability coefficient B^o than γ-alumina. After correction for the resistance of the support, it appears that B^o of titania is $3.1 \cdot 10^{-14}$ m, while that of γ-alumina is $3.7 \cdot 10^{-15}$ m, i.e., the permeability of titania is ~8 times larger. The permeabilities of all titania-based membranes are approximately the

same, as would be expected for macroporous and mesoporous systems with mean pore size >10 nm [26,32,33]. Apparently, the microstructural differences between materials with different levels of zirconia doping do not have an influence on liquid permeability. Similar flux experiments were done with TiO_2 80 mol% / ZrO_2 20 mol% membranes using hexane as hydrophobic liquid.

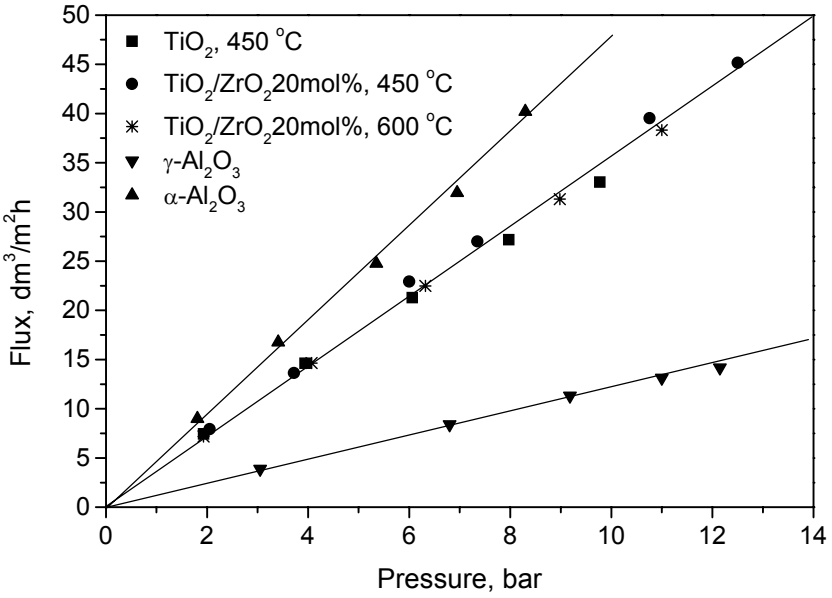

Figure 3.8: Water fluxes as a function of pressure for an α-alumina support, α-alumina supported undoped and doped titania membranes calcined at 450 °C and 600 °C, and a supported γ-alumina membrane.

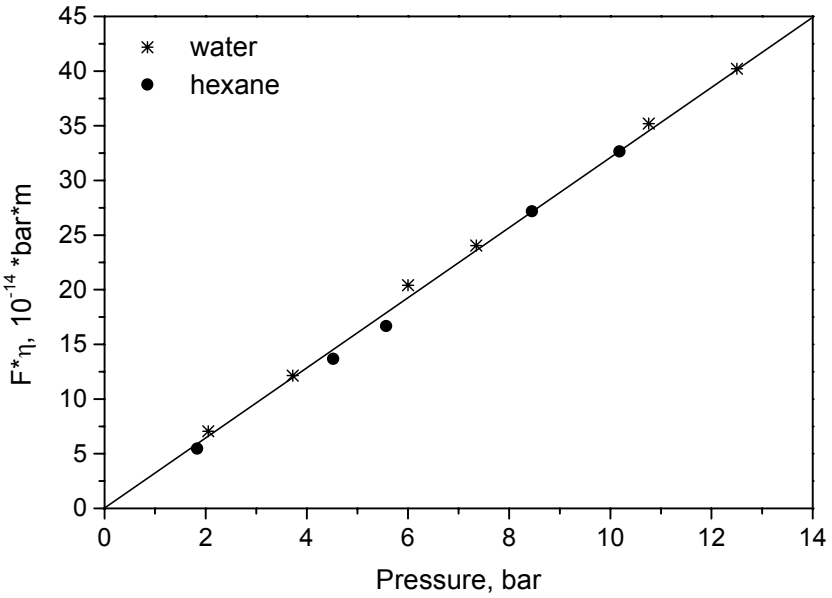

Figure 3.9: Product of liquid flux *F* and viscosity η versus applied pressure for TiO_2 80 mol% / ZrO_2 20 mol% membrane, with water and hexane as permeating liquids.

Figure 3.9 shows the product of flux and solvent viscosity as a function of applied pressure. Following Eq. (3.3), the slope of this line equals the permeability B^o. The close agreement between the plots of water and hexane indicates that the membrane permeability does not depend on the nature of the permeating liquid, in contrast to what has been found for mesoporous γ-alumina [26]. Assuming a microstructure made up of randomly close-packed particles with a corresponding tortuosity τ of ~3, the hydrodynamic pore radiuses r_p calculated from Eq. (3.3) and (3.4) were 2.3 and 1.9 nm for undoped and 20 mol% ZrO_2 doped titania membranes, respectively. The corresponding r_p of γ-alumina is ~1 nm, adopting a tortuosity of 10 for γ-alumina with assumed platelet microstructure [34].

The considerable disagreement with the pore sizes obtained from permporometry can be understood by considering the actual dimensions that are measured with the two methods. Permporometry measures capillary condensation in a pore at equilibrium conditions, giving as a result the dimensions of a pore "body", i.e. the widest part of a pore. However, ceramic membranes consist of packed spherical particles, resulting in an undulating pore structure. The hydrodynamic pore size is measured under non-equilibrium conditions, i.e., the effective pore size corresponds roughly with the smallest openings in the pore structure where the transport resistance is highest, and actually represent the pore "neck" dimensions. Hence, obtaining pore diameters from flux measurements yields significantly smaller values than permporometry.

3.4 Conclusions

The synthesis procedure for mesoporous titania membranes is optimised. Crack-free layers with an average pore size of 7 nm are obtained, with a reproducibility of ~50%. It is believed that cracking is caused by stresses developed due to the phase transformation at the calcination temperature and the low elasticity of the layers, which is caused by the low binder content. Zirconia is shown to be a suitable dopant that not only retards the phase transformation of anatase into rutile to temperatures above 700 °C, but also leads to a material with more porosity, smaller pore sizes, higher pore connectivities, larger internal surface areas and crack-free layers formed with the reproducibility ~100%. It is suggested that zirconia may form clusters between anatase particles, thus preventing direct contact of anatase particles, thereby suppressing its transformation to rutile. When larger amounts of dopant (≥10 mol%) are present, an additional crystalline zirconia phase is formed. It is

demonstrated that α-alumina supported zirconia-doped titania membranes have a much higher mechanical strength than undoped titania layers, which is attributed to both the absence of rutile grains in zirconia-doped films, and to the much higher allowed calcination temperatures. The liquid permeability of undoped and doped titania membranes is ~8 times higher than that of γ-alumina. The permeability is not influenced by the level of zirconia doping, or by the nature of the permeating liquid.

References

1. C. Guizard, A. Julbe, A. Larbot, L. Cot, "Nanostructures in sol—gel derived materials: application to the elaboration of nanofiltration membranes", Journal of Alloys and Compounds, 188 (1992) 8-13.
2. C.–H. Chang, R. Gopalan, Y.S. Lin, "A comparative study on thermal and hydrothermal stability of alumina, titania and zirconia membranes", J. Membr. Sci. 91 (1994) 27-35.
3. G. San Vincente, A. Morales, M.T. Gutierrez, "Preparation and characterization of sol–gel TiO_2 antireflective coatings for silicon", Thin Solid Films, 391,1 (2001) 133-137.
4. O. Harizanov, A. Harizanova, "Development and investigation of sol–gel solutions for the formation of TiO_2 coatings", Solar Energy Materials & Solar Cells, 63 (2000) 185-195.
5. C. Guillard, J. Disdier, C. Monnet, J. Dussaud, S. Malato, J. Blanco, M.I. Maldonado, J. Herrmann, "Solar efficiency of a new deposited titania photocatalyst: chlorophenol, pesticide and dye removal applications", Applied Catalysis B: Environmental, 46, 2 (2003) 319-332.
6. G. Phani, G. Tulloch, D. Vittorio, I. Skryabin, "Titania solar cells: new photovoltaic technology", Renewable Energy 22, 1-3 (2001) 303-309.
7. D.B. Haddow, S. Kothari, P.F. James, R.D. Short, P.V. Hatton, R. van Noort, "Synthetic implant surfaces; The formation and characterization of sol-gel titania films", Biomaterials, 17, 5 (1996) 501-507.
8. K-N.P. Kumar, "Nanostructured ceramic membranes; layer and texture formation", PhD Thesis, University of Twente, 1993.
9. Y.S. Lin, C.H. Chang, R. Gopalan, "Improvement of thermal stability of porous nanostructured ceramic membranes", Ind. Eng.Chem. Res. 33 (1994) 869-870.
10. K.-N.P. Kumar, "Textural stability of titania-alumina composite membranes", J. Mater. Chem. 3,9 (1993) 917-922.
11. H. Zhang, J.F. Banfield, "A new kinetic model for the nanocrystalline anatase-to-rutile transformation revealing rate dependence on number of particles", American Mineralogist, 84 (1999) 528-535.
12. J. Yang, J.M.F. Ferreira, "On the Titania Phase Transition by Zirconia Additive in a Sol-Gel-Derived Powder", Mat. Res. Bull. 33 (1998) 389-394.
13. W.D. Kingery, H.K. Bowen, D.R. Uhlmann, "Introduction to ceramics", 2nd edition, Wiley & Sons, New York, 1976.
14. K. Okada, N. Yamamoto, Y. Kameshima, A. Yasumoti, "Effect of silica additive on the anatase-to rutile phase transition", J. Am. Ceram. Soc. 84 (2001) 1591-1596.

15. P.J. Sanchez-Soto, M.A. Avies, G. Colon, M. Macias, J.A. Navia, "Thermal evolution of TiO_2-ZrO_2 composites prepared by chemical coating processing", Mater. Lett. 20 (1994) 339-343.

16. Y.S. Lin, C.H. Chang, R. Gopalan, "Improvement of thermal stability of porous nanostructured ceramic membranes", Ind. Eng. Chem. Res. 33 (1994) 860-865.

17. R. Gopalan, Y.S. Lin, "Evaluation of pore structure and phase structure of sol-gel derived lanthanum doped titania at high temperatures", Ind. Eng. Chem. Res. 34 (1995) 1189-1196.

18. R. Aroyo, G. Cordoba, J. Pedilla, V.H. Lara, "Influence of manganese ions on the anatase – rutile phase transition of TiO_2 prepared by the sol-gel process", Mater. Lett. (2001) 3432-3439.

19. T. Van Gestel, C. Vandecasteele, A. Buekenhoudt, C. Dotremont, J. Luyten, R. Leysen, B. Van der Bruggen, G. Maes, "Alumina and titania multilayer membranes for nanofiltration: preparation, characterization and chemical stability", J. Membr. Sci. 207 (2002) 73-51.

20. D.-S. Bae, K.-S. Han, S.-H. Choi, "Fabrication and microstructure of TiO_2-ZrO_2 composite membranes", J. Mater. Sci. Lett. 16 (1997) 658-660.

21. D.-S. Bae, K.-S. Han, S.-H. Choi, E.J.A. Pope, "Synthesis and characterization of TiO_2-ZrO_2 composite membranes", Sol-Gel Processing of Advanced Materials, Ceramic Transactions, Vol. 81, American Ceramic Society, 1998.

22. F.F. Lange, "Powder processing science and technology for increased reliability", J. Am. Ceram. Soc. 72,1 (1989) 3-15.

23. F. Rouquerol, J. Rouquerol, K. Sing, "Adsorption by powders & porous solids – principles, methodology and application", Elsevier Academic Press, Amsterdam, 1999.

24. F.P. Cuperus, D. Bargeman, C.A. Smolders, "Permporometry: the determination of the size distribution of active pores in UF membranes", J. Membr. Sci. 71,1 (1992) 57-67.

25. G.Z. Cao, J. Meijerink, H.W. Brinkman, A.J. Burggraaf,, "Permporometry study on the size distribution of active pores in porous ceramic membranes", J. Membr. Sci. 83,2 (1993) 221-235.

26. S. R. Chowdhury, R. Schmuhl, J.E. ten Elshof, K. Keizer, D.H.A. Blank, "Pore size and surface chemistry effects on the transport of hydrophobic and hydrophilic solvents through mesoporous γ-alumina and silica MCM-48", J. Membr. Sci. 225,1 (2003) 177-186.

27. W.B.S. de Lint, "Transport of electrolytes through ceramic nanofiltration membranes", PhD Thesis, University of Twente, 2003.

28. J. Livage, M. Henry, C. Sanchez, "Sol-gel chemistry of transition metal oxides", Solid St. Chem. 18 (1988) 259-262.

29. C. Lijzenga, V.T. Zaspalis, C.D. Ransijn, K.P. Kumar, K. Keizer, A.J. Burggraaf, "Nanostucture characterisation of titania membranes", Key Engin. Mater. 61-62 (1991) 379-383.

30. K.S.W. Sing, "The use of gas adsorption for the characterization of porous solids", Colloids and Surfaces, 38, 1 (1989) 113-124.

31. G.S. Armatas, C.E. Salmas, M. Louloudi, G.P. Androutsopouls, P.J. Pomonis, "Relationships among pore size, connectivity, dimensionality of capillary condensation, and pore structure tortuosity of functionalized mesoporous silica"**,** Langmuir 19 (2003) 3128-3136.

32. M.L. Gee, P.M. McGuiggan, J.N. Israelachvili, A.M. Homola, "Liquid to solidlike transitions of molecularly thin films under shear", J. Chem. Phys. 93 (1990) 1895-1906.

33. Y. Wang, C. Bryan, H. Xu, P. Pohl, Y. Yang, C.J. Brinker, "Interface Chemistry of Nanostructured Materials: Ion Adsorption on Mesoporous Alumina", J. Colloid. Int. Sci. 254,1 (2002) 23-30.

34. A.F.M. Leenaars, K. Keizer, A.J. Burggraaf, "The preparation and characterisation of alumina membranes with ultra-fine pores. Part 1. Microstructural investigations on non-supported membranes", J. Mater. Sci. 19 (1984), 1077-1088.

4

Synthesis and characterisation of microporous titania membranes from polymeric titania sols

Abstract

A procedure for the synthesis of amorphous microporous TiO_2 membrane by the polymeric sol–gel technique was developed. The influence of several processing variables on particle size and sol stability was investigated. It was found that low molecular weight polymeric sols could be obtained only when the hydrolysis conditions were strictly controlled. The use of titanium-tetra-ethoxide was shown to yield smaller polymeric species than the corresponding precursors with i-propoxide or n-butoxide side groups, probably due to the formation of trimeric ethoxide units in the alcohol solution that make it the slowest reacting precursor. Upon variation of process parameters, sols with a stability of at least one month were obtained. The polymeric sol particles of 1.5-5 nm size were found to be highly branched with a fractal dimension >1.5. Calcination of unsupported material at 300 °C resulted in mixed microporous and mesoporous titania, with average pore sizes of <1.0 nm and ~3.5 nm in the microporous and mesoporous range, respectively. The porosity of the powder was estimated to be ~34%. Membrane layer characteristics and quality were evaluated by means of SEM, reflectivity, positron annihilation, pure water permeation and molecular retention measurements. Highly reproducible, homogeneous, crack-free amorphous titania layers with pore size ≤0.9 nm, porosity ~18% and thickness 30-150 nm can be obtained on both mesoporous γ-alumina and titania coated substrates. The upper limit of thermal stability of the membrane layers is ~425 °C. Higher calcination temperatures leads to crystallization of amorphous material into anatase, which is accompanied by a collapse of the microstructure and severe cracking. The material was found to be chemically stable in a pH interval 2-13.

4.1 Introduction

Sol-gel processing has gained scientific interest and technological importance during the last decades mainly due to the relative simplicity of the procedure and the almost unlimited number of possibilities for the formation of various improved or new materials. One of the most important applications of the method is in the field of production of porous materials [1,2]. The sol-gel chemistry of silica is one of the most widely studied topics in this area [1-7]. Besides application of microporous materials in membrane technology, sol-gel coatings have high application potential as thin films in electronic, optical, chemical and gas-sensing devices, semiconductor devices, aerogels and various protective coatings [1].

4.1.1 Polymeric route for titania sol synthesis

The chemistry involved in the sol-gel process is based on polymerisation [8] of inorganic metallo-organic compounds such as alkoxides $M(OR)_n$ (M=Si, Ti, Zr, Al; OR=OC_nH_{2n+1}). Hydrolysis and condensation reactions lead to the formation of metal-oxo-based macromolecular networks. The main problem in microporous titania membrane synthesis by the polymeric sol-gel technique is the high reactivity of titanium-alkoxides, which form precipitates rather than stable sols and gels when water is added [8]. Thus, the success of the sol-gel route to obtain an oxide with given properties depends on the ability to control the hydrolysis-condensation process [8-14]. These reactions are controlled by the process parameters, mainly by the precursor properties, and the hydrolysis and inhibition ratios.

One of the most important properties of a metal alkoxide that has to be taken into account is its molecular structure. The full coordination of many metals is often not satisfied in metal alkoxides $M(OR)_n$. This is due to the fact that the oxidation state Z of the metal is lower than its usual coordination number N. In such cases coordination expansion of the metal occurs via oligomerisation or charge transfer complex formation. The oxidation state of titanium is Z=4 while its preferred coordination number is N=6. However, coordination expansion of titanium already occurs by alkoxy-bridging when the alkoxide is dissolved in a weak complexing medium (for example alcohol).

Under normal conditions, the hydrolysis-condensation reactions of titanium alkoxides in solution lead to precipitation of titanium-oxo polymers. Control of the reaction conditions is usually performed through the use of inhibitors, which may be inorganic acids or complexing ligands such as organic acids, β-diketones or related derivates [14-17]. The

simplest and most commonly used inhibitors for the condensation reaction are H^+ ions [14]. Inorganic acids favour the hydrolysis reaction by making protonated alkoxy ligands better leaving groups. However, an increase of the acidity will also increase the protonation of nucleophilic species (Ti-OH) causing selective inhibition of some condensation reactions. Thus it can be expected that for very high H^+ concentrations the condensation process is nearly completely inhibited, so that only oligomers or very small polymers are obtained, while for low H^+ concentrations the hydrolysis and condensation reactions are both catalysed and occur simultaneously, yielding highly cross-linked polymers or even precipitates. A more detailed description of growth mechanisms involving polymer recombination and dense growth mechanism as a function of the acid concentration is given in the work of Kallala *et al.* [14].

4.1.2 Microporous titania membrane

Microporous ceramic membranes have a high application potential due to their chemical, mechanical and thermal stability. Many research groups have studied microporous membranes made of amorphous silica with pore sizes of 0.3-0.5 nm [1-6,18-21]. Although silica membranes show good performance in gas separation [18] and pervaporation [6], its hydrothermal and chemical stability is limited [20,21]. Amorphous microporous titania is expected to exhibit a better performance in these respects [22,23]. However, in contrast with the large variety of available literature about microporous silica membranes, the synthesis and characterisation of amorphous microporous titania has been studied and reported only by very few research groups [22-30]. Xu *et al.* [23,24], and later Peterson *et al.* [25,26], extensively studied the hydrolysis/condensation reactions of titanium and zirconium alkoxides, the sol stability, the thermal stability, and possible applications for microporous titania and zirconia membranes. They reported a preparation procedure for a material with a mean pore size of 1.5 nm and an upper thermal stability limit of 200-300 ^{o}C. Voigt *et al.* prepared amorphous, microporous membranes with a mean pore size of ~1 nm, and a porosity of 28% [28]. The material kept its amorphous structure till 250 ^{o}C. These membranes were applied in nanofiltration, and a molecular weight cut off of <500 Da was reported. More recently, Van Gestel reported the successful preparation of amorphous, microporous material with an average pore size of 1.6 nm. However, above 200 °C, transformation of amorphous into a crystalline (anatase) structure took place, increasing the average pore size to 2.4 nm upon calcination at 300 ^{o}C, and 3.4 nm upon calcination at 400 ^{o}C [22].

In this chapter a procedure for the preparation of microporous titania membrane by the polymeric sol–gel technique is reported. The aim was to study the chemistry of the titanium-alkoxide hydrolysis-condensation reactions and the influence of process parameters on the properties of the resulting polymeric sol and porous material. Several titanium alkoxide precursors were employed to promote the formation of polymeric sols in acidic conditions. The influence of precursor type, hydrolysis and inhibition ratio on particle size and sol stability is reported. The thermal phase evolution, thermal and chemical stability, and microstructural characteristics of calcined powders were analysed. Furthermore, the structural characteristics, and the gas and liquid permeation properties were studied for anatase titania and γ-alumina supported microporous titania membranes.

4.2 Experimental

Polymeric titania sols were prepared according to the procedures outlined in general by Livage *et al.* [8]. Several titanium alkoxides were used as precursor, and nitric acid (65% solution, Merck) was employed as acid catalyst to promote the formation of polymeric sols. Titanium tetra-ethoxide, titanium tetra-i-propoxide and titanium tetra-n-butoxide were obtained from Aldrich and used without further purification. The parent alcohol of the precursor was used as solvent in all cases, except for the synthesis with titanium-tetra-n-butoxide, in which case ethanol instead of butanol was used as solvent for water. In all cases a given amount of a water/nitric acid solution was dissolved in a large volume of alcohol to keep the local concentration of water low. The resulting solution was added under vigorous stirring to a titanium alkoxide/alcohol solution. All experiments were performed in a dry nitrogen atmosphere to avoid possible reactions of the alkoxides with water from ambient air. Microporous titania powder was prepared by drying the sol in air, and subsequent calcination at 300 °C for 3 h.

Titania top layers were deposited by the dip coating technique on mesoporous γ-alumina [31] or (anatase) titania [32] coated α-alumina substrates [33]. To avoid the effect of strong capillary forces drying was performed in an alcohol-saturated atmosphere over a period of 48 h. The dried membranes were calcined in air at 300 – 450 ^{o}C for 3 h.

The theoretical background of the techniques employed in the structural characterisation of the material is described in more detail in chapter 2 of this thesis.

The size of the polymeric species in the sols (particle size) was measured by a ZetaSizer (Malvern, UK). The lower limit for accurate detection as specified by the manufacturer is around 2 nm. Therefore, values below 2 nm mentioned in the text below should be considered as approximate values.

Further information about the structure of the polymeric species was obtained from small-angle x-ray scattering measurements [18] on a PW3373/10 (Panalytical, The Netherlands). Measurements were carried out with a Cu Kα anode (λ=0.15418 nm), in the range 0.005-5^{o} in Bragg mode, with step size of 0.01^{o} and a measurement time of 50 s at each angle. A reference measurement was performed with a pure ethanol-filled capillary. The background scattering curve (including solvent and capillary contributions) was subtracted prior to analysis. The scattering curve was fitted by the Texeira function, as described elsewhere [34].

The amorphous to anatase phase transformation of dried uncalcined powder was studied by temperature programmed X-ray diffraction experiments (Philips SR5056, Panalytical, The Netherlands). The thermal evolution of TiO_2 was investigated by thermogravimetric analysis (TGA) and differential scanning calorimetric analysis (DSC). Measurements were performed in a nitrogen flow with a heating rate of 10 °C/min in the temperature interval 25-600 ^{o}C, using coupled TGA/DSC equipment (Setsystem 16/18, Setaram, France).

The internal surface area, pore volume, and average pore size distribution of titania powders were obtained from nitrogen sorption isotherms using a Sorptomatic 1990 (Horiba, USA). The BET method was used in data processing [35].

The chemical stability of amorphous titania was determined at room temperature by static solubility tests [22] in water at pH 1-13 using calcined unsupported material. In all cases, 1 g of powder was immersed in 50 ml of water solution. The pH of the solutions was adjusted with nitric acid or ammonium hydroxide and the total weight loss of the powder after 120 h immersion was calculated by measuring the concentration of dissolved titanium in the solution using atomic adsorption spectroscopy (Thermo-Optec BV SOLAAR system 939). The material was regarded as stable when the amount of dissolved titania in the solution was lower than or close to the AAS detection limit of 0.1 mg/l for titanium.

The thickness and quality of the layers was checked with HR-SEM (LEO Gemini 1550 FEG-SEM, UK).

Additional examination of the layer was carried out using X-ray reflectivity measurements (XRR) on a 4-circle diffractometer (PHILIPS, The Netherlands) [36,37]. The instrumental resolution stays within a range of 0.035 - 0.15° for parafocusing geometry and within 0.0015 - 0.3° for parallel beam geometry. Data processing was carried out using Philips software X'Pert Reflectivity.

Further information about pore size, porosity and internal pore structure were obtained from positron annihilation studies on unsupported material. This technique is based on a positron "interaction" with a porous structure [38]. All the experiments were performed with the positron beams at the Delft Positron Center [38,39]. The analysis of the data was done with the aid of the VEPFIT program [39].

The liquid permeability of the membranes was measured in a pressurized dead-end filtration cell with fully desalinated, pre-filtered water, over the pressure range of 0-18 bar [40]. Retention measurements were performed with 3 wt% solutions of various molecular weight polymers (ethylene glycol (EG), diethylene glycol (DEG), triethylene glycol (TEG), and polyethylene glycol (PEG), all obtained from Merck) at a pressure of 8 bar [41]. For transport only driven by convection the volume flow rate (F) is directly proportional to the pressure difference (ΔP):

$$F = \frac{B^o}{\eta}\Delta P, \tag{4.1}$$

where η is the liquid viscosity, and B^o the total permeability, which is defined as:

$$B^o = \frac{\varepsilon r_p^2}{8\tau L}. \tag{4.2}$$

r_p is the (hydrodynamic) pore radius, L the membrane layer thickness, ε the porosity, and τ the tortuosity. The retention (R_i) for each molecular weight (component i) was calculated using the following formula:

$$R_i = (1 - \frac{C_{i,feed}}{C_{i,permeate}}) \cdot 100. \tag{4.3}$$

The permeates were analysed using capillary gas chromatography (VARIAN CP-3800, USA).

Single gas permeation experiments were performed at 200 °C in a cross-flow gas permeation set-up, with H_2, CH_4, C_3H_8, n-C_4H_{10} and SF_6 [5]. Prior to the permeance

experiments, the membranes were dried at 300 °C under a He stream to remove any moisture from the pore structure. The membranes were placed in stainless-steel cells with the microporous membrane top-layer at the feed side. The composition of the gas mixture at the feed side was controlled by mass flow controllers. The feed pressure and the pressure difference over the membrane were measured by electronic pressure transducers. Argon was used as sweep gas with a flow of 120 ml/min. The gas composition of the permeate and retentate were analysed by a gas chromatograph (Varian, Star 3400CX, with a molecular sieve and Haysep column).

4.3 Results and discussion

4.3.1 Polymeric titania sol

The procedure for polymeric titania sol synthesis was optimised. It was found that low molecular weight polymeric sols could be obtained only when the hydrolysis conditions were strictly controlled. As a solvent, the parent alcohol was used with high dilution ratios (<2 mol Ti/dm^3, and <5 mol H_2O/dm^3 alcohol). This was crucial to obtain small particles, but also to avoid precipitation in some cases. Mixing has to be done under high-speed stirring to avoid high local concentrations of water, because otherwise formation of dense agglomerates occurred. In addition, a moisture-free atmosphere is required.

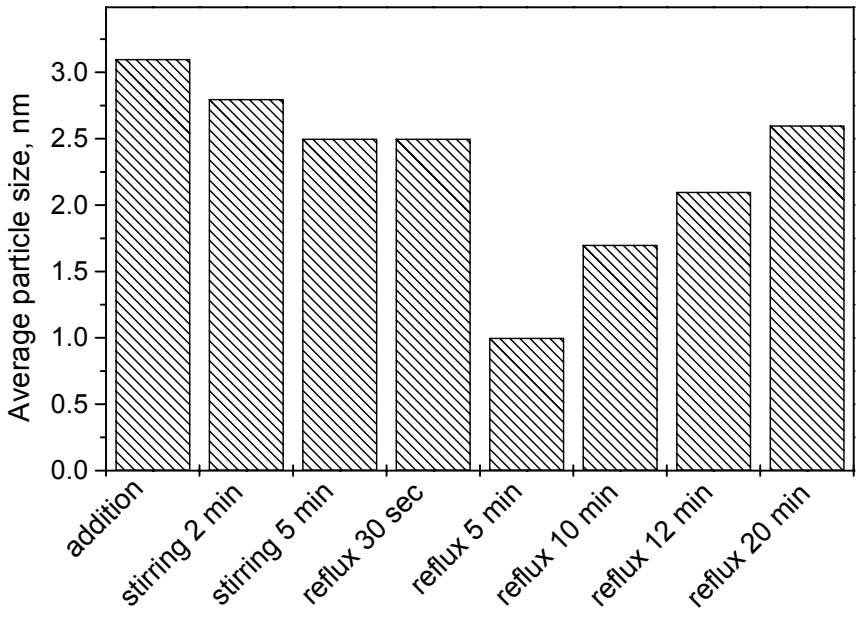

Figure 4.1: Average particle size in the sol (titanium-ethoxide, r_w=1.9, r_a=0.1, reflux at 60 °C) in various phases of the synthesis.

Figure 4.1 shows the average particle size in various stages of sol synthesis. Very small particles were formed shortly after the reactants were mixed. Further aging of the sol at room temperature had an almost negligible effect on particle size. Elevated temperatures led to the breaking of polymeric chains into small pieces that continued to rearrange into relatively larger but also more highly branched polymers, as shown by the SAXS experiments below. Prolonged exposure of the sol to high temperatures led to continued growth of the species, and finally to gelation. Based on these findings, it was decided to carry out peptisation at 60 ^{o}C for 10 minutes in all further experiments.

4.3.1.1. Influence of process parameters on sol properties

Precursor: The influence of alkyl chain length, steric hindrance and oligomerisation on the hydrolysis-condensation reaction was studied by using titanium-tetrabutoxide, tetra-isopropoxide and tetra-ethoxide as precursors.

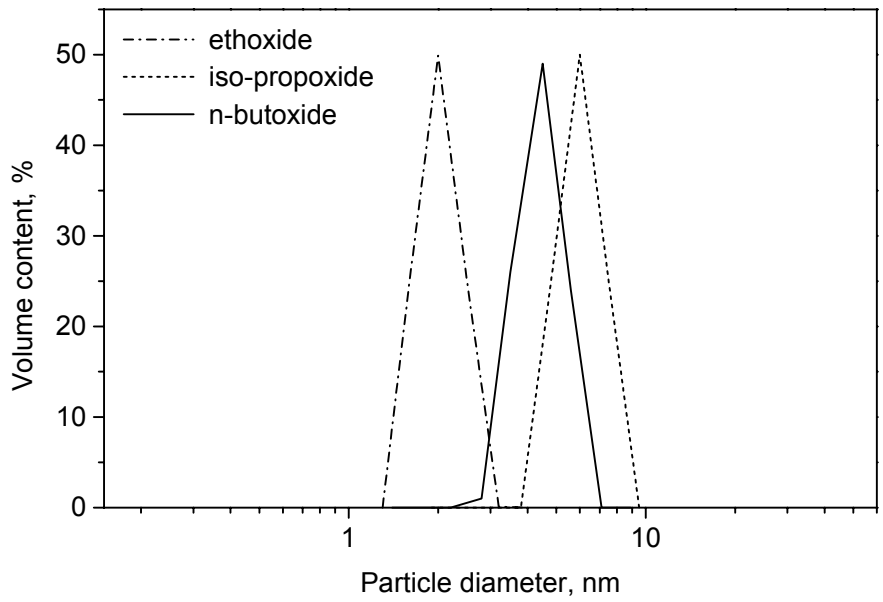

Figure 4.2: Particle size distribution in the sol 24 h after synthesis depending on the precursor used.

As can be seen in Figure 4.2, the mean particle size increases in the order ethoxide < butoxide < iso-propoxide. The large size of the particles obtained from titanium isopropoxide can be expected because of the steric hindrance effect caused by the secondary group [8]. On the other hand, titanium-tetraethoxide is expected to give larger particles than the corresponding butoxide precursor, due to the shorter alkyl chain length, and considering the fact that they both form pentacoordinated trimers in alcoholic solution [8,11,14]. However, it seems that in this case steric hindrance of the bulkier butoxide group

has a negative effect on the hydrolysis rate. Because of its small particle size, titanium tetra-ethoxide was selected as precursor for further studies.

Sol particle size estimates were also made by SAXS experiments. Titania polymeric systems are fractal objects and can be characterised by a mass fractal dimension D_f that is related to its mass m and size r in the following way:

$$m \propto r^{D_f} \tag{4.4}$$

A SAXS curve of a stable amorphous titania sol obtained by the hydrolysis of titanium-ethoxide is shown in Figure 4.3.

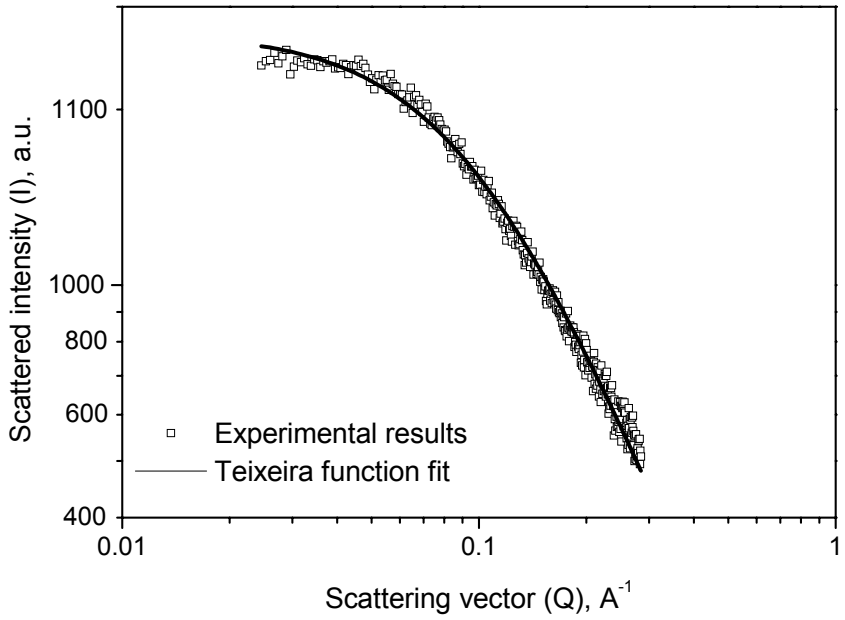

Figure 4.3: SAXS spectrum of titania sol (titanium-ethoxide, r_w=1.9, r_a=0.1 and fit by the Texeira function of the experimental data.

The Teixeira function, which describes the scattering curve of fractal objects, was used to fit the experimental data [34]. This provided three parameters, namely the radius of the individual scatterer R_o, the correlation length of self-similar behaviour of the sol particles ξ, and the fractal dimension of the particles D_f. The value of R_o should be roughly equal to the Ti-O monomer bond length of ~0.19 nm, and ξ can be related to the Guinier radius of the inorganic polymer R_g via $R_g^2 = \frac{1}{2} D_f (D_f + 1) \xi^2$.

The best fits were obtained with R_o~0.2 nm, ξ~1.1–1.4, and D_f~1.5–1.7. This corresponds to a radius of gyration R_g between 1.7 and 1.9 nm, which is equivalent to an average particle size of 3.4–3.8 nm. This value is similar to size of 3.6 nm that was measured by light scattering as shown in Figure 4.2.

The value of D_f provides information on the microstructure of the final microporous material. As the tendency of two fractal particles m_1 and m_2 with dimension D_f to interpenetrate is inversely related to the number of intersections, the relationship between two merged particles $m_{12}=m_1+m_2$ [18] can be described as

$$m_{12} \propto r^{2D_f-3}. \tag{4.5}$$

This indicates that dense packing of particles is only possible when $D_f < 1.5$. The amorphous titania sols have a slightly higher value of ~1.6, which suggests that very dense packing and a very high degree of interpenetration, as occurs for microporous silica with $D_f < 1.5$ [18], can not occur. Hence, it is expected that the average pore size of titania material will be larger than in microporous silica.

Hydrolysis and inhibition ratio; For a given precursor and titanium concentration the hydrolysis-condensation reactions are mainly governed by the initial hydrolysis ratio $r_w=[H_2O]/[Ti]$ and the inhibition ratio $r_a=[H^+]/[Ti]$. The hydrolysis of titanium-tetraethoxide in the presence of different amounts of acid and water led to sols, turbid or clear gels or precipitates, depending on r_w and r_a as shown in Figure 4.4.

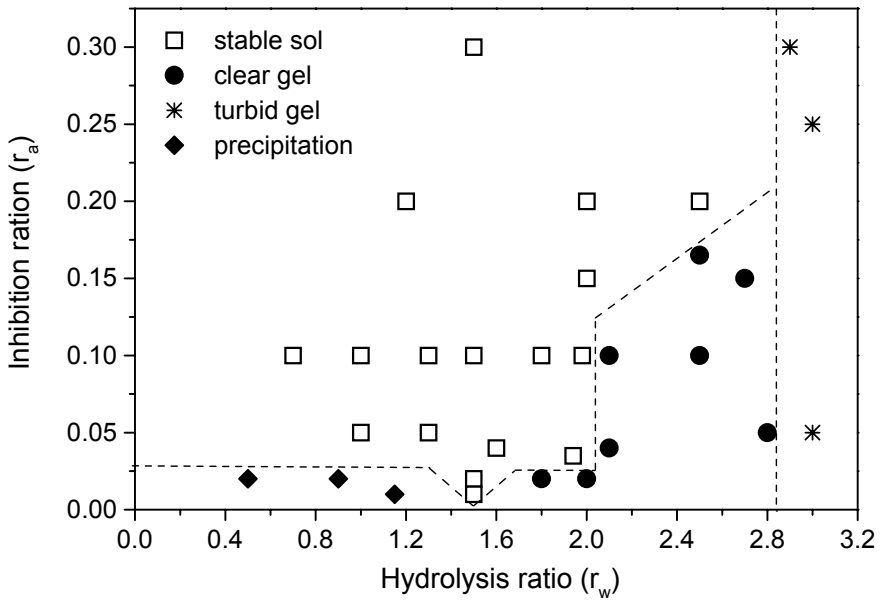

Figure 4.4: Pseudo-phase diagram of polymeric titania sol made from titanium ethoxide, showing influence of hydrolysis (r_w) and inhibition (r_a) ratios on sol state.

The main parameter that determined the formation and stability of sols is found to be the hydrolysis ratio, which had to be kept at values below 2 to prevent fast gelation. The average particle size (24 h after synthesis) varied between 1.6 and 3.6 nm, depending on the amount of water used (r_w) as shown in Table 4.1.

Table 4.1: Average sol particle size 24 h after synthesis and corresponding internal surface areas of the material calcined at 300 °C depending on hydrolysis ratio; titanium-ethoxide was used as a precursor, and the inhibition ratio (r_a) was fixed at 0.1.

$r_w=[H_2O]/[Ti]$	Average particle size, nm	BET surface area, m^2/g
0.7	1.6	138.3
1.0	1.7	133.7
1.3	3.1	165.5
1.5	3.4	171.2
1.7	3.6	193.5
1.9	3.7	195.7
2.1	GEL	/

It was found that a pH of 3 or lower was required to form polymeric sols. This corresponds to an inhibition ratio of 0.02 or higher. For lower inhibition ratios either precipitation or gelation occurred depending on the actual value of r_w. At low H^+ concentrations, hydrolysis and condensation were both catalysed and occurred almost simultaneously, yielding precipitates or gels, depending on r_w. On the other hand, at higher H^+ concentrations, hydrolysis occurs faster than condensation and this results in the formation of long chain polymers and stable sols.

4.3.1.2. Sol aging

The stability of the sol polymers derived from different precursors was studied as a function of hydrolysis ratio, as shown in Figures 4.5 (a) and 4.5 (b), respectively.

When titanium-tetraethoxide was used as precursor, the hydrolysis ratio had a significant influence on the mean particle size, but also on the sol behaviour during aging. In case of small hydrolysis ratios (r_w=0.7-1.5) a significant increase of particle size was observed during the first 24 h (Figure 4.5 (a)), indicating chemical activity and polymer rearrangement. Upon further aging, no significant change was seen. The sol stability was found to be at least one month, provided that it was not exposed to high humidity atmospheres. As shown in Figure 4.5 (b), both titanium-tetraethoxide and titanium-tetra-n-butoxide gave sols with small particle sizes that did not change significantly over a period of approximately two weeks. On the other hand, sols from titanium tetra-isopropoxide became unstable after 5 days.

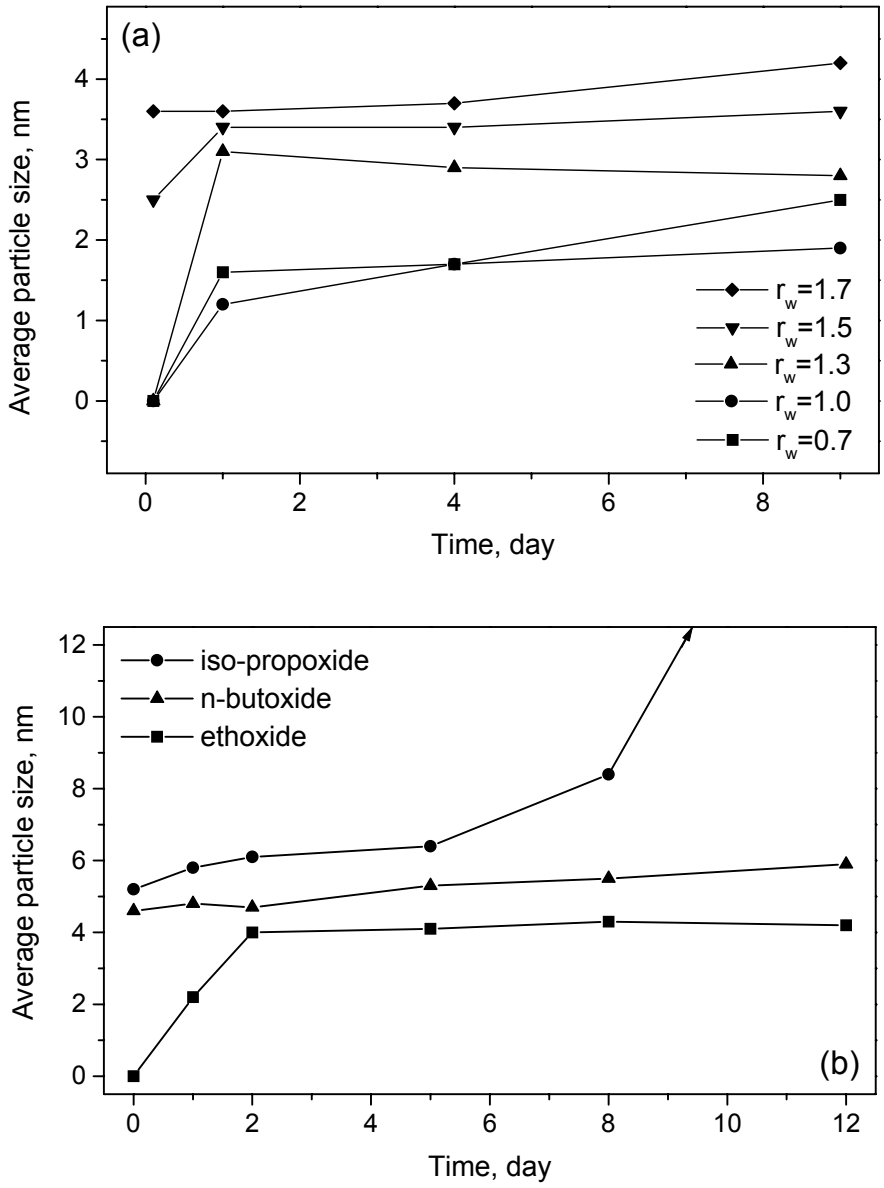

Figure 4.5: Aging behaviour of the sol depending on hydrolysis ratio (a), and precursor (b); (a): precursor is titanium-ethoxide, r_a=0.1, and (b): r_a= .1, r_w=1.9.

4.3.2 Structural characteristics of the unsupported material

4.3.2.1 Thermal evolution and stability

The temperature programmed XRD diagrams shown in Figure 4.6 were obtained from TiO_2 material synthesised from titanium-tetraethoxide with a hydrolysis ratio r_w of 1.7. The material kept its amorphous structure until 350 °C, where slight crystallisation into anatase occurred. Crystallisation proceeded rapidly above this temperature and at 400 °C distinctive anatase peaks can be observed.

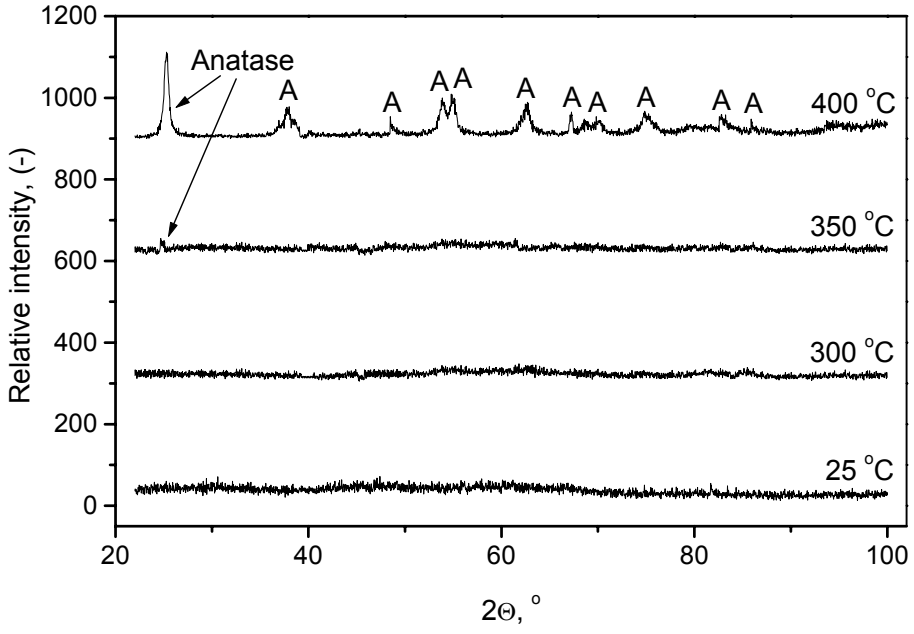

Figure 4.6: Temperature programmed XRD spectra of air-dried titania powder.

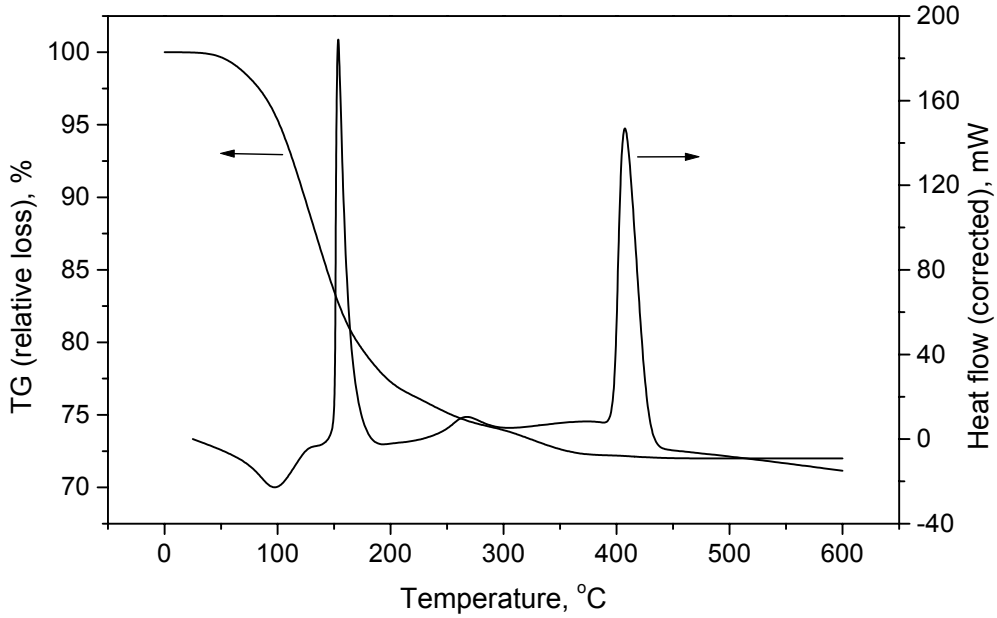

Figure 4.7: Differential scanning calorimetry and thermo-gravimetric analysis of TiO_2 in temperature interval 25-600 °C.

Figure 4.7 shows a typical TGA/DSC pattern of a dried TiO_2 gel. The TGA pattern reveals weight losses occurring in two temperature intervals. A sharp weight loss occurred in the temperature interval 80-120 °C indicating the loss of water and solvent, followed by slower weight losses of organic substances in the interval 120-425 °C. The weight loss beyond 425 °C was negligible. The DSC curve shown in Figure 4.7 contains information about water and solvent evaporation, structural changes, organic oxidation, and nitrate

decomposition [42]. The first endothermic peak at ~100 °C in the DSC pattern corresponds to the removal of physisorbed water. A distinctive exothermic peak at 150 °C may be attributed to the evaporation of ethoxy groups in the form of ethanol. The heat effect is due to the heats of the hydrolysis and condensation reactions (minus the heat of evaporation of ethanol) that irreversibly occur when ethanol is removed from the polymers. Decomposition of organics and dehydroxylation occur between 200 °C and 400 °C. A sharp exothermic peak at 405 °C corresponds to the amorphous to crystalline (anatase) phase transition.

The crystallisation temperature recorded by DSC is slightly higher than that obtained by XRD, where it occurred from 350 °C onwards. This can be attributed to the fact that the temperature programmed XRD experiment was performed with a heating rate of 0.25 °C/min, while faster heating in the TGA/DSC apparatus (10 °C/min) led to more sudden crystallisation at a higher temperature.

4.3.2.2. Pore structure characteristics

According to the interpretation by Rouquerol *et al.* [35], nitrogen isotherms such as the one that is shown in Figure 4.8 is characteristic for a microporous material containing some additional larger pores. The hysteresis loop is due to network percolation effects [43]. The large pores, which were determined to be up to 4 nm in diameter, with an average value of 3.5 nm, are most likely the consequence of prolonged drying of the powder and formation of a thick unit. An alternative reason could be that drying was carried out in air, which may have led to uncontrolled reactions with water vapor into dense particles forming relatively large pores. The average pore size in the microporous range cannot be calculated with the existing models, but the occurrence of substantial sorption at low P/P_o indicate the presence of a considerable number of micropores in the subnanometer range. A rough estimate can be obtained from the similarity of the sorption isotherm with the one obtained according to the Saito-Foley model [44]. This function gives a pore size distribution in the range of 0.8 - 2.0 nm, with the majority of pores below 1.2 nm. The porosity was estimated to be 34% from the cumulative pore volume value, assuming a skeleton density of 3.1 g/cm^3 [45] for amorphous titania.

Nitrogen sorption measurements were also employed to study the influence of the hydrolysis ratio on the surface area of calcined material. As can be seen in Table 4.1, larger hydrolysis ratios gave rise to larger particles, but also to larger surface areas. By increasing the hydrolysis ratio from 0.7 to 1.9, the internal surface area calculated according to the

BET model increased from 138 m^2/g to 196 m^2/g. Hence, although a small particle size appears to be more favourable for microporous thin film development, it seems that larger quantities of unreacted alkoxide remain, which have a negative effect on microstructure formation, i.e., surface area development, in later processing steps.

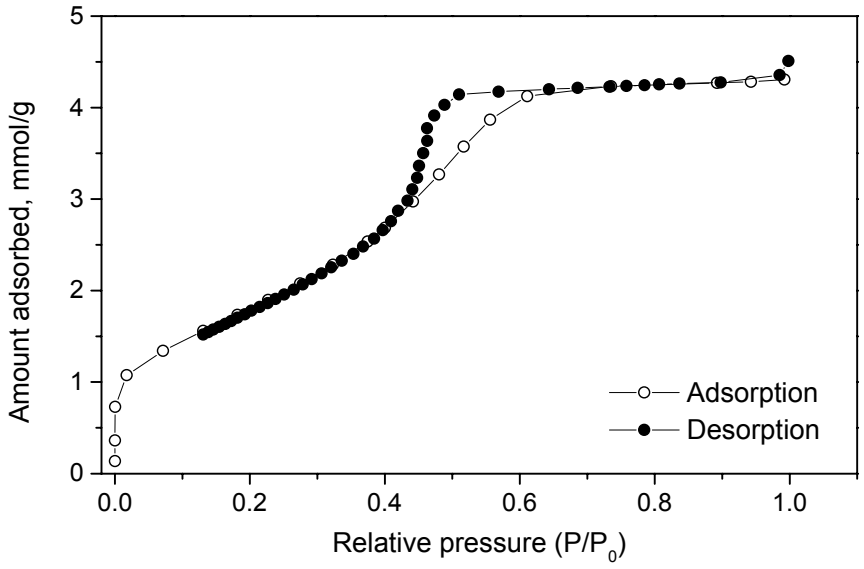

Figure 4.8: Nitrogen sorption isotherms for amorphous TiO_2 material calcined at 300 °C.

4.3.2.3. Chemical stability

The amorphous titania phase was found to be chemically stable at room temperature in the pH range 2-13. However, the weight loss at pH=0 was 21%, and at pH=1 it was approximately 1%. This is a considerable improvement of chemical stability in comparison with microporous silica, which is found to be stable in the pH range 1-9 [7]. As shown by Van Gestel, the results of static stability tests are in good agreement with tests under dynamic conditions [22], therefore it is expected that amorphous titania membranes will be stable under similar dynamic conditions.

4.3.3 Microporous titania membrane

4.3.3.1 Thermal stability

As can be seen from the XRD studies of unsupported material, crystallisation of the amorphous titania phase starts at 350 ^oC, and proceeds rapidly until 400 ^oC, where the material has mainly transformed into anatase [46]. Slightly different behaviour was observed when the material was in a thin layer form. Using scanning electron microscopy, uniform crack-free layers were observed up to a calcination temperature of 425 ^oC, while severe cracking occurred when the membrane was calcined at 450 ^oC, indicating rapid

crystallization of the material in the temperature range 425-450 ^{o}C. In conclusion, the crystallisation of titania in thin layer form occurs at higher temperatures than in the unsupported material. This is supported by other studies that show that phase transformation of oxides in thin layer form occurs at higher temperatures than in powder form [46]. For example, Kumar found that the anatase-to-rutile phase transformation temperature and transformation rate differed significantly for unsupported and supported materials, due to the important contribution of the rigid support in the stabilization of the porous structure [46,47]. This phenomenon may be attributed to the decrease of driving force for sintering due to the stress developed during constrained sintering of a film attached to a rigid support.

4.3.3.2 Morphology of the membrane layer

Highly reproducible, homogeneous, crack-free amorphous titania layers were obtained on both mesoporous γ-alumina and titania coated substrates. It was found that the thickness of the layer could be easily varied by changing the sol concentration prior to deposition of the layer. For example, when a sol with [Ti]=0.01 mol/l was used, a layer thickness of ~150 nm was obtained after calcination (see Figure 4.9), while the layer thickness was ~40 nm when the Ti concentration was decreased to 0.005 mol/l. The maximum layer thickness that could be achieved in a single coating step was ~250 nm. Above this value additional stresses developed, and cracking occurred upon drying.

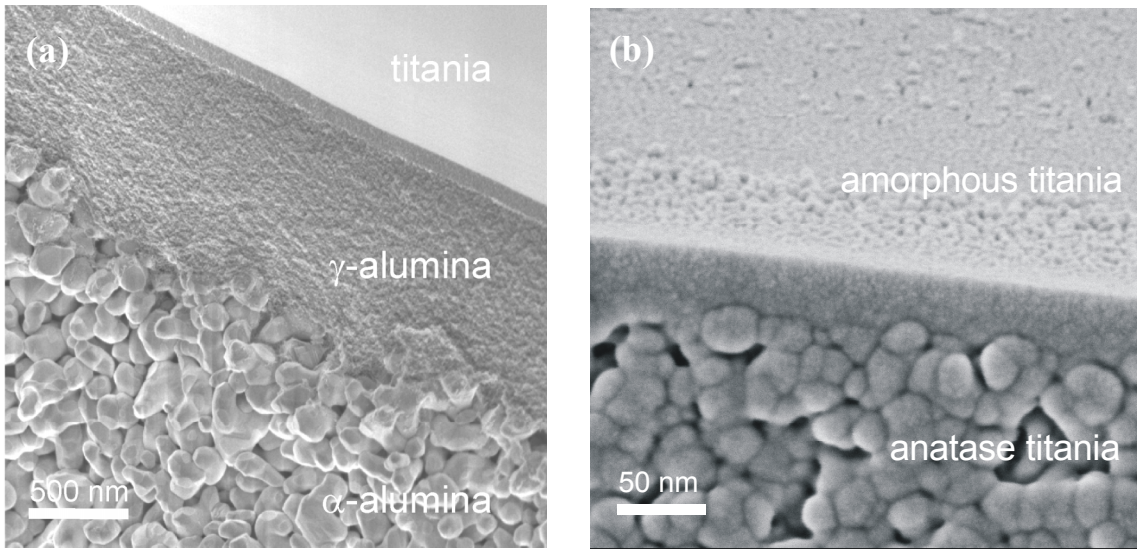

Figure 4.9: SEM picture of a cross section of an amorphous TiO_2 layer on a γ-Al_2O_3 (a) or anatase titania (b) coated α-Al_2O_3 substrate.

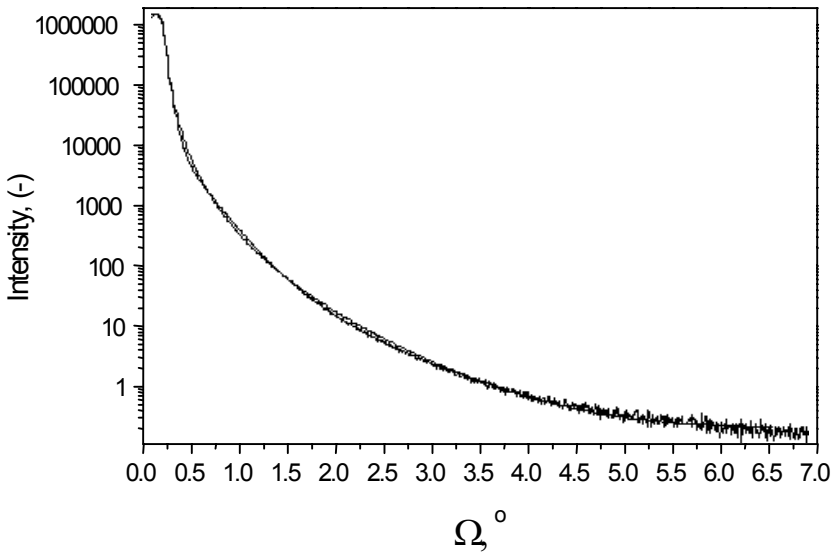

Figure 4.10: Reflectivity curves (experimental and fitted values) of amorphous TiO_2 layer.

For further characterisation of the layers, reflectivity measurements were carried out. X-ray reflectivity is a non-destructive technique used for estimation of layer thickness, density and surface (or interface) roughness. It is based on total external reflection of x-rays and a measurement of the scattering from a set of layers (not atomic planes) that have a contrast of density and scattering power [36,37]. An advantage of the method is that it is insensitive to the crystallinity of the layer and it may therefore be applied to amorphous, polycrystalline or epitaxial layers. A wide angle XRD scan was made prior to the reflectivity measurement to ensure the absence of additional crystalline phases that could disturb the reflectivity measurements. No trace of a crystalline titania phase was found. The reflectivity data are shown in Figure 4.10. After data processing, the thickness of the top layer was found to be 88.4 nm, the roughness 0.189 nm and the porosity 18%. The measured layer thickness is in good agreement with the thickness of ~100 nm estimated from SEM examination of a cross section of a similar sample. The porosity was calculated assuming a theoretical density of the amorphous titania phase of 3.1 g/cm^3 [45].

Formation of a defect-free layer was confirmed by permporometry measurements [35]. After saturation with cyclohexane, membranes did not allow any oxygen flow, which is an indication of the formation of a defect-free layer with pore sizes in the microporous range.

The calcined supported membranes were also characterised with positron beam analysis (PBA). The PBA results obtained with the aid of the VEPFIT program are shown in Figure 4.11. This program provides an algorithm that simulates the implementation and

solves the diffusion equation, taking into account the trapping and annihilation of positrons inside the material.

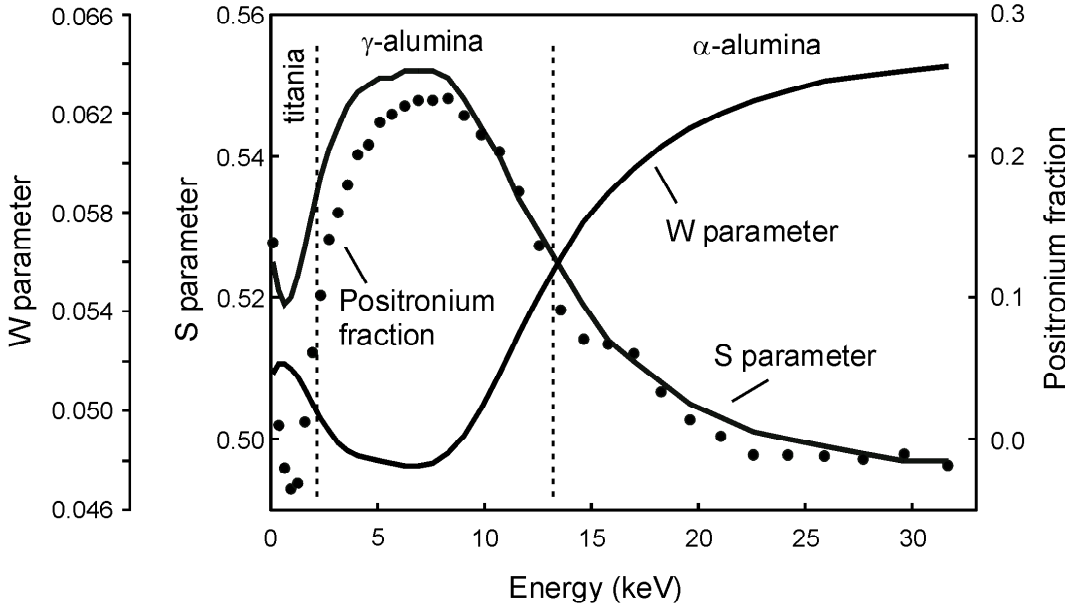

Figure 4.11: Positronium fraction, S and W parameters as a function of positron implementation energy.

The ~80 nm thick titania top layer, ~550 nm thick γ-alumina intermediate layer, and part of the α-alumina support structure are indicated in the figure. In terms of positron annihilation the formation of positronium, a hydrogen-like quantum-mechanical particle of ~1 nm size consisting of a positron-electron pair, in a layer indicates a percolative pore structure with pore size >1 nm. The presence of positronium is revealed by the observation of certain γ-events that occur when positronium is (self)annihilated [39]. As shown in the figure the positronium fraction in the titania top layer was very low, which strongly suggests that the pore size in this layer was smaller than 1 nm, thereby making it impossible for positronium to form. In contrast, a high fraction of positronium was formed in the underlying γ-alumina layer, which is known to have a percolative pore structure with pore sizes in the range of 4.5-7 nm. The *S* parameter in the titania layer, which is a measure of the porosity of a layer, was found to have values in between that of γ-alumina (55% porosity) and α-alumina (30% porosity), indicating porosity higher than the value calculated from reflectivity measurements. The *W* parameter, which is related to the chemical nature of the pore walls, varied little over the different layers, which is due to their oxidic nature.

4.3.4 Permeation properties

Single gas permeances *F*, i.e., the molar gas flux per unit driving force, of several gases are shown in Figure 4.12. The permeance of microporous silica [48] calcined at 400 °C is shown for comparison. Clearly, microporous titania allows diffusion of larger molecules than silica, which indicates the presence of larger pores than in silica. The ideal H_2/n-C_4H_{10} permselectivity was found to be 9-12, while the theoretical upper limit for Knudsen diffusion is ~5.4. With the exception of SF_6 the ideal permselectivities $F_{H_2}/F_{C_xH_y}$ of all gases exceeded the theoretical upper limit for Knudsen (mesopore) diffusion [48]. This indicates that micropore diffusion plays a dominant role in the transport of alkanes through this membrane. The higher flux of SF_6 may be attributed to its inertness, i.e low and/or weak adsorption on the pore surface, and hence to a lower contribution of surface diffusion. In contrast, hydrocarbons are condensable gasses that may adsorb strongly to the surface.

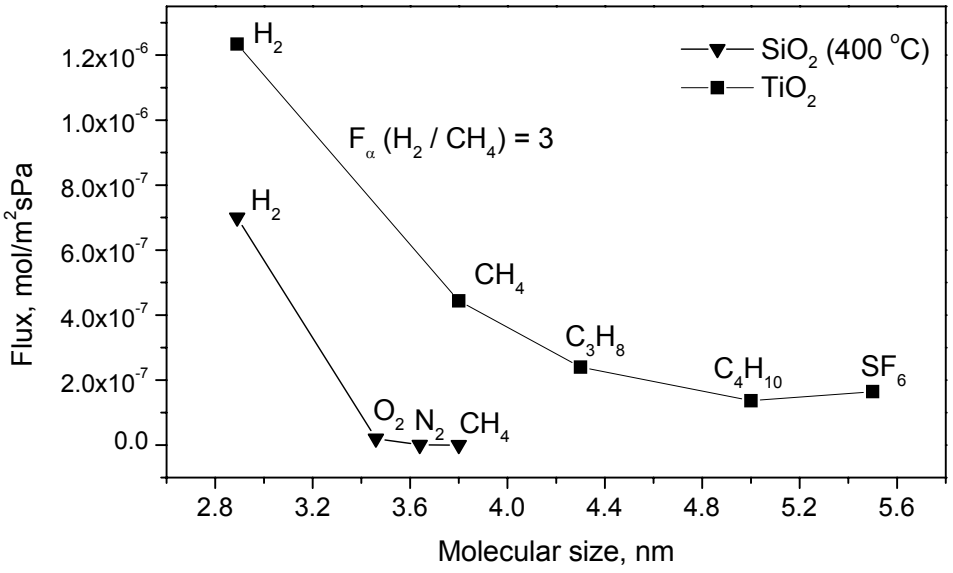

Figure 4.12: Single gas permeances of gases with various kinetic diameter through a 100 nm thick microporous titania membrane at 200 °C and comparison with 400 °C-calcined microporous silica.

Figure 4.13 shows the volumetric water flux at steady state. A linear dependency between flux and pressure applied over the membrane is observed, which indicates that the pressure difference is the only driving force for permeation. Relatively low fluxes of 3-6 dm^3/m^2h were measured in the pressure range of 9 - 16 bar, which are typical values for a microporous material. The same graph (Figure 4.13) shows results obtained on a macroporous α-alumina support (pore size ~100 nm [31]) and an α-alumina supported

mesoporous γ-alumina nanofiltration membrane (pore size ~5.0 nm, layer thickness ~1 μm [31]) for the sake of comparison [40]. The low total permeance (J/ΔP) of ~0.4 dm^3/m^2h bar of the microporous titania layer can be expected in view of the microporous nature of this material [41]. Corrected for the support contribution, the permeability of the microporous titania layer is B^0 ~$1.0 \cdot 10^{-16}$ m. For mesoporous systems such as γ-alumina and anatase, B^0 values are typically in the range of 10^{-15}-10^{-14} m (as shown in Chapter 3 of this thesis), i.e., 1 to 2 orders of magnitude larger.

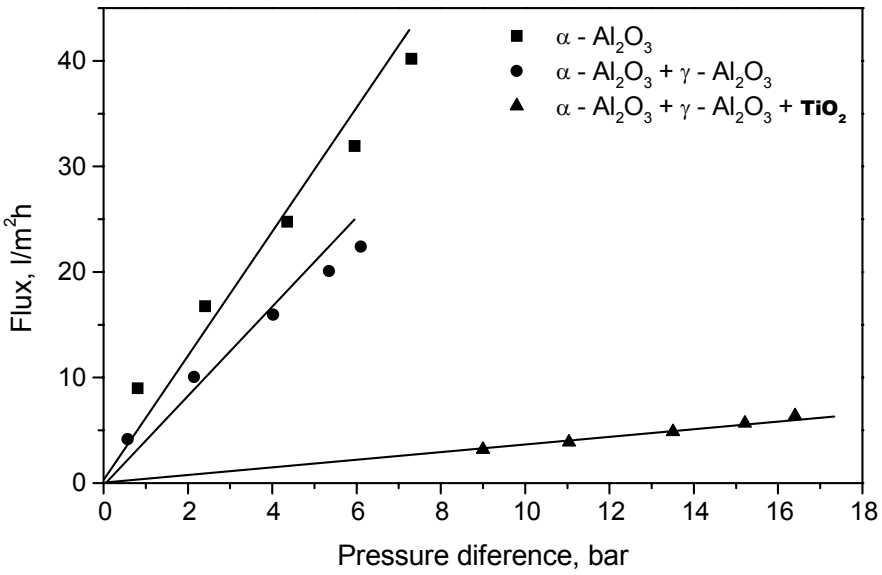

Figure 4.13: Water fluxes as a function of pressure for an α-alumina support, γ-alumina coated support and titania coated γ-alumina membranes .

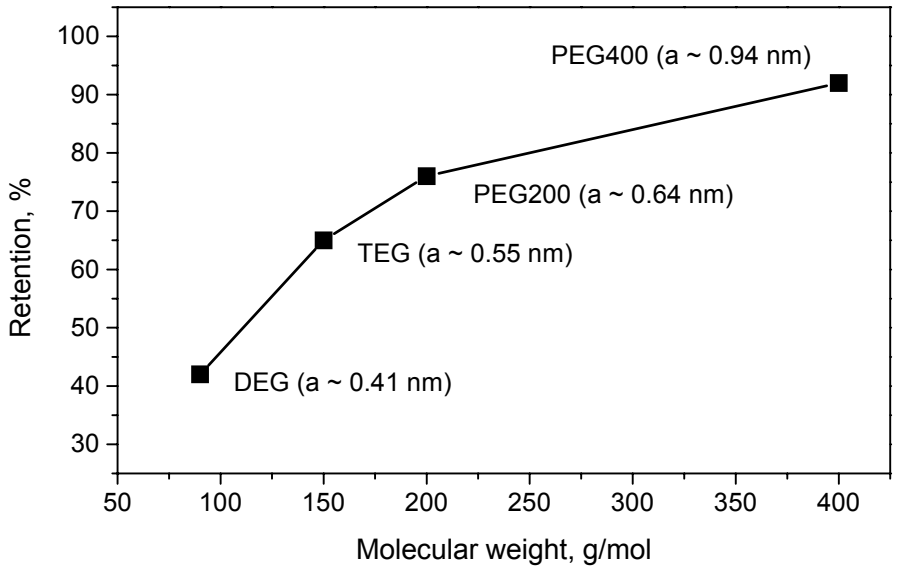

Figure 4.14: Retention behaviour of microporous titania membrane.

The maximum pore size of the titania membrane was also estimated by nanofiltration tests with solutions containing ethylene glycol based compounds with molecular weights in the range of 60-400 g/mol. The molecular weights of the glycol molecules were correlated with their molecular sizes via the Stokes radius model, according to the equation:

$$a \approx 0.1673 \cdot M^{0.557}, \tag{4.6}$$

where a is the Stokes radius in Å, and M is the molecular weight in g/mol [28,49].

As can be seen in Figure 4.14, the retention of ethylene-glycol molecules increases with molecular size, and exceeds a value of 90% for PEG, M_w=400 g/mol. A relatively high retention is observed for all employed molecular sizes.

Molecular weight cut-offs of microporous titania membranes were reported as <200 g/mol, and <500 g/mol by Van Gestel *et al.* [30] and Voigt *et al.* [28], respectively. Furthermore, higher total permeabilities (not corrected for the support contribution) were reported by both authors in comparison with the present work: a permeability of around 2 l/m^{2}hbar was reported by Van Gestel *et al*., and ~20 l/m^{2}hbar by Voigt *et al.* [28,30]. The lower permeability measured in this work can be a consequence of the low porosity of the material. However, it should be noted that in all cases the permeability was determined from pure water flux measurements, while the cut-off measurements were either carried out with solutions containing one type of organic molecule (present work), or with mixtures of molecules with a wide range of molecular sizes [28,30]. The combination of low molecular cut-off and high water permeability as reported by Van Gestel and Voigt may possibly indicate pore blocking by large organic molecules. Therefore, the pure water flux indicates a material with larger pores and/or porosity, while adsorption or physical clogging of the pores determines their molecular cut-off values.

Taking the calculated Stokes radii (Eq. 4.6) of various molecules into account, the pore size of the titania membrane can be estimated to be ≤0.9 nm. Although the molecular weight cut-off measurements can only give a rough estimate of a membrane pore size, the result is in good agreement with the observations of the other used characterisation techniques. This confirms the successful formation of a stable, defect-free titania membrane with pore size in a sub-nanometer range.

4.4 Conclusions

Variation of precursor, hydrolysis and inhibition ratios, and peptisation conditions leads to significant differences in the sols and microstructural properties of the final microporous materials. Depending on process conditions, sols with titanium polymeric species down to 2 nm in diameter and a stability of at least one month can be obtained. The use of titanium-tetra-ethoxide is shown to yield the smallest sol particles, and these are found to be highly branched polymeric chains. Stable polymeric sols can also be obtained from titanium precursors with iso-propoxide and n-butoxide side groups. Hydrolysis ratios below 2, and pH values below 3 are crucial for the formation of transparent, stable polymeric sols.

The upper limit of thermal stability of the amorphous phase of the unsupported material is ~300 °C. Calcination at higher temperatures leads to the crystallization of material into anatase. The calcined material exhibits microporosity, with pore sizes mainly in the sub-nanometer range, and an overall porosity of ~34%. A small number of larger mesopores with size ~3.5 nm is also present.

Highly reproducible amorphous microporous titania layers can be obtained on both mesoporous γ-alumina and titania/zirconia coated substrates. The upper limit of thermal stability of the amorphous phase in thin layer form is ~425 °C. Calcination at higher temperatures leads to crystallization into anatase, accompanied by a collapse of the microstructure and layer cracking. Moreover, the material shows a high chemical stability. Although a technique that would directly measure pore size distribution is not available, the gathered results from reflectivity, positron annihilation, permporometry and molecular cut-off experiments indicate the formation of a defect-free titania membrane, with pore size ≤0.9 nm and porosity ~18%. The liquid permeation experiments showed a high potential for these membranes in nanofiltration, and possible application in gas separation and pervaporation.

References

1. C.J. Brinker, "Sol-gel science: the physics and chemistry of sol-gel processing", Harcourt Brace Jovanovich, Boston, 1990.
2. H. Schmidt, "Chemistry of material preparation by the sol-gel process", J. Non-Crys. Solids, 100 (1988) 51-64.
3. A.M. Buckley, M. Greenblatt, "The sol-gel preparation of silica gels", J. Chem. Educ. 71,7 (1994) 599 – 601.
4. B.N. Nair, K. Keizer, T. Okubo, S.I. Nakao, "Evolution of pore structure in microporous silica membranes: sol-gel procedures and strategies", Adv. Mater. 10 (1998) 249-252.
5. R.M. de Vos, H. Verweij, "High-selectivity, High-flux silica membranes for gas separation", Science 279 (1998) 1710-1711.
6. H.M. van Veen, Y.C. van Delft, C.W.R. Engelen, P.P.A.C. Pex, "Dewatering of organics by pervaporation with silica membranes", Sep. Purif. Tech. 22-23 (2001) 361-66.
7. J. Sekulic, M.W.J. Luiten, J.E. ten Elshof, N.E. Benes, K. Keizer, "Microporous silica and doped silica membrane for alcohol dehydration by pervaporation", Desalination, 148 (2002) 19-23.
8. J. Livage, M. Henry, C. Sanchez, "Sol-gel chemistry of transition metal oxides", Prog. Solid State Chem. 18 (1988) 259-268.
9. J. Blanchard, S. Barboux-Doeuff, J. Maquet, C. Sanchez, "Investigation on hydrolysis-condensation reaction of titanium (IV) butoxide", New J. Chem. 19 (1995) 929-935.
10. D.C. Bradley, R.C. Mehrota, D.P. Gaur, "Metal alkoxides", Academic Press, London, 1978.
11. F. Babonneau, C. Sanchez, J. Livage, "Spectroscopic characterisation of sol-gel processing,", J. Non-Cryst. Solids 106 (1988) 170-178.
12. C. Sanchez, J. Livage, M. Henry, F. Babonneau, "Chemical modification of alkoxide precursors", J. Non-Cryst. Solids 100 (1988) 65-73.
13. J. Livage, M. Henry, J.P. Jolivet, C. Sanchez, "Chemical synthesis of fine powders" MRS Bull. (1990) 18-25.
14. M. Kallala, C. Sanchez, B. Cabane, "SAXS study of gelation and precipitation in titanium-based systems", J. Non-Cryst. Solids 147-148 (1992) 189-196.
15. S. Barboux-Doeuff, C. Sanchez, "Synthesis and characterization of titanium oxide-based gels synthesized from the acetate modified titanium butoxide precursors" Mat. Res. Bull. 29 (1993) 1-14.
16. A. Bleuzen, S. Barboux-Doeuff, P. Flaud, C. Sanchez, "Rheological study of titanium oxide-based gels", Mat. Res. Bull. 29, 12 (1994) 1223-1232.
17. S. Benfer, U. Popp, H. Richter, C. Siewert, G. Tomandl, "Development and characterization of ceramic nanofiltration membranes", Sep. Purif. Tech. 22-23 (2001) 231-238.
18. B.N. Nair, "Structure-property relations in silica sols, gels and molecular-sieving membranes" PhD Thesis, University of Tokyo, 1998.

19. R.W. van Gemert, F.P. Cuperus, "Newly developed ceramic membranes for dehydration and separation of organic mixtures by pervaporation", J. Membr. Sci. 105 (1995) 287-291.
20. G.P. Fotou, Y.S. Lin, S. E. Pratsinis, "Hydrothermal stability of pure and modified microporous silica membranes", J. Mater. Sci. 30 (1995) 2803-2808.
21. H. Imai, H. Morimoto, A. Tominaga, H. Hirashima, "Structural changes in sol-derived SiO_2 and TiO_2 films by exposure to water vapour", J. Sol-Gel Sci. Tech. 10 (1997) 45-54.
22. T. Van Gastel, "Alumina and titania multilayer membranes for nanofiltration in aqueous solutions and non-aqueous solvents - Preparation, characterization and chemical stability", PhD Thesis, Catholic University Leuven, 2003.
23. Q. Xu, M.A. Anderson, "Sol-gel route to synthesis of microporous ceramic membranes: preparation and characterization of microporous TiO_2 and ZrO_2 xerogels", J.Am. Ceram. Soc. 77,7 (1994) 1939-1945.
24. Q. Xu, M.A. Anderson, "Synthesis of porosity controlled ceramic membranes", J. Mater. Res. 8,5 (1991) 1073-1079.
25. R.A. Peterson, M.A. Anderson, C.G. Hill, "Development of TiO_2 membranes for gas phase nanofiltration", J. Membr. Sci. 94 (1994) 103-111.
26. R.A. Peterson, E.T. Webster, G.M. Niezyniecki, M.A. Anderson, C.G. Hill, "Ceramic membranes for novel separations", Sep. Sci. Tech. 30, 7-9 (1995) 1689-1710.
27. P. Puhlfürss, A. Voigt, R. Weber, M. Morbé, "Microporous membrane with a cut off <500 Da", J. Membr. Sci. 174 (2000) 123-133.
28. I. Voigt, P. Puhlfuss, J. Topfer, "Preparation and characterization of microporous TiO_2 membranes", Key Engin. Mater. 132-136 (1997) 1735-1739.
29. T. Van Gestel, C. Vandecasteele, A. Buekenhoudt, C. Dotremont, J. Luyten, R. Leysen B. Van der Bruggen, G. Maes, "Alumina and titania multilayer membranes for nanofiltration: preparation, characterization and chemical stability", J. Membr. Sci. 207,1 (2002) 73-89.
30. T. Van Gestel, C. Vandecasteele, A. Buekenhoudt, C. Dotremont, J. Luyten, B. Van der Bruggen, G. Maes, "Corrosion properties of alumina and titania NF membranes", J. Membr. Sci. 214,1 (2003) 21-29.
31. R.J. van Vuren, B.C. Bonekamp, K. Keizer, R.J.R. Uhlhorn, H.J. Veringa A.J. Burggraaf, "Formation of ceramic alumina membranes for gas separation" in "High Tech Ceramics", Edited by P. Vincenzini. Elsevier Science Publ. B.V., Amsterdam, Oxford, New York, Tokyo, 1987, pp. 2235-2245.
32. J. Sekulić, A. Magrasso, J.E. ten Elshof, D.H.A. Blank, "Influence of ZrO_2 doping on microstructure and liquid permeability of mesoporous TiO_2 membranes", Micropor. Mesopor. Mater. 72 (2004) 49-57
33. F.F. Lange, "Powder processing science and technology for increased reliability", J. Am. Ceram. Soc. 72,1 (1989) 3-15.
34. J. Teixeira, "Small-angle scattering by fractal systems", J. Appl. Cryst. 21 (1988) 781-786.
35. F. Rouquerol, J. Rouquerol, K. Sing "Adsorption by powders and porous solids: principles, methodology and applications" Academic Press, San Diego, 1999.
36. V. Kogan, K. Bethke, R. de Vries, "Applying X-rays in material analysis", Nuclear Instruments and Methods in Physics Research (A), 509 (2003) 290-293.

37. S. Kundu, "Interface modification of Ag/Co system: X-ray reflectivity study ", Nuclear Instruments and Methods in Physics Research (B) 212 (2003) 489-495.
38. A. van Veen, R. Escobar Galindo, H. Schut, S. W. H. Eijt, C. V. Falub, A. R. Balkenende, F. K. de Theije, "Positron beam analysis of structurally ordered porosity in mesoporous silica thin films", Mater. Sci. Eng. (B) 102, 1-3, (2003) 2-8.
39. A. van Veen, H. Schut, M. Clement, J.M.M. de Nijs, A. Kruseman, M.R. Ijpma, "VEPFIT applied to depth profiling problems", Appl. Surf. Sci. 85 (1995) 216-224.
40. S. Roy Chowdhury, R. Schmuhl, J.E. ten Elshof, K. Keizer, D.H.A. Blank, "Pore size and surface chemistry effects on the transport of hydrophobic and hydrophilic solvents through mesoporous γ-alumina and silica MCM-48", J. Membr. Sci. 225,1 (2003) 177-186.
41. T. Tsuru, T. Sudoh, T. Yoshioka, M. Asaeda, "Nanofiltration in non-aqueous solutions by porous silica–zirconia membranes", J. Membr. Sci. 185, 2, (2001) 253-261.
42. J. Ragai, "Effect of preparative pH and ageing media on the crystallographic transformation of amorphous TiO_2 to anatase and rutile", Colloids and Surfaces, 61 (1991) 97-101.
43. T. Yamada, K. Johkan, T. Okuhara, "Micropore size distribution by argon porosimetry for cesium hydrogen salts of 12-tungstophosphoric acid", Micropor. Mesopor. Mater. 26 (1998) 109-115.
44. A. Saito, H.C. Foley, "Argon porosimetry of selected molecular sieves: experiments and examination of the adapted Horvath-Kawazoe", Micropor. Mater. 3, 4-5, (1995) 531-542.
45. E.A. Barringer, H.K. Bowen, "High-purity, monodisperse TiO_2 powders by hydrolysis of titanium tetraethoxide; Synthesis and physical properties", Langmuir, 1,4 (1985) 414-420.
46. K-N. P. Kumar, "Nanostuructured ceramic membranes", PhD Thesis, University of Twente, 1993, pp 96-99.
47. E.G. Liniger, R. Raj, D.B. Marshall, "The instability of polycrystalline thin films: experiments and theory," J. Mater. Res. 5,1 (1990) 151-160.
48. A.J. Burggraaf, "Fundamentals of inorganic membrane science and technology", Ed. by A.J. Burggraaf, L. Cot, Elsevier, Amsterdam 1996, pp. 1-35, 331-433.
49. S. Singh, K.C. Khulbe, T. Matsuura, P. Ramamurthy, "Membrane characterisation by solute transport and atomic force microscopy", J. Membr. Sci. 142 (1998) 111–127.

5

Pervaporation separation of ethylene glycol - water mixtures using microporous titania membranes

Abstracts

In this chapter the pervaporation characteristics of amorphous microporous titania membranes in dewatering of organic mixtures are described. The influence of process parameters like temperature and feed component concentrations on the pervaporation properties of α-Al_2O_3 – anatase $TiO_2(ZrO_2)$ – amorphous TiO_2 membranes were studied. The microporous titania membrane was found to be non-selective for small molecules (e.g. lower alcohols), because its relatively large micropores exclude molecular sieving as possible separation mechanism. However, high separation factors and reasonable fluxes were measured for ethylene glycol/water mixtures with ≤5 wt% water in the temperature range of 40-90 °C. The results can be explained on the basis of an adsorption-diffusion model. Under dynamic conditions, the membrane becomes selective for water, probably because of adsorption of ethylene glycol on the membrane material surface. As the level of interaction between ethylene glycol and the pore wall is rather high, the adsorbed ethylene glycol molecules cannot diffuse and insufficient space is left for other ethylene glycol molecules to pass. Therefore, only water transport occurs, although the layer of adsorbed ethylene glycol molecules decreases the effective pore size substantially, so that relatively low water fluxes (<0.6 kg/m^2h) are obtained under these conditions. At higher water contents, the ethylene glycol adsorbed on the pore wall is replaced by water and the effective pore size widens. Consequently, the flux increases, while the membrane selectivity disappears.

5.1 Introduction

Pervaporation, in its simplest form, is an energy efficient combination of membrane permeation and evaporation [1]. In a pervaporation process, components of a liquid feed permeate through a membrane and evaporate into the downstream due to the partial pressure on the permeate side being lower than the saturation vapour pressure. The fact that feed components undergo a phase change makes pervaporation unique among membrane processes. The driving force behind the separation process is the difference in chemical activity of components in the feed and the permeate. Separation occurs because of different rates of sorption and diffusion of the feed components in the membrane. One component preferentially permeates across the membrane due to a concentration or vapor pressure gradient. A vacuum applied to the permeate side is coupled with a cold trap for immediate condensation of the permeated vapours. Another method of inducing a partial pressure gradient is to sweep an inert gas over the permeate side of the membrane. These methods are referred as vacuum and sweep gas pervaporation, respectively. Similar to pervaporation, in vapour permeation one of the components is separated from the vapour phase feed mixture by gas transport through a membrane.

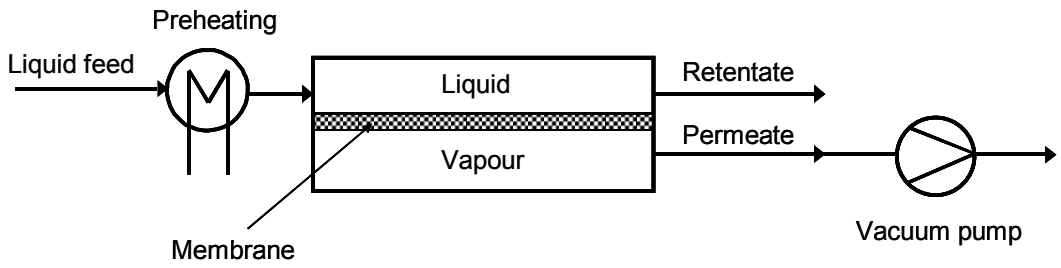

Figure 5.1: Schematic representation of the pervaporation process.

A schematic representation of the vacuum pervaporation process is shown in Figure 5.1. The feed is allowed to flow along one side of the membrane and a fraction of the feed (permeate) passes through the membrane, leaving the reactor as vapour on the opposite side of the membrane. The permeate is collected in the liquid state after condensation. The retentate, composed of the feed materials that did not pass through the membrane, is usually recycled to the feed container in order to increase process efficiency.

The separation performance of a membrane is characterised by two parameters: flux and separation factor. Flux is defined as the rate of permeation of feed components through a

unit of membrane surface area during a unit of time. The most commonly used flux unit in pervaporation processes is kg/m^2 h:

$$J_i = \frac{m_i}{A_m \cdot t} \tag{5.1}$$

J_i is the flux of component *i* or the total flux, and m_i is the mass of permeated component *i* or the total permeate mass, through an effective membrane surface area A_m during time *t*.

Two types of selectivities are defined for a membrane: ideal selectivity and actual selectivity. The ideal selectivity is simply the ratio of fluxes of pure substances through a membrane, and the actual selectivity of a membrane in a binary system is defined as the ratio of concentrations of components *i* and *j* in the permeate relative to that in the feed:

$$\alpha = \frac{y_i / x_i}{y_j / x_j}, \tag{5.2}$$

in which *y* and *x* are the fractions of components *i* and *j* in the permeate and feed, respectively.

The selectivity of a membrane is strongly influenced by two factors: the affinity of the membrane towards one (or more) component(s) of the feed, and the ease of diffusion of the permeating molecules through the membrane matrix. The overall selectivity of a membrane is defined as the product of sorption selectivity, α_S, and diffusion selectivity, α_D [2,3]:

$$\alpha = \alpha_S \cdot \alpha_D \tag{5.3}$$

Either one, or both of these selectivities contribute to the preferential permeation of feed components through a given membrane. Therefore, the choice of a proper membrane material for a specific separation process is crucial. In most cases, the selectivity of a membrane is mainly governed by the diffusion component. However, a material with a high affinity towards one component of the feed may also lead to a high selectivity. Hence sorption can also be a determining factor in membrane selectivity.

In addition to specific characteristics of feed components and membrane, the operating parameters also influence the overall performance of a pervaporation process. These parameters include feed temperature, concentration of the components in the feed, and downstream pressure [1]. It is generally believed that feed pressure has an insignificant effect on the permeability and selectivity of pervaporation membranes.

In principle, pervaporation and vapour permeation technologies have better separation capacity and energy efficiency than competing distillation, adsorption and extraction technologies, and their application may lead to considerable energy reductions [3]. The main advantage of pervaporation over distillation is that it is independent of the relative volatilities of the components, and is therefore not limited by the vapour–liquid equilibrium. Pervaporation is considered to be an attractive alternative to other separation methods for a variety of processes. For example, with the low temperatures and pressures involved in pervaporation, there are often cost and performance advantages for the separation of constant-boiling azeotropes [4]. Pervaporation is also used for the dehydration of organic solvents, the removal of organics from aqueous streams, as well as various organic/organic separations [4-6]. Additionally, pervaporation has emerged as a good choice for the separation of heat sensitive products [7].

Using well-known polymeric membranes, pervaporation established itself relatively quickly as a new type of unit operation [3,8]. However, the applicability of such membranes is limited to temperatures up to ~130 °C, while their performance in terms of flux and selectivity is often limited to a narrow range of solvents and feed concentrations. On the other hand, zeolite and microporous ceramic membranes exhibit superior thermal, mechanical and chemical stabilities. Zeolite membranes are known to be very selective because of their well-defined pore structure and size and are particularly useful for dehydration processes in which low water concentrations should be reached [8-12]. Also, the separation of organic components using zeolites with high Si/Al ratio has been reported [8,9]. However, a disadvantage of some zeolites is that due to their ion-exchange nature they may be susceptible to degradation in acidic and alkaline media. On the other hand, ceramic pervaporation membranes are more robust and exhibit higher fluxes, although they are often less selective than zeolite and polymeric membranes [8].

Generally, ceramic membranes are virtually chemically inert in non-aqueous organic solvents and they offer high temperature stability relative to polymeric membranes. However, their instability in aqueous corrosive liquids like strong acids and alkaline solutions has often been mentioned [13-15]. One of the most commonly applied systems α-alumina / γ-alumina / silica is stable in a very narrow range of pH of 4-10 that is mainly determined by the poor chemical stability of the γ-alumina phase [13-15]. If γ-alumina would be replaced by crystalline titania, and silica with amorphous microporous titania, it is expected that the chemical stability the resulting system would be much higher.

In this chapter, the pervaporation characteristics of amorphous microporous titania membranes in the separation of water from selected binary liquids are studied. The application window is evaluated based on the separation properties of the membranes for various organic solvent/water mixtures. The influence of process parameters (temperature and water concentration in the feed) on pervaporation properties is investigated and interpreted on the basis of an adsorption-diffusion model.

5.2 Experimental

5.2.1 Membranes

The membrane system α-Al_2O_3 - $TiO_2(ZrO_2)$ – TiO_2 was applied in the separation of organic liquid/water mixtures. α-Al_2O_3 was used as a macroporous support. These supports are disc-shaped, with a diameter of 39 mm, a thickness of 2 mm, a mean pore radius of 100 nm, and a porosity of ~30% [16]. The intermediate (mesoporous) layer was either anatase titania (calcined at 450 ^oC), or zirconia-doped titania containing 5-20 mol% of zirconia and calcined at 450-700 ^oC [17,18]. The top layer, made of amorphous microporous titania, had an average thickness of 50-100 nm, and a maximum pore size of ~0.9 nm [19].

5.2.2 Pervaporation

Pervaporation experiments were carried out using a laboratory scale pervaporation unit, shown in Figure 5.2.

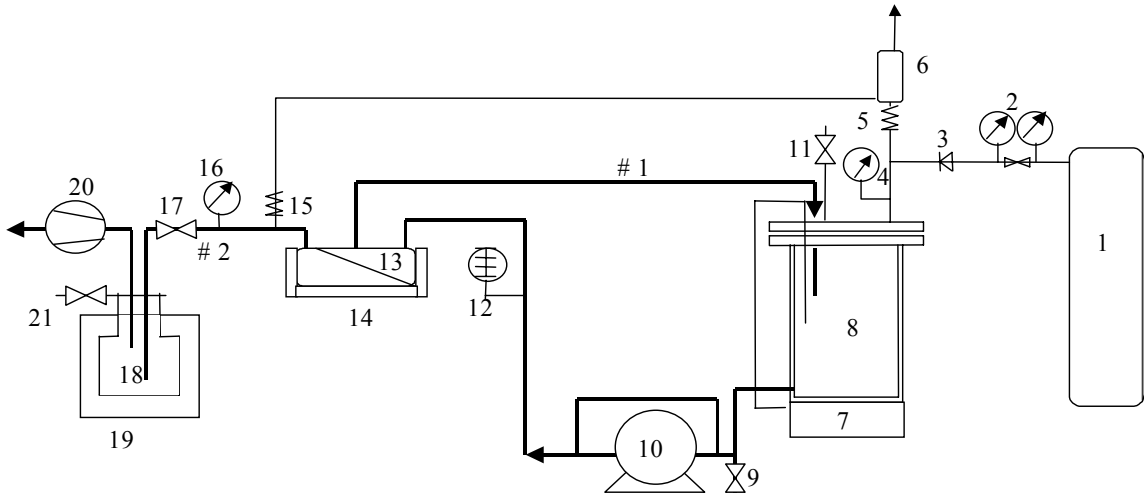

Figure 5.2: Pervaporation unit.

The main parts of this unit are a nitrogen bottle (marked as 1), feed container (8), membrane module (13), oil bath (14), membrane pump (10), vacuum pump (20), cold trap (18), together with a number of controlling and safety valves, flow and temperature meters. The unit is built to withstand pressures of up to 7 bar, and temperatures of up to 120 ^{o}C. The membrane module (13) is replaceable and adaptable for flat and tubular membrane geometries. The feed mixture, contained in a 2 l heated vessel under a pressure of 2-3 bar, is pumped continuously in the pulls mode through the feed compartment of the pervaporation unit, where it came into direct contact with the top layer of the membrane. The retentate is recycled to the feed vessel. The permeate side of the membranes was kept under near-vacuum (6-8 mbar) with a vacuum pump. Steady state fluxes were determined by collecting the permeate side vapors in an ethanol-based cold trap and measuring the weight increase with time. The feed and permeate compositions were determined by Karl Fischer titration (784 KFP Titrino, Metrohm, Switzerland).

The pervaporation experiments that are described in this chapter were performed in the temperature range of 40-90 °C. The feed mixtures were binary liquids with 2-20 wt% water (on total weight) in 2-propanol, 2-butanol, p-dioxane or ethylene-glycol (all obtained from Merck).

5.3 Results and discussion

Screening pervaporation experiments with feed mixtures containing 2-propanol, 2-butanol or p-dioxane showed no separation in the case of propanol and butanol, and low separation factors (α=2-4) for p-dioxane/water mixtures. On the other hand, excellent separation factors were measured for ethylene glycol/water mixtures. The poor separation in the case of alcohols or dioxane/water mixtures can be explained by the relatively large pore size (~0.9 nm) of the microporous titania membrane in comparison with the molecular sizes of the permeating species, which excludes the possible occurrence of a molecular sieving mechanism. Although it is difficult to identify reliable values for the molecular diameters of permeants, approximate values as adopted from both literature sources and theoretical modelling are ~0.24, ~0.45, ~0.55, and ~0.7 nm for water, 2-propanol, 2-butanol and p-dioxane, respectively [20-22]. However, as will be discussed below in detail, water concentrations in the permeate close to 100% as were measured under some conditions for ethylene-glycol/water mixtures can hardly be explained by the difference in kinetic diameter between ethylene-glycol (~0.45 nm) and water (~0.24 nm).

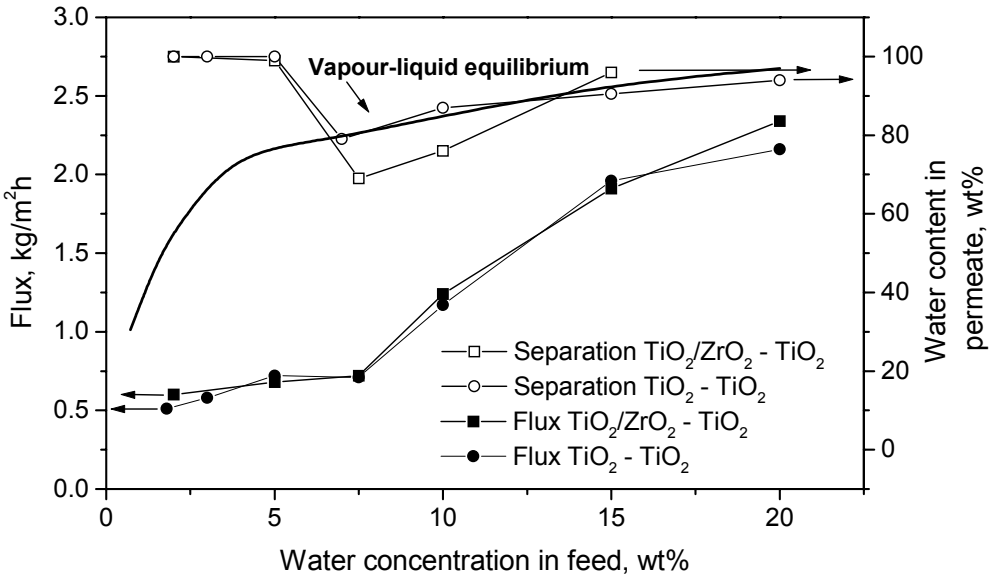

Figure 5.3: Influence of water content in the feed on separation and permeation properties of a microporous titania membrane at 80 °C.

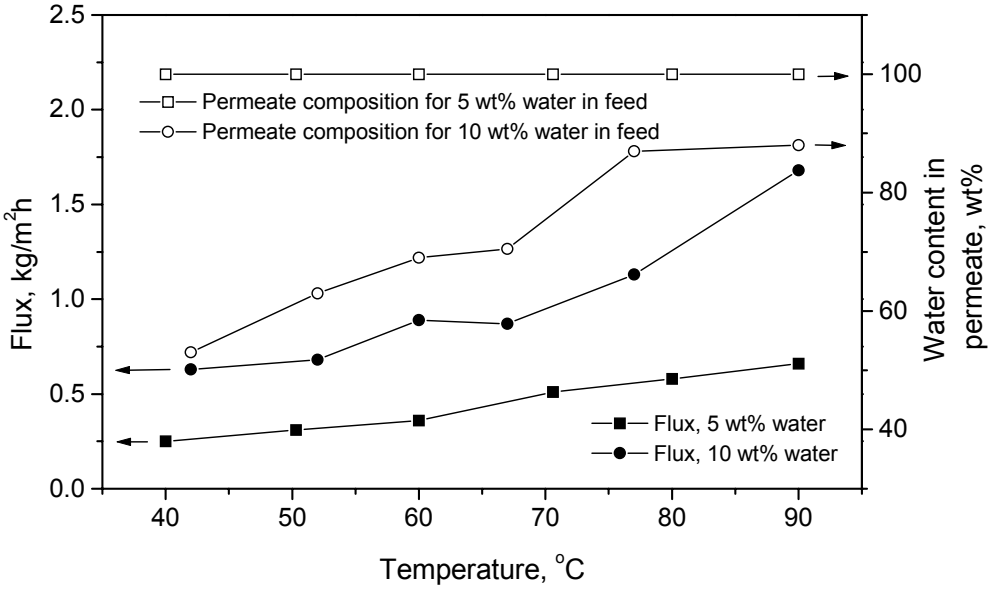

Figure 5.4: Influence of temperature on separation and permeation properties of a microporous titania membrane at feed compositions of 5 and 10 wt% water / 95 and 90 wt% ethylene-glycol, respectively.

The influence of temperature and water concentration in the feed on the separation properties of microporous titania membranes in the pervaporation of ethylene-glycol/water mixtures are shown in Figure 5.3 and 5.4. As the separation factor reaches extremely high values in some cases, the separation performance is shown in terms of water concentration in the permeate instead of separation factor.

In Figure 5.3, separation properties are shown for both an anatase-supported microporous membrane, and for a zirconia-doped titania-supported microporous membrane. No significant differences in flux and separation factors between these two systems can be observed, which confirms the reproducibility of results and the absence of an influence of the intermediate layer on the pervaporation performance of the microporous top layer.

In general, high separation factors (permeate contained almost 100% water) were measured at water contents of 2-5 wt% in the feed. In the same range of feed compositions, rather low fluxes were measured (0.25-0.66 kg/m^{2}h), indicating that water transport was substantially hindered by the presence of glycol molecules. It is most likely that water and ethylene glycol transport take place by an adsorption-diffusion mechanism [20,22]. Since glycol has a relatively large dipole moment (2.28 D) and two –OH groups, it is expected that relatively strong attractive interactions between ethylene glycol and the titania surface will occur, resulting in substantial ethylene glycol sorption on the titania pore wall. In addition, ethylene glycol molecules might form hydrogen bonded macroclusters, due to their dihydric nature, as suggested by Kurihara *et al*. [23]. Interaction between ethylene glycol molecules and pore walls, as well as interaction between "free" and adsorbed molecules may lead to partially filled pores where the small water molecule can still pass, but the transport of larger ethylene glycol molecules is inhibited almost completely. The adsorbed ethylene glycol molecules will probably not diffuse quickly because of their strong H-bond interactions with the titania surface, while the remaining unsorbed ones can not pass due to lack of space. Such a situation would lead to an increased selectivity for water transport. At the same time, the effective space available for diffusion of water molecules will be smaller than when no ethylene glycol sorption occurs, which will effectively result in relatively low water fluxes.

As shown in Figure 5.3, the separation factor decreased considerably when more than 5 wt% water was present in the feed. At higher water contents the composition of the permeate side stream was essentially similar to the equilibrium vapour composition of the liquid feed [24], indicating "free" flow of vapour molecules through the titania membrane, i.e., the separation factor is entirely due to preferential evaporation of water from the feed, rather than being caused by the membrane. We interpret these results by assuming that an increasing number of water molecules is available for adsorption with increasing water concentration in the feed. At higher water contents, it is likely that a stronger competition between water (dipole moment 1.85 D) adsorption and ethylene glycol adsorption occurs.

Beyond a certain water concentration the water molecules will effectively replace the adsorbed ethylene glycol molecules. Moreover, ethylene glycol molecular clusters are very likely to be disturbed with the fast diffusing water species. Since water molecules are considerably smaller than the ethylene glycol molecules, steric blocking of pores will not be pronounced and the effective pore size will be close to the "real" pore size. Consequently, a higher flux and a lower separation factor are expected at higher water concentrations, in agreement with the experimental findings.

Similar behavior was observed by Shah *et al.* for DMF/water mixtures through hydrophilic zeolite NaA membranes [11]. They attributed the low fluxes to the effect of strong DMF adsorption on the internal zeolite surface, thereby blocking the channels for water transport. For microporous silica membranes, Ten Elshof *et al.* compared the pervaporation characteristics of methanol/water, 1,4 dioxane/water and N,N-dimethyl formamide (DMF)/water mixtures, and observed anomalously low fluxes (<0.5 kg/m^2h) in combination with reasonable separation factors for DMF/water mixtures [22]. The authors explained the behaviour by strong adsorption of DMF molecules on the silica surface, due to their large dipole moment, which caused an effective pore size decrease. Hence, DMF molecules that were in the pores diffused slowly, hindering water transport as well. Although no data on the adsorption behaviour of ethylene glycol on titania was found in the available literature, the adsorption can be considered to be qualitatively similar for different oxides. Therefore, the types of interactions described for amorphous silica surfaces can be expected for titania as well.

A gradual increase of flux was measured with increasing temperature, as shown in Figure 5.4. Surprisingly, the separation factor did not change with temperature when the water contents in the feed was 5 wt%. In this case, the permeate contained 100% water anywhere in the temperature range 40-90 ^{o}C. However, when the water content in the feed was increased to 10 wt%, the water content in the permeate was slightly below the vapour-equilibrium line, and both flux and separation factor increased with increasing temperature.

The total and partial fluxes in pervaporation generally show an Arrhenius type temperature dependency, as described by Feng and Huang [25].

$$J_i = \frac{J_{0i}}{l}(P_{i0} - P_{i1}), \tag{5.4}$$

$$\frac{J_i}{\Delta P_i} = \frac{J_{oi}^{\ 0}}{l} e^{\frac{-E_{act,i}}{R \cdot T}}, \qquad (5.5)$$

where J is the permeate flux of component i, $\Delta P_i=(P_{i0} - P_{i1})$ the transmembrane partial pressure difference, E_{act} the activation energy of permeability, J_{oi} and $J_{oi}^{\ 0}$ prexponential factors that contain the diffusivity and solubility of component i, L the membrane thickness, R the molar gas constant, and T the temperature. As the driving force for molar transport depends on the vapour pressure, the values of E_{act} of flux (Eq. 5.4) contain a contribution from the increase of the component feed side vapor pressures with increasing temperature. The temperature dependency of the permeability $F_i=J_i/\Delta p_i$ provides a better measure to compare the thermally activated nature of transport of different species through a membrane. Therefore, the activation energy is usually calculated from Eq. 5.5, i.e. using the $\ln(J/dP) - (1/T)$ diagram [22]. The activation energies, calculated for the case of 10 wt% water in the feed mixture, are $E_{act,water}$ ~11 kJ/mol and $E_{act,glycol}$ ~10 kJ/mol, and $E_{act,water}$ ~22 kJ/mol for the case of 5 wt% water in the feed mixture.

The low separation factor (2-4) masured for the p-dioxane/water mixtures cannot be described with the concept of increased selectivity by effective pore size decrease due to strong adsorption of larger molecules, as p-dioxane is a considerably larger molecule (~0.7 nm) than ethylene glycol, and interacts relatively weakly with the pore wall (net dipole moment equal to zero, no OH groups present). The adsorption of p-dioxane molecules is therefore not competitive with the adsorption of water, hence no effectively decreased pore size due to blocking by larger molecules occurs in this case. The measured selectivity is most likely the consequence of a molecular sieving effect of dioxane molecules by the smaller pores of the titania membrane.

5.4 Conclusions

The microporous titania membrane is generally non-selective for smaller molecules (e.g. lower alcohols), due to its relatively large micropores which exclude a molecular sieving effect as a possible separation mechanism for most separations. However, under dynamic conditions the membrane may become selective for water, probably due to strong adsorption of ethylene glycol on the membrane surface. Very high selectivities (~100% water in the permeate) were measured for ethylene-glycol/water mixtures with water contents in the feed of 2-5 wt%, in the temperature range 40-90 ^{o}C. It is hypothesised that

due to strong adsorption of glycol molecules on the surface, insufficient space may be left for other glycol molecules to pass. As the interaction between glycol and pore wall is rather strong, the adsorbed glycol molecules cannot diffuse either. Therefore, only water transport can occur, although the layer of adsorbed glycol molecules decreases the effective pore size so much that low water fluxes (<0.6 kg/m^2h) are obtained under these conditions. At higher water contents, the glycol on the pore wall becomes replaced by water and the effective pore size widens. Consequently, the flux increases, while the selectivity decreases. The high separation factors obtained with glycol/water under some conditions indicate separation based on a molecular sieving mechanism. It was shown that the membrane became selective under dynamic conditions, despite the fact that the pores were insufficiently small for selective separation. According to this picture, microporous titania membranes might be applied in dewatering of various organic compounds that show strong adsorption on the internal pore surface. In general, these would be molecules with a reasonable molecular size, a large dipole moment and/or the possibility to form hydrogen bonds, e.g., ethylene-glycol, dimethyl formamide, dimethyl sulfoxide, etc.

References

1. G.H. Koops, C.A. Smolders, "Pervaporation membrane separation process", Ed. by R.Y.M Haung, Elsevier, Amsterdam, 1991.
2. S.-H. Chen, R.-M. Liou, C.-S. Hsu, D.-J. Chang, K.-C. Yu, C.-Y. Chang, "Pervaporation separation water/ethanol mixture through lithiated polysulfone membrane", J. Memb. Sci. 193, 1 (1986) 59-67.
3. X. Feng, R.Y.M. Huang, "Liquid separation by membrane pervaporation; a review, Industrial & engineering chemical research", ISSN 0888-05885, 36, 4 (1997) 1048-1066.
4. H.M. van Veen, Y.C. van Delft, C.W.R. Engelen, P.P.A.C. Pex, "Dewatering of organics by pervaporation with silica membranes", Separ. Purif. Tech. 22-23 (2001) 361-366.
5. M. Asaeda, Y. Sakou, J. Yang, K. Shimasaki, "Stability and performance of porous silica–zirconia composite membranes for pervaporation of aqueous organic solutions", J. Membr. Sci. 209, 1 (2002) 163-175.
6. R.W. Gemert, F.P. Cuperus, "Newly developed ceramic membranes for dehydration and separation of organic mixtures by pervaporation", J. Membr. Sci. 105 (1995) 287-291.
7. W. Yoshida, Y. Cohen, "Ceramic-supported polymer membranes for pervaporation of binary organic/organic mixtures", J. Membr. Sci. 213, 1-2, (2003) 145-157.
8. T. Gallego-Lizon, E. Edwards, G. Lobiundo, L. Freitas dos Santos, "Dehydration of water/t-butanol mixtures by pervaporation: comparative study of commercially available polymeric, microporous silica and zeolite membranes", J. Membr. Sci. 197, 1-2 (2002) 309-319.
9. A. Navajas, R. Mallada, C. Tellez, J. Coronas, M. Menendez, J. Santamaria, "Preparation of mordenite membranes for pervaporation of water-ethanol mixtures", Desalination 148 (2002) 25-30.
10. S. Li, V.A. Tuan, R.D. Noble, J.L. Falconer, "Pervaporation of water/THF mixtures using zeolite membranes", Ind. Eng. Chem. Res. 40 (2001) 4577-4586.
11. D. Shah, K. Kissick, A. Ghorpade, R. Hannah, D. Bhattacharyya, "Pervaporation of alcohol-water and dimethylformamide-water mixtures using hydrophilic zeolite NaA membranes: mechanisms and experimental results", J. Membr. Sci. 179 (2000) 185-192.
12. S. Li, V.A. Tuan, J.L. Falconer, R.D. Noble, "Properties and separation performance of Ge-ZSM-5 membranes", Micropor. Mesopor. Mater. 58 (2003) 137-141.
13. T. Van Gestel, C. Vandecasteele, A. Buekenhoudt, C. Dotremont, J. Luyten, B. Van der Bruggen, G. Maes, "Corrosion properties of alumina and titania NF membrane"s, J.Membr. Sci. 214, 1 (2003) 21-29.
14. T. Van Gestel, C. Vandecasteele, A. Buekenhoudt, C. Dotremont, J. Luyten, R. Leysen, B. Van der Bruggen, G. Maes, "Alumina and titania multilayer membranes for nanofiltration: preparation, characterization and chemical stability", J.Membr. Sci. 207, 1 (2002) 73-89.
15. J. Sekulic, M.W.J. Luiten, J.E. ten Elshof, N.E. Benes, K. Keizer, "Microporous silica and doped silica membrane for alcohol dehydration by pervaporation", Desalination, 148, 1-3, (2002) 19-23.

16. F.F. Lange, “Powder processing science and technology for increased reliability”, J. Am. Ceram. Soc. 72,1 (1989) 3-15.
17. R.J. van Vuren, B.C. Bonekamp, K. Keizer, R.J.R. Ulhorn, H.J. Veringa, A.J. Burggraaf, “Formation of ceramic alumina membranes for gas separation”, High Tech. Ceram. (1987) 2235-2245.
18. J. Sekulić, A. Magrasso, J.E. ten Elshof, D.H.A. Blank, “Influence of ZrO_2 doping on microstructure and liquid permeability of mesoporous TiO_2 membranes”, Micropor. Mesopor. Mater. 72 (2004) 49-57.
19. J. Sekulić, J.E. ten Elshof, D.H.A. Blank, “A microporous titania membrane for nanofiltration and pervaporation”, Adv. Mater. 16,17 (2004) 1546-1550.
20. T.C. Bowen, J.C. Wyss, R.D. Noble, J.L. Falconer, “Measurements of diffusion through a zeolite membrane using isotopic-transient pervaporation”, Micropor. Mesopor. Mater. 71, 1-3 (2004) 199-210.
21. A. Heintz, W. Stephan, “A generalized solution diffusion-model of the pervaporation process through composite membranes. 2. Concentration polarization, coupled diffusion and the influence of the porous support layer”, J. Membr. Sci. 89 (1994) 153-161.
22. J.E. ten Elshof, C. Rubio Abadal, J. Sekulic, S.R. Chowdhury, D.H.A. Blank, “Transport mechanisms of water and organic solvents through microporous silica in the pervaporation of binary liquids”, Micropor. Mesopor. Mater. 65, 2-3 (2003) 197-208.
23. K. Kurihara, N. Yasuhiro, M. Masashi, ”Hydrogen-bonded macrocluster formation of ethylene glycol on silica surface in ethylene glycol-cyclohexane binary liquids”, Chemistry Letters 32,1 (2003) 84-85.
24. J. Gmehling, U. Onken, W. Arlt, ”Vapour-liquid equilibrium data collection”, Dechema, Frankfurt, 1981.
25. X. Feng, R.Y.M. Huang, “Estimation of activation energy for permeation in pervaporation process”, J. Membr. Sci. 118 (1995) 127-135.

6

Separation mechanism in pervaporation

Abstract

The pervaporation properties of three asymmetric stacked membrane systems that differ with respect to the used oxide materials and the average pore size of the separating layer are discussed. The adsorption-diffusion model and Maxwell-Stefan theory are applied to explain the influence of process parameters on the pervaporation of selected binary liquids. The temperature, feed concentration and chemical nature of the permeating species were varied. The membrane system α-Al_2O_3 - anatase TiO_2 (or γ-Al_2O_3) - microporous SiO_2 was found to be selective in dewatering of various solvents (e.g., ethanol, 2-butanol, ethylene glycol, etc.) due to the combination of small pores of the microporous silica layer, and hydrophilicity of this layer. It was found that the hydrophilicity of the silica top layer is influenced by the nature of the underlying supporting layer. On the other hand, microporous titania membranes, having larger pores (~0.9 nm) and insufficient hydrophilicity showed poor separation properties in pervaporation of the same mixtures.

6.1 Introduction

Pervaporation and vapour permeation are separation technologies in which one of the components of a liquid mixture (pervaporation), or a vapour phase (vapour permeation) is separated from the feed mixture by selective evaporation (pervaporation) or gas transport (vapour permeation) through a membrane. In principle, these technologies have better separation capacity and energy efficiency than competing distillation, adsorption and extraction technologies and their application may lead to energy reductions of 40-60% [1]. However, the application of pervaporation/vapour permeation in the chemical industry has been restricted due to severe limitations of the current generation of commercially available membranes, i.e., their low chemical and thermal stability, insufficient selectivity and low flux [2-19].

Although ceramic membranes are virtually inert in non-aqueous organic solvents and offer high temperature stability, they have limited stability in aqueous corrosive liquids like strong acids and alkaline solutions [2-7]. Typical pH ranges in which certain ceramic membrane materials are stable at room temperature, i.e., do not dissolve and do not change pore characteristics, are given in Table 6.1. These data are summarized from the studies described in Chapters 3 and 4 of this thesis, and from literature data on static and dynamic corrosion tests [6-8,20]. Since ceramic membranes are commonly stacked layer systems, consisting of a macroporous support, a mesoporous intermediate layer and a microporous top layer, the stability of each layer material may determine the stability of the complete system. α-Alumina is usually used as a macroporous support, because of its high thermal and chemical stability [4]. It can be concluded that the most commonly applied system γ-alumina / silica is stable in a narrow range of pH (4-10), and that this is mainly caused by the poor stability of the γ-alumina phase. Replacing γ-alumina by crystalline titania the stability of the system considerably improves, especially in acidic environments since the titania/silica system is stable in the pH range 1-10. Furthermore, the system crystalline titania / amorphous titania is stable in a very wide pH range (2-14).

It should be noted that, at present, pervaporation is generally not carried out under extreme acidic or basic conditions. However, industrial requirements are set towards more chemically stable membranes in order to enable cleaning and after-treatment with strong acidic or basic solutions, and to expanding the application field towards new processes that involve more corrosive chemicals.

Table 6.1: pH stability range of commonly used ceramic membrane materials.

Material	Stability pH range
α - Al_2O_3	0 – 14
γ - Al_2O_3	4 – 11
TiO_2 (anatase), ZrO_2 (crystalline)	0 - 14
SiO_2 (amorphous)	1 - 10
TiO_2 (amorphous)	2 - 14

An understanding of the transport and separation mechanisms is crucial for further development of a membrane pervaporation process in terms of choice of suitable membrane materials and adjustment of process parameters that lead to enhanced separation and higher fluxes. Historically, two (main) models were proposed to describe the molecular transport process in pervaporation and other membrane processes [9-11]. The solution-diffusion model is based on the dissolution of feed components in a membrane matrix and the subsequent diffusion down a concentration gradient. On the other hand, the pore flow model is based on the assumption of molecular sieving of the permeating species [9]. Nowadays, the solution-diffusion model is generally accepted as a good description of the mechanism of fluid transport, and is widely applied in the area of polymeric membrane research [10]. Applied to zeolite and ceramic membranes, it was renamed into the adsorption-diffusion model. The steps included in this model are the sorption of the permeate at the interface between the feed and the membrane, the subsequent diffusion across the membrane due to concentration gradients (rate determining steps), and finally the desorption into the vapour phase at the permeate side of the membrane. The first two steps are primarily responsible for the final permselectivity [11,9].

The Maxwell-Stefan theory is the most often used model to describe transport of binary mixtures through a membrane [12-16]. It is based on the thermodynamics of irreversible processes, and takes the effect of interactions between the individual mobile components into account explicitly. The Maxwell-Stefan equations regard the steady state transport of a component as a balance between the driving force of that component, and the friction forces exerted by the membrane and the other components.

The first application of the Maxwell-Stefan theory to pervaporation was by Heintz and Stephan for polymeric membranes [12]. It has been used since to describe the pervaporation processes in several polymeric membranes [13,14]. A description of

pervaporation through a ceramic microporous membrane in terms of the Maxwell-Stefan equation was given by Verkerk *et al*. [15]. Unlike the modified Maxwell-Stefan equations for polymeric membranes [12], which consider volume fractions instead of molar fractions, and describe the driving forces in terms of concentration differences across the membrane, they modelled the molecular transport in terms of vapour partial pressure differences and molar fractions, which are more applicable quantities for the description of vapor transport through microporous layers with a fixed pore structure.

Considering the one-dimensional transport of a mobile component *i* from a binary mixture composed of components *i* and *j* through a membrane *M*, the driving force of component *i* can be expressed in terms of the Maxwell Stefan theory as [15]

$$-\frac{1}{RT}\frac{d\mu_i}{dz}=\frac{x_j}{Đ_{ij}}\left(v_i-v_j\right)+\frac{1}{Đ_{iM}'}v_i, \tag{6.1}$$

where z is the direction of transport (perpendicular to the membrane surface area), T the temperature, R the universal gas constant, μ_i the chemical potential of component i, x_j the mole fraction of component j in the adsorbed (membrane) phase, $Đ_{ij}$ the Maxwell-Stefan micropore diffusivity between components i and i, $Đ_{iM}'$ the Maxwell-Stefan micropore diffusivity of component i in the membrane, and v_i and v_j the velocities of components i and j in the membrane, respectively. The first term on the right hand side of Eq. (6.1) describes the friction on species i caused by the presence of species j, while the second term indicates the friction exerted on species i by the membrane. If correlation effects between i and j can be neglected, then $1/Đ_{ij}=0$.

Under the assumption that the components are transported as individual gaseous species via surface or activated gas phase diffusion [17], an expression for the driving force can be obtained using the chemical potential of an ideal gas phase component:

$$\mu_i=\mu_i^0+RT\ln p_i, \tag{6.2}$$

where μ_i^0 and p_i are the standard chemical potential and partial pressure of component i, respectively. Furthermore, the velocity v_i in Eq. (6.1) can be written as the ratio of flux J_i (mol/m^{2}s) and local concentration c_i (mol/m^3), i.e, $v_i=J_i/c_i$, so that

$$-\frac{1}{p_i}\frac{dp_i}{dz}=\frac{x_j}{Đ_{ij}}\left(\frac{J_i}{c_i}-\frac{J_j}{c_j}\right)+\frac{1}{Đ_{iM}'}\frac{J_i}{c_i}. \tag{6.3}$$

For a binary liquid, Eq. (6.3) gives a set of two coupled equations that can be solved numerically if the molar fraction x_j is known as a function of position z inside the membrane. The simplifying assumption that is made here is that x_j can be approximated by the average of the molar fractions on opposite sides of the membrane $\bar{x}_j$ [13].

At low levels of adsorption (Henry's law regime), the concentration of a component is proportional to the local vapuor pressure in the membrane [15], i.e.,

$$c_i = H_i \cdot p_i , \tag{6.4}$$

where H_i is the adsorption coefficient of component i, that depends on temperature according to [15]

$$H_i = H_i^0 \cdot e^{\frac{Q_i}{RT}} . \tag{6.5}$$

An explicit expression for J_i can be obtained from Eq. (6.3) if term J_j/c_j is negligible in comparison with J_i/c_i. For a membrane of thickness L the expression for J_i and J_j then reads [15]:

$$J_i = -K_i \left(\frac{\bar{x}_j}{Đ_{ij}} + \frac{1}{Đ_{iM}'} \right)^{-1} \frac{\Delta p_i}{L} , \tag{6.6a}$$

$$J_j = c_j \left(\frac{x_j}{Đ_{ij}} + \frac{1}{Đ_{jM}'} \right)^{-1} \left(-\frac{1}{p_j} \frac{\Delta p_j}{L} + \frac{x_j}{Đ_{ij}} \frac{J_j}{c_j} \right), \tag{6.6b}$$

The second term on the right hand side of Eq. (6.6 b) shows that minority flux does not depend only on its own driving force, but also on the flux of the majority component. In Eq. (6.6 a) and (6.6 b) $\Delta p_i = p_i^f - p_i^p$, with p_i^f and p_i^p the vapour partial pressures of component i at the feed and permeate side of the membrane, respectively. The factor K is equal to either H (pure surface diffusion) or $1/RT$ (pure gas phase translation). The factor containing the Maxwell-Stefan diffusivities can be regarded as the effective diffusion coefficient $Đ_i^{eff}$:

$$Đ_i^{eff} = \left(\frac{\bar{x}_j}{Đ_{ij}} + \frac{1}{Đ_{iM}'} \right)^{-1} . \tag{6.7}$$

The temperature dependency of $Đ_i^{eff}$ is complex, depending on both physical phenomena such as the activation energy of species hopping along surface adsorption sites and surface

coverage, but also on external process variables such as the composition at the feed and permeate sides of the membrane. However, in sufficiently small temperature intervals it may be approximated by an Arrhenius-type expression

$$Đ_i^{eff} = Đ_i^{eff,0} e^{\frac{-E_i^D}{RT}}, \tag{6.8}$$

where E_i^D and $Đ_i^{eff,0}$ are the apparent activation energy of diffusion and a pre-exponential constant, respectively.

From Eqs. (6.6a) and (6.7) the permeability F_i can be expressed as

$$F_i = \frac{J_i}{\Delta p_i} = \frac{K_i Đ_i^{eff}}{L}, \tag{6.9}$$

so that the activation energy of permeability E_i^F is either $E_i^F = E_i^D - Q_i$ (surface diffusion), or $E_i^F \approx E_i^D$ (gas translation).

6.2 Experimental

6.2.1 Membranes

Three different membrane systems were considered in this study.

1. α-Al_2O_3 - γ-Al_2O_3 - SiO_2
2. α-Al_2O_3 - $TiO_2(ZrO_2)$ - SiO_2
3. α-Al_2O_3 - $TiO_2(ZrO_2)$ - TiO_2

In all cases, α-Al_2O_3 was used as macroporous support. Supports were made from α-alumina powder (AKP30, Sumimoto, Japan). The final supports were disc-shaped, with diameter 39 mm, thickness 2 mm, mean pore radius 100 nm, and porosity ~30% [18].

The intermediate (mesoporous) layer was either γ-Al_2O_3 (calcined at 600 ^oC) [19], or based on the anatase phase of titania (calcined at 450 ^oC). In some cases, the titania phase was doped with 5-20 mol% of zirconia and calcined at 450-700 ^oC [20]. The intermediate layers were applied onto the α-Al_2O_3 discs by a dip-coating technique. After calcinations, these layers had similar structural characteristics: a thickness of 1-2 μm, pore sizes of 5-8 nm, and porosities of ~40-55%.

Polymeric silica and titania sols for microporous top layers were made by acid-catalysed hydrolysis and condensation of suitable alkoxides, as described in more detail elsewhere [21,22]. The sols were deposited onto the surface of the mesoporous layer by dip-coating. The silica and titania membranes were calcined at 400 °C and 300 °C, respectively. The resulting silica layers were amorphous, with a thickness of ~100 nm and pore sizes in the range of 0.3-0.5 nm [21]. The amorphous titania layers had a thickness of 50-100 nm and a maximum pore size of ~0.9 nm [22].

6.2.2 Pervaporation

Pervaporation experiments were carried out using a laboratory scale pervaporation unit. The feed mixture, contained in a 2 l heated vessel under a pressure of 2-3 bar, was pumped continuously in the pulls mode through the feed compartment of the pervaporation unit, where it came into direct contact with the top layer of the membrane. The retentate was recycled to the feed vessel. The permeate side of the membranes was kept under near-vacuum (6-8 mbar) with a vacuum pump. Steady state fluxes were determined by collecting the permeate side vapours in an ethanol-based cold trap and measuring the weight increase with time. The feed and permeate compositions were determined by Karl Fischer titration (784 KFP Titrino, Metrohm, Switzerland).

The pervaporation experiments described in this chapter were performed in the temperature range of 30-100 °C. The feed mixtures were binary liquids with 2-20 wt% water (on total weight) in ethanol, 2-propanol, 2-butanol or p-dioxane (all obtained from Merck, Germany).

The partial vapor pressures at the feed side was calculated from $p_i^f = x_i \gamma_i p_i^0$, where x_i is the molar fraction of component *i* in the liquid phase, γ_i the activity coefficient, and p_i^0 the vapor pressure of pure component *i* at a given temperature. The values of γ_i were calculated with the Wilson equation, and p_i^0 using the Antoine equation [23]. The partial vapor pressures at the permeate side were calculated from the molar fractions in the permeate and the total pressure.

Gas separation experiments were performed with H_2/CH_4 feed mixtures at 200 °C in a cross-flow gas permeation set-up as described elsewhere [24]. Prior to the permeation experiments the membranes were dried at 300 °C under a helium stream to remove any moisture from the pore structure. The membranes were placed in a stainless-steel cell with

the microporous membrane top-layer at the feed side. The composition of the gas mixture at the feed side was controlled by mass flow controllers. The feed pressure and the pressure difference over the membrane were measured by electronic pressure transducers. Argon was used as sweep gas with a flow of 120 ml/min. The gas composition of the permeate and retentate were analysed by a gas chromatograph (Varian, Star 3400CX).

NH_3 Temperature programmed desorption (TPD) [25,26] was performed in order to determine the presence of acidic sites on the membrane pore surface. About 80 mg of the sample was activated at 400 °C for 2 h, then evacuated for 30 min, cooled to room temperature, and equilibrated with NH_3 at 50 °C, at a pressure of 6.5 mbar. The time for reaching the adsorption equilibrium was 75 min. The excess ammonia was evacuated from the sample. A temperature program was set from 50 to 500 °C with a heating rate of 10 °C/min.

X-ray Photoelectron Spectroscopy (XPS, PHI Quantera Scanning ESCA Microprobe, USA) with Ar^+ sputtering (sputter rate 5.1 nm/min; 2 keV Ar^+) was carried out to identify the atomic concentrations of silica, alumina and titania by measuring the Si *2p*, Al *2p* and Ti *2p* spectra as a function of depth inside the layer [27].

6.3 Results and discussion

6.3.1 Influence of process parameters

Fluxes and separation factors of titania-supported silica membranes (system α-Al_2O_3 - $TiO_2(ZrO_2)$ – SiO_2) in the separation of 2-butanol/water and 2-propanol/water mixtures are shown in Figure 6.1. Separation factors up to 500 and 100, and total fluxes up to 1.7 and 2.2 kg/m^{2}h were measured for 2-butanol/water and 2-propanol/water, respectively (Figure 6.1). Experiments were also carried out with ethanol/water mixtures (results not shown in the figure), where separation factors up to 20 and fluxes up to 1.3 kg/m^{2}h were measured.

In general, the membranes showed the highest separation factors and the lowest fluxes for 2-butanol/water mixtures, followed by 2-propanol and ethanol/water mixtures. This trend is expected, having in mind the average pore size of the silica membrane of ~0.3 nm, and molecular sizes of ~0.55, 0.5 and 0.45 nm for 2-butanol, 2-propanol, and ethanol respectively [11,16].

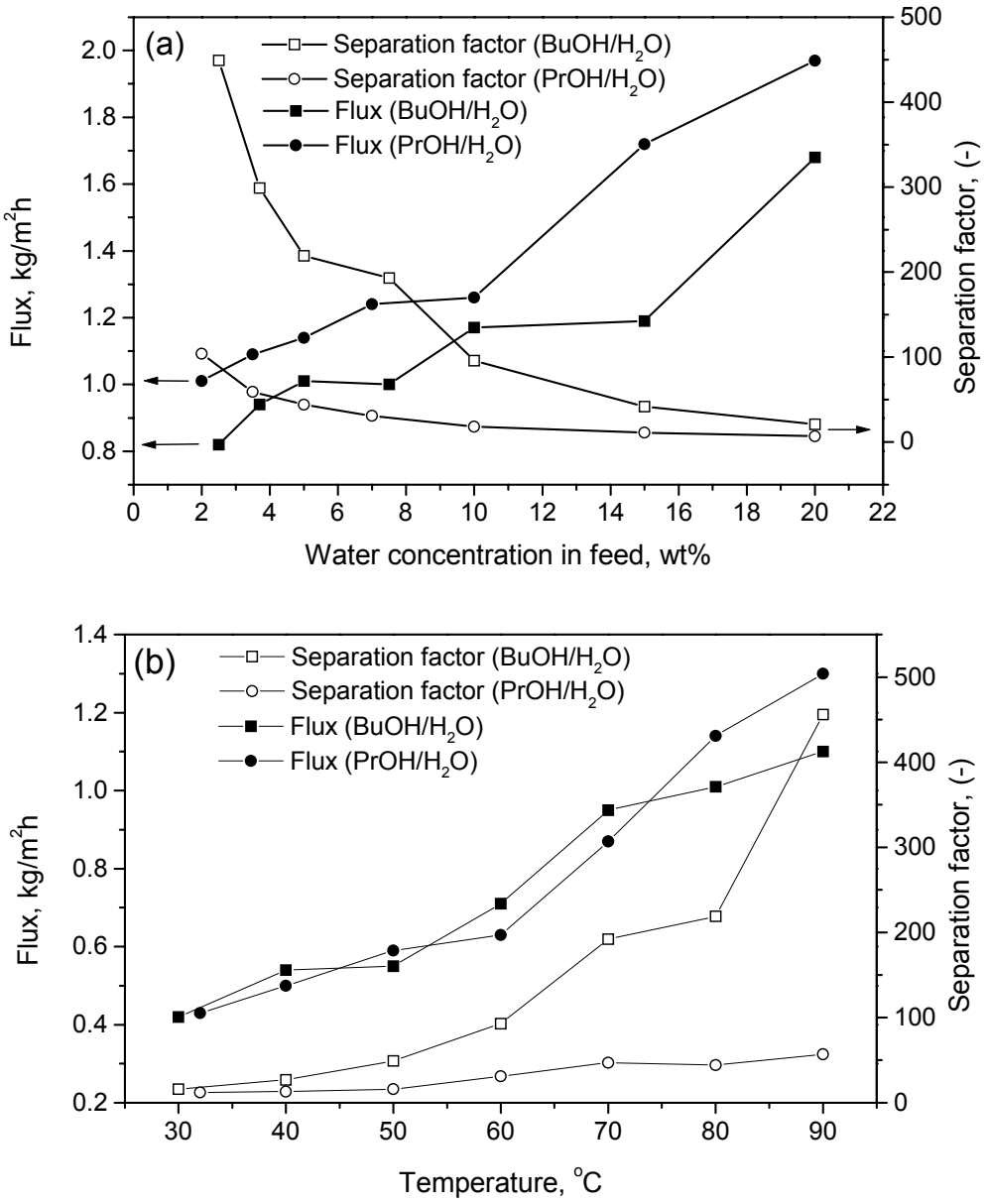

Figure 6.1: Separation factors and total fluxes as a function of feed content at 80 °C (a), and temperature at feed content of 5% H_2O / 95% alcohol (b), for an α-Al_2O_3-TiO_2/ZrO_2-SiO_2 membrane.

The total flux increases, whereas the separation factor decreases with increasing water content in the mixture (Figure 6.1 (a)). Competitive adsorption of liquid molecules onto the membrane surface is the first step taking place. Water adsorption onto the surface of the membrane should increase with increasing concentration in the feed, therefore the flux should also increase. The decrease in selectivities is often attributed to the so-called "drag" effect. Since alcohol molecules are dragged by water through the membrane, the pure alcohol flux increases to a larger extent than the water flux. In terms of the Maxwell Stefan theory, since the velocity of water is higher than the velocity of alcohol ($v_i > v_j$), the

alcohol flux behaves according to Eq. (6.6 b), where the second term on the right hand side shows that the alcohol flux does not depend only on its own driving force, but also on the water flux [15,16].

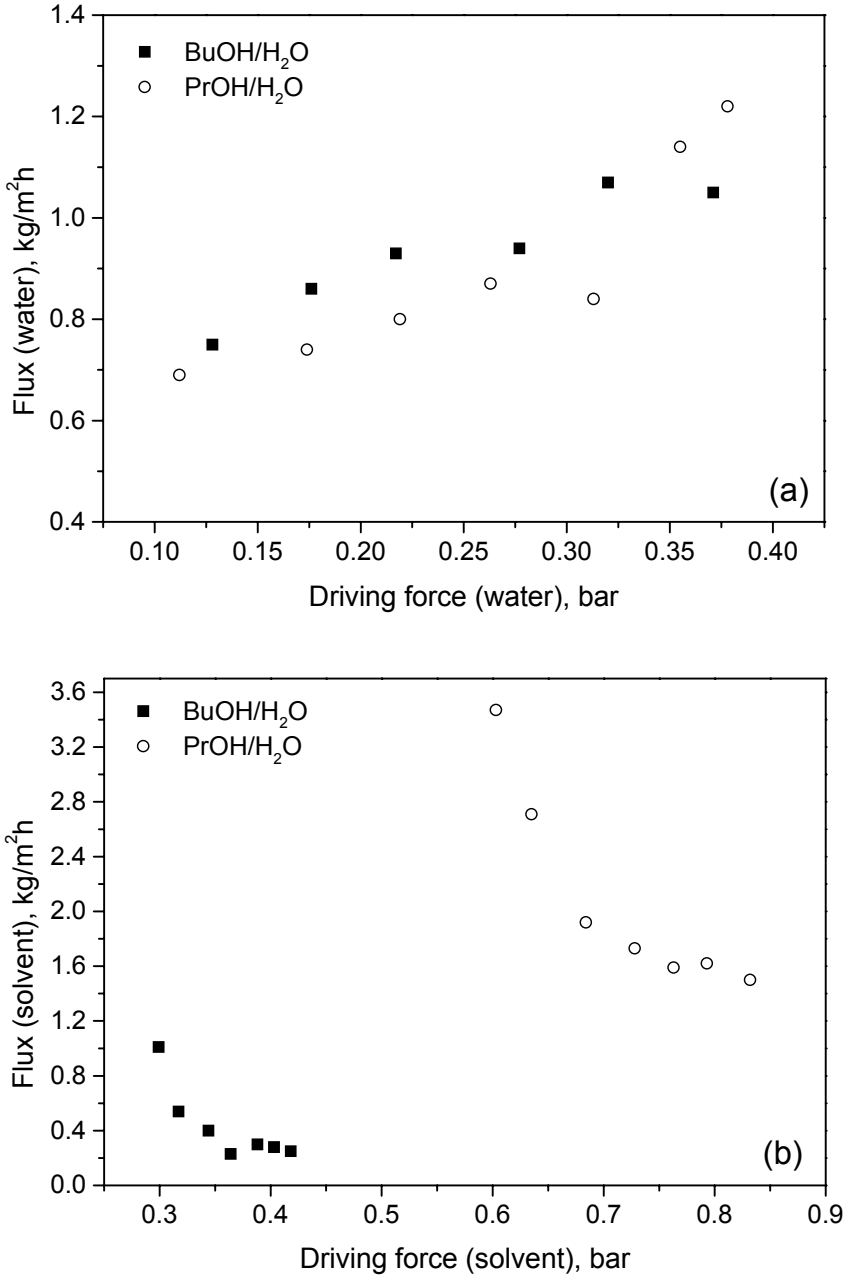

Figure 6.2: Component flux versus partial vapor pressure difference across the membrane at 80 °C; water fluxes (a) and correspondent solvent fluxes (b).

The total flux increases, whereas the separation factor decreases with increasing water content in the mixture (Figure 6.1 (a)). Competitive adsorption of liquid molecules onto the membrane surface is the first step taking place. Water adsorption onto the surface of the membrane should increase with increasing concentration in the feed, therefore the flux

should also increase. The decrease in selectivities is often attributed to the so-called "drag" effect. Since alcohol molecules are dragged by water through the membrane, the pure alcohol flux increases to a larger extent than the water flux. In terms of the Maxwell Stefan theory, since the velocity of water is higher than the velocity of alcohol ($\nu_i > \nu_j$), the alcohol flux behaves according to Eq. (6.6 b), where the second term on the right hand side shows that the alcohol flux does not depend only on its own driving force, but also on the water flux [15,16].

As can be seen in Figure 6.1 (b), both separation factor and flux increases with temperature for all studied mixtures, confirming the improved pervaporation characteristics at elevated temperatures [15]. In accordance with the adsorption-diffusion model, a higher flux is a consequence of an increased driving force due to the increased vapor pressure of the components in the feed, but also due to the increased mobility of the adsorbed species.

The fluxes of components at 80 °C versus their partial pressure differences over the membrane are shown in Figure 6.2. The water fluxes in Figure 6.2 (a) increase with increased partial pressure difference of water, confirming that the water flux is only dependent on its own driving force. However, the decreasing alcohol fluxes with increasing driving force in Figure 6.2 (b) clearly show that the alcohol flux is not dependent only on the concentration gradient of alcohol vapour, but also on the dragging effect from the faster diffusing water species. Furthermore, the 2-butanol flux is substantially lower than the 2-propanol flux, which explains the higher separation factors for 2-butanol/water in comparison with that of the 2-propanol/water mixture.

The total and partial fluxes in pervaporation generally follow an Arrhenius-type temperature dependency [28], which can be written as:

$$J_i = \frac{J_{i0}}{L}(P_{i0} - P_{i1}), \tag{6.10}$$

$$\frac{J_i}{\Delta P_i} = \frac{J_{oi}^{\ 0}}{L} e^{\frac{-E_{act,i}}{R \cdot T}}, \tag{6.11}$$

where J is the permeate flux of the component i, ΔP the transmembrane partial pressure difference, E_{act} the activation energy of permeability, J_{oi} and $J_{oi}^{\ 0}$ prexponential factors that contain the diffusivity and tendency to adsorption of component i, L the membrane thickness, R the molar gas constant, and T the temperature. The activation energy of the

majority permeating component is in general a combination of activation energy of diffusion and the enthalpy of adsorption:

$$E_{act} = E_D + \Delta H_{ads} \,. \tag{6.12}$$

This energy is often viewed as the energy required to facilitate a diffusional jump of a penetrating molecule, minus the enthalpy of sorption. While E_D is positive, ΔH_{ads} is negative for an exothermic sorption process.

The calulated activation energies of permeability $F_i = J_i/\Delta P_i$ of all components are listed in Table 6.2. Since the activation energy of water permeability is (close to) zero in both cases, this suggests that water is transported either by gas-phase diffusion, in which case $E_{act} = E^D \approx 0$, or by surface diffusion, in which case $|E^D| \approx |\Delta H_{ads}|$. Verkerk *et al*. [15] and Ten Elshof *et al*. [16] also reported an activation energy for water permeation of around zero, for γ-alumina supported silica membrane. Negative activation energy calculated for butanol suggests that in this case at lower temperature more energy is needed for the sorption process than for the diffusional jump of butanol molecules.

Table 6.2: Apparent activation energies of permeability in the pervaporation of binary liquids with 10 wt% water in the feed.

Binary liquid	E_{act}, kJ/mol	E_{act}, kJ/mol
	water	alcohol
water/2-butanol	3.8 ± 1.3	-15.6 ± 1.0
water/2-propanol	2.9 ± 1.2	3.1 ± 1.0

Table 6.3: Estimated Maxwell-Stefan micropore diffusion coefficients.

Binary liquid	$Đ_{water,M}'$ (m^2/s)	$Đ_{water,alcohol}$ (m^2/s)
water/2-butanol	$1.2 \cdot 10^{-13}$	$6.3 \cdot 10^{-15}$
water/2-propanol	$1.0 \cdot 10^{-13}$	$6.9 \cdot 10^{-15}$

Since the fluxes of 2-propanol and 2-butanol are low compared to the water fluxes, and both organic solvents are expected to adsorb considerably on silica, Eq. (6.6a) can be used to estimate $Đ'_{water,M}$ and the friction coefficients $Đ_{water,alcohol}$, adopting $H_{water} = 3.8$ molm^{-3}Pa^{-1} from literature [15,16]. For the sake of simplicity it was assumed that the friction coefficients have constant values over the entire feed composition interval.

Good fits were obtained with the parameters listed in Table 6.3. The water diffusion coefficient $Đ_{water,M}'=1\cdot10^{-13}$ m^2/s obtained from the fits is lower than the value reported by Verkerk *et al.*, who estimated $Đ_{water,M}'=9\cdot10^{-13}$ m^2/s [15]. However, they assumed that H_{water} is 0.8 mol m^{-3} Pa^{-1}, which leads to higher predicted values for $Đ_{water,M}'$. This also holds for the values of the friction coefficient ($Đ_{water,alcohol}\sim6\cdot10^{-15}$) of both 2-propanol and 2-butanol, which are smaller than the reported friction coefficient of $0.8–2.0\cdot10^{-13}$ m^2/s [15] for iso-propanol/water.

6.3.2 Influence of membrane material characteristics

A selection of pervaporation data with various membrane systems and feed mixtures is shown in Table 6.4. These measurements were carried out at 80 °C. High separation factors (800 – 1000) and reasonable fluxes were measured with γ-alumina supported silica membranes (experiments I and II). Surprisingly, the separation factor decreased considerably when the intermediate layer material was changed from γ-alumina into mesoporous titania (experiments III and IV). Moreover, significantly different separation factors were measured for ethanol/water and 2-butanol/water mixtures (19 and 220, respectively). The microporous titania membrane did not show any selectivity for ethanol/water, propanol/water or butanol/water mixtures. For p-dioxane/water mixtures (dioxane has a molecular size of ~0.7 nm), low separation factors were measured (experiments V and VI). The separation factor was slightly higher when γ-alumina was used as intermediate layer instead of titania.

Table 6.4: Selected results of pervaporation fluxes and separation factors of various membrane material systems at 80 °C; all feed mixtures contained 5-10% of water.

Experiment	Membrane system	Feed mixture	Total flux, kg/m^{2}h	Separation factor
I	γ-Al_2O_3 - SiO_2	EtOH / H_2O	1.0	800
II	γ-Al_2O_3 - SiO_2	2-BuOH / H_2O	1.0	1000
III	TiO_2 - SiO_2	EtOH / H_2O	1.3	19
IV	TiO_2 - SiO_2	2-BuOH / H_2O	0.6	220
V	γ-Al_2O_3 - TiO_2	p-dioxane / H_2O	1.9	4
VI	TiO_2 - TiO_2	p-dioxane / H_2O	2.8	2

Since the pore size of a silica membrane is small (0.3-0.5 nm), and is similar to the molecular sizes of ethanol (~0.45 nm) and 2-butanol (~0.55 nm) while water is much smaller (~0.24 nm) [11,16], a molecular sieving effect could be the main separation mechanism for this membrane. However, the high separation factors found for the ethanol/water mixture (even though the molecular size of ethanol does not exceed the upper limit of the silica membrane pore size), and the relatively low separation factor for the 2-butanol/water mixture obtained with the mesoprous titania-supported silica membrane, implies some influence of the intermediate layer on overall selectivity.

Gas permeation experiments were carried out on the same γ-alumina and titana-supported silica membranes to examine the presence of defects that might explain the differences in membrane permselectivity during pervaporation. At 200 °C, the H_2 permeability was ~$7 \cdot 10^{-7}$ mol/m^{2}sPa, and the separation factor for a 1:1 H_2/CH_4 gas mixture was ~50 for both membranes. This high permselectivity strongly suggests that the membranes are virtually defect-free. Hence, the observed difference in separation factor cannot be explained by an increased defect concentration, nor by an increase of the average pore size in the mesoporous titania - silica membrane. Certain differences in morphology of the top silica layer due to different layer thicknesses and different silica penetration depths may still be possible, but as seen from the gas permeation data, the intermediate layers seem to have no substantial influence on the intrinsic membrane separation properties associated with a sieving mechanism.

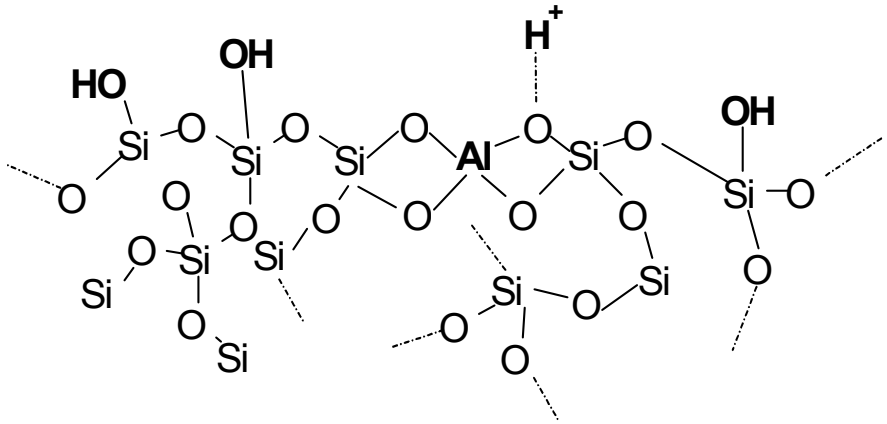

Figure 6.3: Chemical structure of a mixed Al^{3+} / SiO_2 system.

Therefore, is seems more likely that the surface properties of the membranes somehow play a definite role in the separation process. Considering the fact that the main difference between the γ-alumina and titania membranes are the elemental compositions, it is possible that if an aluminium atom becomes embedded into a silica matrix (as shown in Figure 6.3),

an acid (H^+) site will be formed due to the trivalent nature of Al. Consequently, the membrane surface would become more hydrophilic, water molecules would adsorb more strongly, and the value of Henry's constant would increase (Eq. 6.6). On the other hand, an increase of the number of acidic sites is not expected when titanium would be present in the silica matrix, as it oxidation state (4+) is the same as that of silicon.

The questions that remain are: a) are the aluminium (or titanium) atoms incorporated into the silica matrix, forming a "mixed" layer at the interface between the intermediate and top layer, and b) how to experimentally verify the existence of acidic sites when alumina is present in the system.

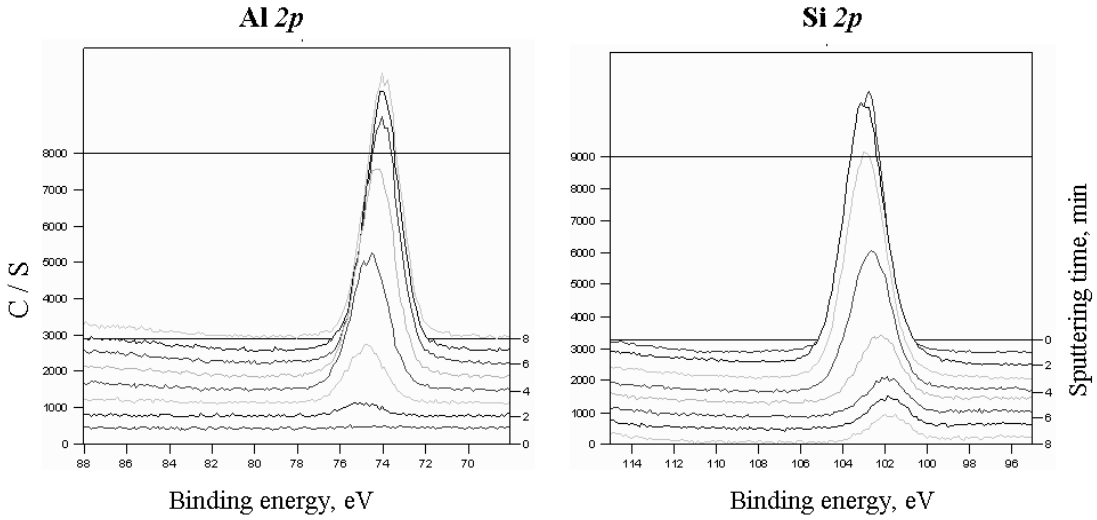

(a) γ-alumina – silica system

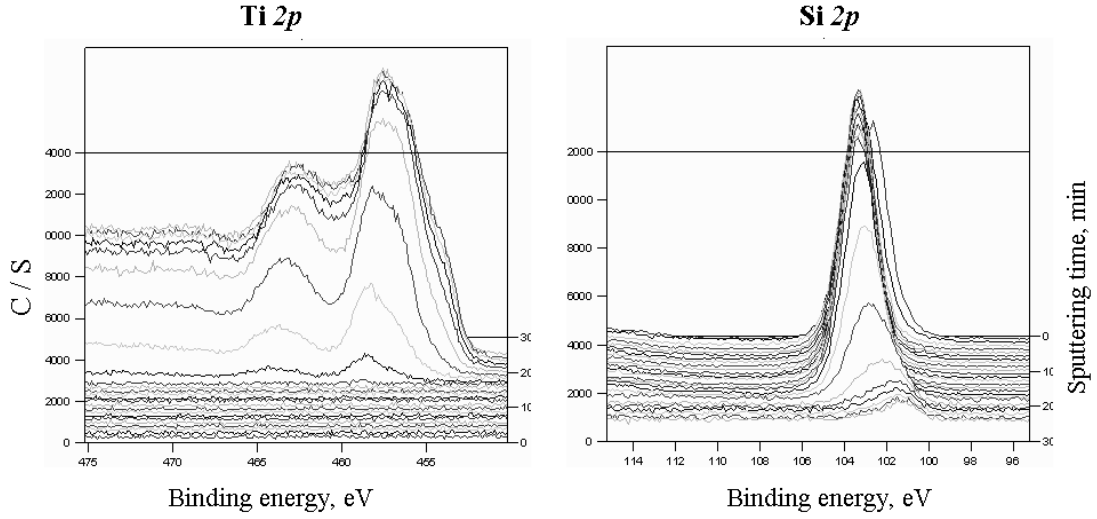

(b) titania – silica system

Figure 6.4: XPS analysis of the γ-alumina / silica interfacial region; Al *2p* and Si *2p* (a) and Ti *2p* and Si *2p* (b) spectrum.

a) The existence of "mixed" silica/alumina and silica/titania layers was proven by XPS analysis. From the "bulk" alumina layer (upper line of the diagram in Figure 6.4 (a)) towards the Si surface, a clear shift in the Al 2*p* spectrum from 74 eV (the binding energy that corresponds to Al_2O_3) to 75.1 eV can be observed in Figure 6.4 (a) [27].

In the Si 2*p* spectrum, shown in Figure 6.4 (b), a binding energy peak shift from 103.2 (SiO_2) to 101.6 eV can be seen. These shifts indicate the existence of compounds other than SiO_2 and Al_2O_3 in the interfacial region, for example Al_2OSiO_4 (corresponding binding energy 74.8 eV in Al 2*p* spectra), $Al_4Si_4O_{10}(OH)_8$ (102.6 eV) etc. [27]. Although the given examples correspond to crystalline materials, the existence of various silicon-aluminate-like compounds confirms the interfacial chemical reactions that may occur, leading to the incorporation of aluminum atoms into the silica matrix. Therefore, it appears that a thin layer near the alumina / silica interface is formed, with a structure as schematically shown in Figure 6.3. Similar results were obtained by XPS analysis of the mesoporous titania/silica interface, which also indicated the formation of a mixed element matrix. It is not entirely clear in which stage of the synthesis these layers are formed, but mutual penetration of silica into the underlying material (and vice versa) is evident.

(b) The presence of acidic sites in the mixed alumina/silica material was verified by Temperature Programmed Desorption (TPD) using NH_3.

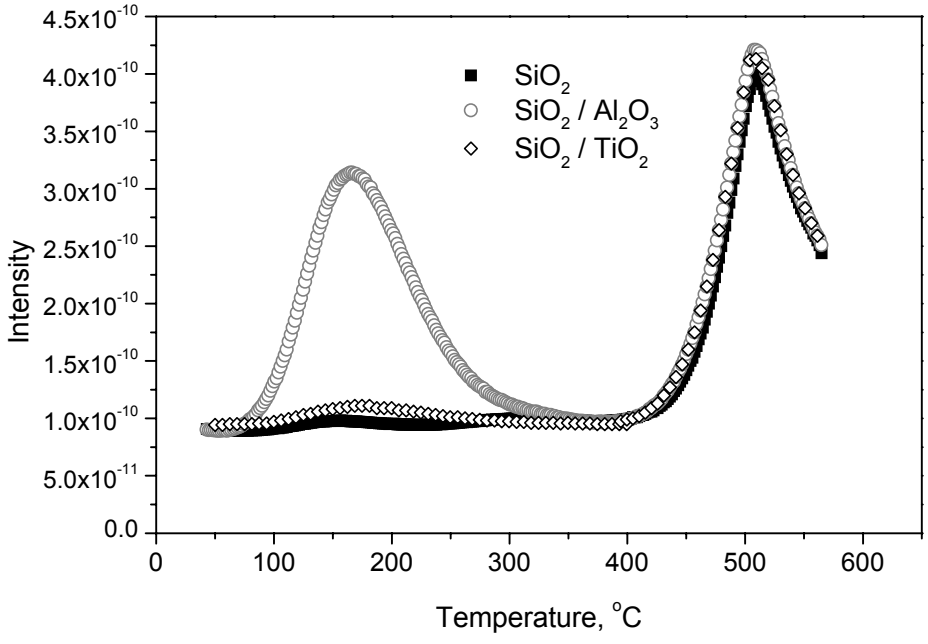

Figure 6.5: Temperature programmed desorption of NH_3 from silica and mixed alumina/silica powders.

Composite silica/alumina and silica/titania material was prepared by simultaneous hydrolysis of silicon- and aluminium-alkoxides, as described by de Lange *et al.* [29]. This material is chemically similar to the material that is formed at the interface between the silica and γ-alumina or titania layer in the membrane system.

As shown in Figure 6.5, NH_3 desorbed around ~100 ^oC from the mixed alumina/silica material, while no desorption around this temperature was observed on the pure silica and silica/titania powder. The desorption peak at ~100 °C corresponds well with the adsorption/desorption of NH_3 due to the presence of acidic sites. On the other hand, the peaks of similar intensity that were recorded in the temperature region around 500 ^oC for all of the samples can be attributed to desorption of OH groups [25,26].

The flux and separation of permeants will be determined by the membrane-permeant affinity and the permeant mobility inside the pore. Hence, membrane parameters that will determine if separation occurs are pore size and internal pore chemistry. From the results presented above it can be concluded that the presence of H^+ (which increases the hydrophilicity) has a beneficial influence on the separation properties of the membrane. Namely, by creating more acidic sites, the concentration of adsorbed water in the membrane is increased leading to a higher driving force for permeation of water, yielding a higher selectivity. The second factor that has a beneficial influence on the separation properties is the small pore size, as in the case of the silica membrane. Therefore, in the case that a stacked membrane system contains γ-Al_2O_3 and SiO_2, the separation of water appears to be improved by the pronounced hydrophilic nature of the material due to the presence of acidic sites. When the membrane system consists of a mesoporous TiO_2 intermediate layer and a SiO_2 top layer, the hydrophilicity is determined only by native OH groups on the silica surface, hence it is significantly lower than when it contains the combination γ-Al_2O_3 - SiO_2. All systems with a microporous TiO_2 membrane as the separating layer will have an increased hydrophilic nature only if γ-alumina is present as intermediate layer, but the ability of this membrane to separate water is determined more strongly on differences between pore size and molecular size. A separation mechanism based on the hydrophilic nature of the membrane, in accordance with the adsorption-diffusion model, has been studied extensively for zeolite membranes [30]. Using mordenite membranes, Casada *et al.* obtained high separation factors in the pervaporation of ethanol/water mixtures, although a molecular sieving mechanism could be ruled out completely, since the size of the mordenite channels of 6.5x7.0 Å allow an easy entrance of

both water and ethanol [30]. Similarly, the differences in activated diffusion rates of water and ethanol did not seem large enough to justify the high separation factors obtained, especially when it was taken into account that the experiments were carried out in the range where surface adsorption processes exert a considerable influence. Instead, separation was thought to take place primarily due to the hydrophilic character of mordenite, hence preferential water adsorption occurred, thereby hindering the passage of ethanol through zeolitic and small non-zeolitic pores. Since the chemical nature of mordenite is roughly similar to the one formed in the interfacial region between γ-alumina and silica, the same explanation may apply in this work for the high separation factors obtained in pervaporation of ethanol/water mixtures by the α-alumina - γ-alumina - silica membrane system.

In conclusion, due to its small pores, silica membranes can be used for separation of water from a wide range of molecules (e.g., dehydratation of BuOH, p-dioxane, etc.), and separation probably occurs primarily due to a molecular sieving effect. On the other hand, it can also be used for separation of molecules with molecular size lower than the maximum pore size (e.g., ethanol /water mixtures), where separation may occur at least partly due to the hydrophilic effect originating from the presence of acidic sites in aluminum doped silica. In the case of the microporous titania membrane, the main separation mechanism seems to be a molecular sieving effect. However, the pore size of this membrane (~0.9 nm) exceeds the molecular size of most industrially important organic molecules. Hence, the microporous titania membrane, although superior with respect to chemical stability, has an application potential that is limited to separation of water and/or small organic molecules from very large molecules as, e.g., in polymerisation reactions.

6.4 Conclusions

According to the adsorption diffusion model, the permeants' flux and separation factors will be determined by the membrane-permeant affinity and the permeant mobility inside the pores. Based on measurements on three types of ceramic membrane systems for various organic/water mixtures, three main factors influencing separation properties are identified: (1) the nature of the permeant (its molecular size and ability to interact with the pore material); (2) the pore size of the separation layer, and (3) the membrane material. The system α-Al_2O_3 - (anatase)TiO_2 - SiO_2 has an improved chemical stability in

comparison with the one containing γ-Al_2O_3 and it can be applied in dewatering of alcohols. However, the choice of an intermediate layer material may also have a pronounced effect on separation factor when the permeants' molecular sizes do not exceed the maximum pore size of the membrane (e.g. as in separation of ethanol/water mixtures). The use of γ-alumina as intermediate layer increases the hydrophilicity of the system, promoting water adsorption and consequently, increasing water flux that is in accordance with the adsorption-diffusion permeation model. In general, the system γ-alumina/silica showed the highest separation factors in pervaporation, followed by the system titania/silica, and titania/titania. However, the chemical stability window increases in the same order. Therefore, the choice of a membrane and support material strongly depends on the requirements of the specific application.

References

1. X. Feng, R.Y.M. Huang, "Liquid separation by membrane pervaporation; a review, Industrial & engineering chemical research", ISSN 0888-05885, 36, 4 (1997) 1048-1066.
2. G.P. Fotou, Y.S. Lin, S. E. Pratsinis, "Hydrothermal stability of pure and modified microporous silica membranes", J. Mater. Sci. 30 (1995) 2803-2808.
3. H. Imai, H. Morimoto, A. Tominaga, H. Hirashima, "Structural changes in sol-derived SiO_2 and TiO_2 films by exposure to water vapour", J. Sol-Gel Sci. Tech. 10 (1997) 45-54.
4. C.–H. Chang. R. Gopalan, Y.S. Lin, "A comparative study on thermal and hydrothermal stability of alumina, titania and zirconia membranes", J. Membr. Sci. 91 (1994) 27-45.
5. R.W. van Gemert, F.P. Cuperus, "Newly developed ceramic membranes for dehydration and separation of organic mixtures by pervaporation", J. Membr. Sci. 105 (1995) 287-291.
6. T. Van Gestel, C. Vandecasteele, A. Buekenhoudt, C. Dotremont, J. Luyten, B. Van der Bruggen, G. Maes, "Corrosion properties of alumina and titania NF membranes", J. Membr. Sci. 214,1 (2003) 21-29.
7. T. Van Gestel, C. Vandecasteele, A. Buekenhoudt, C. Dotremont, J. Luyten, R. Leysen B. Van der Bruggen, G. Maes, "Alumina and titania multilayer membranes for nanofiltration: preparation, characterization and chemical stability", J. Membr. Sci. 207,1 (2002) 73-89.
8. J. Sekulic, M.W.J. Luiten, J.E. ten Elshof, N.E. Benes, K. Keizer, "Microporous silica and doped silica membrane for alcohol dehydration by pervaporation", Desalination, 148, 1-3 (2002) 19-23.
9. J.G. Wijmans, R.W. Baker, "The solution diffusion model: a review", J. Membr. Sci. 107 (1995) 1-21.
10. F. Lipnizki, G. Trägårdh, "Modelling of pervaporation: models to analyse and predict the mass transport in pervaporation", Sep. Purif. Methods, 30 (2001) 49-54.
11. T. Bowen, S. Li, R.D. Noble, J.L. Falconer, "Driving force for pervaporation through zeolite membranes", J. Membr. Sci. 225, 1-2 (2003) 165-176.
12. A. Heintz, W. Stephan, "A generalized solution diffusion-model of the pervaporation process through composite membranes. 2. Concentration polarization, coupled diffusion and the influence of the porous support layer", J. Membr. Sci. 89 (1994) 153-161.
13. P. Izák, L. Bartovská, K. Friess, M. Šípek, P. Uchytil, "Description of binary liquid mixtures transport through non-porous membrane by modified Maxwell-Stefan equations", J. Membr. Sci. 214 (2003) 293-299.
14. X. Ni, X. Sun, D. Ceng, F. Hua, "Coupled diffusion of water and ethanol in a polyimide membrane", Polym. Eng. Sci. 41 (2001) 1440-1445.
15. A.W. Verkerk, P. van Male, M.A.G. Vorstman, J.T.F. Keurentjes, "Description of dehydration performance of amorphous silica pervaporation membranes", J. Membr. Sci. 193 (2001) 227-239.

16. J.E. ten Elshof, C. Rubio Abadal, J. Sekulic, S.R. Chowdhury, D.H.A. Blank, "Transport mechanisms of water and organic solvents through microporous silica in the pervaporation of binary liquids", Micropor. Mesopor. Mater. 65, 2-3 (2003) 197-208.
17. J. Xiao, J. Wei, "Diffusion mechanism of hydrocarbons in zeolites", Chem. Eng. Sci. 47,5 (1992) 1123-1141.
18. F.F. Lange, "Powder processing science and technology for increased reliability", J. Am. Ceram. Soc. 72,1 (1989) 3-15.
19. R.J. van Vuren, B.C. Bonekamp, K. Keizer, R.J.R. Ulhorn, H.J. Veringa, A.J. Burggraaf, "Formation of ceramic alumina membranes for gas separation", High Tech. Ceram. (1987) 2235-2245.
20. J. Sekulić, A. Magrasso, J.E. ten Elshof, D.H.A. Blank, "Influence of ZrO_2 doping on microstructure and liquid permeability of mesoporous TiO_2 membranes", Micropor. Mesopor. Mater. 72 (2004) 49-57.
21. K. Keizer, R.S.A. de Lange, J.H.A. Hekkink, A.J. Burggraaf, "Polymeric-silica-based sols for membrane modification applications: Sol-gel synthesis and characterization with SAXS", J. Non-Cryst. Solids, 191, 1-2 (1995) 1-16.
22. J. Sekulić, J.E. ten Elshof, D.H.A. Blank, "A microporous titania membrane for nanofiltration and pervaporation", Adv. Mater. 16,17 (2004) 1546-1550.
23. J. Gmehling, U. Onken, W. Arlt, "Vapor-liquid equilibrium data collection", Dechema, Frankfurt, 1981.
24. R.M. de Vos, H. Verweij, "High-selectivity, high-flux silica membranes for gas separation", Science, 279 (1998) 1710-1711.
25. A. Auroux, R. Monaci, E. Rombi, V. Solinas, A. Sorrentino, E. Santacesaria, "Acid sites investigation of simple and mixed oxides by TPD and microcalorimetric techniques", Thermochimica Acta, 379,1-2 (2001) 227-231.
26. M. Sasidharan, S.G. Hegde, R. Kumar, "Surface acidity of Al-, Ga- and Fe-silicate analogues of zeolite NCL-1 characterized by FTIR, TPD (NH_3) and catalytic methods", Micropor. Mesopor. Mater. 24, 1-3 (1998) 59-67.
27. http://srdata.nist.gov/xps
28. X. Feng, R.Y.M. Huang, "Estimation of activation energy for permeation in pervaporation process", J. Membr. Sci. 118 (1995) 127-135.
29. R.S.A. de Lange, "Microporous sol-gel derived ceramic membranes for gas separation", PhD thesis, Unversity of Twente, 1993.
30. L. Casado, R. Mallada, C. Téllez, J.Coronas, M. Menéndez, J. Santamaría, "Preparation, characterization and pervaporation performance of mordenite membranes", J. Membr. Sci., 216, 1-2 (2003) 135-147.

Recommendations

Based on the findings of this work, some recommendations for future research in this field can be given:

Mesoporous titania membranes

❖ The composite system γ-alumina/titania is chemically unstable because separate phases of γ-alumina and titania are formed, causing the stability of the γ-alumina phase to determine the stability of the whole system. If a material would be synthesized in such a way that primarily Ti-O-Al bonds are formed on the atomic level, for example by simultaneous hydrolysis of both metal precursors, this problem could possibly be overcome. In this respect, dopants other than zirconia might prove to be successful in the stabilization of the anatase phase, while the chemical stability of the material would not be decreased.

❖ Mesoporous titania membrane permeation properties can possibly be improved by following template-assisted synthesis routes, instead of a conventional sol-gel route. While in the sol-gel route the development of a porous structure is based on particle packing, which yields materials with high tortuosity, templating routes could yield materials with a lower tortuosity, in theory down to 1, and a much higher porosity than is possible in randomly packed structures.

❖ In comparison with the γ-alumina membrane, the mesoporous titania membrane has similar structural characteristics, yet improved stability and higher permeability. In this respect, the application window of the titania membrane seems to be broader than for γ-alumina membranes. However, their actual performance in nanofiltration still needs to be studied in more detail, e.g., by salt retention experiments.

Microporous titania membranes

❖ To increase the porosity and connectivity of the microporous titania membrane, and consequently its permeability, the sol synthesis route could be optimised so that less branched polymeric species are obtained, for example by increasing the acid concentration in the reaction mixture. More generally, the influence of process parameters on size and

degree of branching of polymeric species in a titania polymeric sol needs to be studied in more detail. The small-angle X-ray scattering technique can be used for that.

❖ To decrease the pore size of the microporous titania phase, doping with, for example, zirconia, lanthanum oxide, alumina etc., could be employed. In that case, simultaneous hydrolysis routes or the synthesis of binary alkoxide precursors might prove successful.

❖ Although stable in dry atmosphere until 400 ^{o}C, very little is known about the behaviour of microporous titania membranes in high humidity atmospheres at elevated temperatures. On the other hand, its stability against strongly acidic or basic liquids at room temperature is proven in this thesis, while the actual stability in combination with high temperatures is not known. In order to precisely define stability, and hence the application window of the titania membrane, more research is needed in this area.

Characterisation

❖ No simple technique for accurate determination of pore size distribution in thin layers, in the range 0.6-2 nm is available. Techniques based on single gas permeation through membranes have an upper limit of ~0.6 nm. On the other hand, molecular cut-off measurements are a rather unreliable probe of pore size, especially for molecules with M_w<300 g/mol. Permporometry, which is currently accurate only for pores larger than 4 nm diameter, could be modified for determination of pore sizes in the microporous range.

❖ Molecular cut-off measurements are not standardized and that makes comparison of membrane properties difficult. Moreover, filtration of a mixture containing several species with different molecular sizes may lead to membrane clogging and underestimation of the cut-off value. Therefore, standardization of the experimental conditions is needed, with a fixed concentration and type of permeating species.

Pervaporation

❖ The water pervaporation properties of the microporous titania membrane might be improved and/or controlled by increasing the layer's hydrophobicity or hydrophilicity.

❖ Details on the adsorption behavior of the components of a binary mixture onto the surface of microporous silica and titania could improve the accuracy of the values of the diffusivity coefficients that can be determined from Maxwell-Stefan theory.

❖ In the pervaporation measurements on flat disc-shaped supported membranes, the fluxes may have been underestimated. Therefore, membrane modules could be modified so that better distribution of liquids over the membrane surface and more favourable hydrodynamic conditions are achieved, so that concentration polarization is prevented and higher fluxes are obtained.

Application

❖ The laboratory-scale membrane manufacturing procedure needs to be transferred into an industrial technology. The manufacturing process design should be carried out with special emphasis on support quality and a dust-free production environment (during any coating step) and moisture-free (during the complete microporous titania membrane manufacturing process). Furthermore, the described synthesis technology needs to be applied first on tubular supports, and then upscaled into membrane modules to increase the surface to volume ratio.

❖ Since the γ-alumina - silica membrane system already proved successful in gas separation and pervaporation, the system α-Al_2O_3 - TiO_2 - SiO_2 has potential in the same processes, with the additional advantage of higher chemical stability at low pH. The microporous titania membrane (system α-Al_2O_3 - TiO_2 - TiO_2) with pore sizes in the higher microporous range and a rather low porosity can be applied in nanofiltration, especially when very a low molecular weight cut-off is required and high permeability is of less importance. However, this membrane system has, at present, a rather limited potential for application in gas separation, while it may be applied in pervaporation for the separation of water from some specific liquid mixtures. Research in this area can go in the direction of membrane properties improvement or optimisation of separation process parameters in order to overcome the present limitations.

Summary

The research described in this thesis deals with the synthesis and properties of ceramic oxide membrane materials. Since most of the currently available inorganic membranes with required separation properties have limited reliability and long-term stability, membranes made of new oxide materials that can improve their performance are developed. Anatase and amorphous titania were chosen as mesoporous and microporous material for membrane development, respectively. The relationship between synthesis conditions and properties of the obtained materials could be understood by applying the theory of sol-gel chemistry of transition-metal alkoxides. The developed membrane systems containing Al_2O_3, SiO_2 and TiO_2 were evaluated regarding their potential for application in gas separation, nanofiltration and pervaporation.

Mesoporous titania membrane

Crack-free anatase-based titania layers with an average pore size of 7 nm can be obtained with a reproducibility of around 50%. On the basis of the hypothesis that cracking is caused by stresses that developed due to (partial) phase transformation at the calcination temperature and the low elasticity of the layers due to the low binder content, doping was employed to increase the reproducibility. Zirconia is a suitable dopant that not only retards the phase transformation of anatase into rutile to temperatures above 700 °C, but also leads to a material with higher porosity, smaller pore sizes, higher degrees of pore connectivities and larger internal surface areas. These zirconia-doped titania crack-free layers can be made with a reproducibility of nearly 100%.

Microporous titania membrane

Highly reproducible defect-free amorphous microporous titania layers with a mean pore size of less than 0.9 nm can be obtained on both mesoporous γ-alumina and titania/zirconia coated substrates. The upper limit of thermal stability of the amorphous phase in thin layer form is around 425 °C. Calcination at higher temperatures leads to crystallization into anatase, and layer cracking. The material is chemically stable in the pH range from 2 to 13.

Application

The development of mesoporous and microporous titania membranes introduces novel stacked membrane systems α-Al_2O_3 - TiO_2 - SiO_2 and α-Al_2O_3 - TiO_2 - TiO_2, along with the previously developed α-Al_2O_3 - γ-Al_2O_3 - SiO_2, for the various membrane technology applications. Since the chemical stability of mesoporous anatase and microporous amorphous titania membranes is higher than those of γ-alumina and silica membranes, the application field of ceramic membranes can be expanded towards new processes that involve more corrosive chemicals. The mesoporous titania membrane can be applied in ultrafiltration, and possibly in nanofiltration. Furthermore, since the γ-alumina - silica membrane system already proved successful in gas separation and pervaporation, the system α-Al_2O_3 - TiO_2 - SiO_2 has potential in the same processes, with the additional advantage of higher chemical stability at low pH. The microporous titania membrane (system α-Al_2O_3 - TiO_2 - TiO_2) with pore sizes in the higher microporous range can be applied in pervaporation and in nanofiltration. Applied in pervaporation, the system γ-alumina/silica shows the highest separation factors, followed by the systems titania/silica, and titania/titania. However, the chemical stability increases in the same order. Therefore, the choice of membrane and support material strongly depends of the requirements of the specific application.

Pervaporation process

The adsorption-diffusion model and Maxwell-Stefan theory are applied in explaining separation mechanism and influence of process parameters on the pervaporation of selected binary liquids. The microporous titania membrane is found to be non-selective for small molecules (e.g. lower alcohols), because its relatively large micropores exclude molecular sieving as a separation mechanism. However, very high separation factors and reasonable fluxes were measured for ethylene glycol/water mixtures with not more than 5 wt% of water. The high separation factors for water obtained with ethylene glycol/water mixtures under water-lean conditions indicate a selective mode of separation that is based on a dynamically induced molecular sieving mechanism. It is shown that the membrane became selective under dynamic conditions, despite the fact that the pores are insufficiently small for size-selective separation. This principle may be applied in other dewatering processes, especially where it involves organic compounds that can strongly

adsorb on the pore surface. In general, these would be molecules with a reasonable molecular size, a large dipole moment and/or the possibility to form one or more hydrogen bonds, e.g., ethylene glycol, dimethyl formamide, dimethyl sulfoxide, etc.

Microporous silica membranes can be used for separation of water from a wide range of alcohols. Separation occurs primarily due to a molecular sieving effect, however the chemical nature of the separating layer also plays a pronounced role. The system α-Al_2O_3 - (anatase)TiO_2 - SiO_2 has an improved chemical stability in comparison with the one containing γ-Al_2O_3 instead of anatase TiO_2 and it can be applied in dewatering of alcohols. However, the choice of an intermediate layer material may also play a crucial role in the separation when the permeants' molecular sizes do not exceed the maximum pore size of the membrane (e.g. for separation of ethanol/water mixtures). The use of γ-alumina as intermediate layer increases the hydrophilicity of the system, promoting water adsorption in accordance with the adsorption-diffusion permeation model.

Samenvatting

Dit proefschrift behandelt de synthese en eigenschappen van keramische membranen. Aangezien de meeste beschikbare anorganische membranen met voldoende scheidingseigenschappen een lage chemische stabiliteit en een betrekkelijk korte levensduur hebben, zijn in dit onderzoek nieuwe oxidische materialen ontwikkeld, nl. mesoporeus anatase en microporeus titania. Er kon een relatie worden gelegd tussen de synthese-condities en de eigenschappen van de uiteindelijke materialen. Tenslotte zijn deze nieuwe membranen, op basis van Al_2O_3, SiO_2 and TiO_2, getest met betrekking tot hun potentieel voor toepassing in gasscheiding, nanofiltratie en pervaporatietechnologie.

Mesoporeus titania membraan

Anatase membranen met een gemiddelde poriegrootte van ~7 nm en een reproduceerbaarheid van ~50% zijn gemaakt. Op basis van de hypothese dat scheurvorming optreedt als gevolg van een (partiële) faseovergang bij de calcineertemperatuur, en als gevolg van de lage elasticiteit van de lagen, is dotering met zirconia toegepast om de reproduceerbaarheid te verhogen. Zirconia remt niet alleen de faseovergang van anatase naar rutiel tot temperaturen boven 700 °C, maar leidt ook tot materialen met hogere porositeit, kleinere poriën, meeer interconnectiviteit tussen de porien, en grotere interne oppervlakken. Deze zirconia-gedoteerde titania lagen konden worden gemaakt met een reproduceerbaarheid van ~100%.

Microporeus titania membraan

Defect-vrije amorfe microporeuze titania lagen met een gemiddelde poriegrootte van minder dan 0.9 nm konden worden gecoat op mesoporeuze γ-alumina en titania/zirconia gecoate substraten. De amorfe fase in de vorm van een dunne laag is thermisch stabiel tot 425 °C. Calcinering bij hogere temperaturen leidt tot kristallisatie van anatase, en tot gescheurde lagen. Het materiaal is chemisch stabiel in het pH bereik van 2 tot 13.

Toepassing

Door de ontwikkeling van nieuwe mesoporeuze en microporeuze titania lagen konden de nieuwe systemen α-Al_2O_3 - TiO_2 - SiO_2 en α-Al_2O_3 - TiO_2 - TiO_2 getest worden in verschillende membraanapplicaties. Aangezien de chemische stabiliteit van mesoporeus anatase en microporeus amorf titania hoger is dan die van γ-alumina en silica membranen, kan het toepassingsgebied van keramische membranen verbreed worden naar nieuwe processen waarin zeer corrosieve chemicaliën voorkomen. Het mesoporeuze titania membraan kan worden toegepast in ultrafiltratie, and mogelijk ook in nanofiltratie. Aangezien het klassieke γ-alumina - silica systeem een goede performance heeft in gasscheiding en pervaporatie, kan het systeem α-Al_2O_3 - TiO_2 - SiO_2 worden toegepast in hetzelfde proces, met als bijkomend voordeel dat de stabiliteit bij lage pH hoger is. Microporeuze titania membranen (α-Al_2O_3 - TiO_2 - TiO_2) met poriegroottes in het hogere microporeuze gebied kunnen worden toegepast in pervaporatie voor de scheiding van enkele specifieke mengsels, en mogelijk ook in nanofiltratie. Het systeem γ-alumina/silica heeft de hoogste scheidingsfactor in pervaporatie, gevolgd door de systemen titania/silica en titania/titania. De chemische stabiliteit neemt echter toe in dezelfde volgorde. De keuze voor een bepaald membraan en support is daarom sterk afhankelijk van de eisen die door de specifieke toepassing gesteld worden.

Pervaporatieproces

Het adsorptie-diffusie model en de Maxwell-Stefan theorie zijn gebruikt om het scheidingmechanisme en de invloed van de procesparameters in kaart te brengen. Microporeus titania bleek niet selectief voor scheiding van mengsels met kleine moleculen, omdat de betrekkelijk grote microporiën het optreden van *molecular sieving* uitsluiten. Er zijn echter wel zeer hoge scheidingsfactoren gerealiseerd voor ethyleenglycol/water mengels met $\leq$5% water. Deze hoge scheidingsfactoren wijzen op een dynamisch optredend moleculair scheidingsmechanisme, waarschijnlijk als gevolg van adsorptie van ethyleenglycol in de microporiën van titania. Dit principe kan mogelijk ook worden toegepast in andere ontwateringsprocessen, met name als er sterk adsorberende componenten in de voedingsstroom aanwezig zijn. Dit zullen in het algemeen redelijk grote moleculen zijn met een hoog dipoolmoment en/of de mogelijkheid tot vorming van

een of meer waterstofbindingen, zoals ethyleenglycol, dimethyl formamide, en dimethyl sulfoxide.

Microporeuze silica membranen kunnen worden gebruikt voor de selectieve scheiding van water/alcohol mengsels. Scheiding treedt hier met name op door middel van een *molecular sieving* mechanisme. De chemische eigenschappen van de scheidende laag spelen echter ook een nadrukkelijke rol. Zo verhoogt het gebruik van γ-alumina als tussenlaag de hydrofiliciteit van de toplaag, waardoor meer wateradsorptie optreedt, en een hogere scheidingsfactor kan worden bereikt dan met een anatase tussenlaag.

Acknowledgments

Many people have been contributed, scientifically or not-scientifically, to the realisation of this thesis. My deepest gratitude to all of you directly involved in my work, but also life in general, during past five years. It has been great honour sharing this time with you.

My first special thanks is to my supervisor *The Boss* André ten Elshof. It is difficult to express in words how much I appreciate your constant involvement in my work, support, constructive discussions, patience and persistence. Thank you!

I am also grateful to my promotor Dave Blank, for all the kind support he gave me in the last two years of my work in IMS.

For giving me opportunity to do PhD research University of Twente thanks to Henk Verweij, and for the inspiring introduction into the scientific and social environment of IMS group thanks to my first supervisor Bas Kerkwijk.

Further, I would like to thank everyone involved in INMEMPERV project for all the interesting discussions and suggestions, all the members of Central materials analysis lab and Analytical group, as well as all the others ever involved into discovering the secrets of my membranes.

One big thanks goes to all the members of IMS group! Each and every one of you contributed to the unforgettable time in Enschede. Very, very special thanks for the very, very special time, also apart from work to Mai, Monse, Anna, José, Ashima, Riaan, Fredo, Samuel, Sankho, and Vittorio.

Furthermore, all my other friends who were with me in the past five years, thanks for the wonderful time we spent together.

To my family thanks for the unlimited love and support.

And finally, but most of all, thank you Boris for all your love that was always, and always will be the moving force for everything I do.